CHEMICAL REVIEWS

Review

Single-Molecule Electron Transfer in Electrochemical Environments

Jingdong Zhang, Alexander M. Kuznetsov, Igor G. Medvedev,
Qijin Chi, Tim Albrecht, Palle S. Jensen, and Jens Ulstrup

Chem. Rev., **2008**, 108 (7), 2737-2791 • DOI: 10.1021/cr068073+ • Publication Date (Web): 11 July 2008

Single-Molecule Electron Transfer in Electrochemical Environments

Jingdong Zhang,[†] Alexander M. Kuznetsov,[‡] Igor G. Medvedev,[‡] Qijin Chi,[†] Tim Albrecht,[§] Palle S. Jensen,[†] and Jens Ulstrup*,[†]

Department of Chemistry, Building 207 and NanoDTU, Technical University of Denmark, DK-2800 Kgs. Lyngby, Denmark, The A.N. Frumkin Institute of Physical Chemistry and Electrochemistry, Russian Academy of Sciences, Leninskij Prospect 31, 119071 Moscow, Russia, and Department of Chemistry, Imperial College London, South Kensington Campus, London SW7 2AZ, U.K.

Received November 27, 2007

Contents

* To whom correspondence should be addressed.
[†] Technical University of Denmark.
[‡] Russian Academy of Sciences.
[§] Imperial College London.

10.1021/cr068073+ CCC: $71.00
Published on Web 07/11/2008

1. Introduction

Interfacial molecular electrochemistry is presently moving toward new levels of structural and functional resolution, approaching even that of the single molecules. This evolution extends, notably to fragile biological molecules and macromolecules such as redox metalloproteins and metalloenzymes. Underlying fundamentals of electron and proton transfer of redox molecules and biomolecules in homogeneous solution are broadly understood, with increasing detail and theoretical sophistication currently added. Fundamentals of interfacial electrochemical electron transfer (ET) are also well understood, but the composite inhomogeneous and anisotropic interfacial solid-electrolyte environment is in current need of new concepts, and rationalization of even new ET phenomena. The latter applies for example to new working configurations such as electrochemical scanning tunneling microscopy (in situ STM) or electrochemically controlled nanoscale electrodes where interfacial electrochemical ET of the single (bio)molecule can now be addressed.

High-resolution, nanoscale molecular electrochemistry has followed a line of evolution beginning in the late 1970s by a new close interaction between electrochemistry on the one side and both solid state physics and physical surface science on the other side.[1–5] In this evolution, almost to be likened by a renaissance of the electrochemical science, single-crystal electrodes with well-defined surface structures were, for example, introduced as a major break-through.[5–7] This also laid the foundation for other novel electrochemical technology, not in the least the scanning probe microscopies. At the same time a range of surface techniques and theory was introduced and developed. These included spectroscopy (UV/vis,[8,9] IR,[10,11] Raman,[12,13] and X-ray photoelectron spectroscopy (XPS)[14]), quartz crystal microbalance,[15] and other physical techniques, as well as both statistical mechanical[16,17] and electronic structural theories and computations,[18–20] warranted by the new electrochemistry. Only slightly later the scanning probe techniques, STM[4,21–23] and atomic force microscopy (AFM)[24,25] signaled a lift of both surface science and interfacial electrochemistry to an unprecedented level of resolution. Atomic resolution of pure metal and semiconductor electrode surfaces, and at least submolecular resolution of electrochemical adsorbates, could now be achieved, opening new worlds of microscopic structures and processes and new approaches to electrochemical nanotechnology.

Jingdong Zhang, born in 1968 has a Ph.D. in chemistry from Changchun Institute of Applied Chemistry (Changchun, Jilin, P.R.China), Chinese Academy of Science in 1996 with Professor Erkang Wang as supervisor. She was a researcher in the Itaya Electrochemiscopy Project (Sendai), led by Professor Kingo Itaya (Tohoku University, Sendai, Japan), Exploratory Research for Advanced Technology (ERATO)/Japan Science and Technology Corporation (JST), Japan from May, 1996-September, 1997. She joined Professor Jens Ulstrup's group at Technical University of Denmark in 1998. Since her graduation, she has been interested in single-crystal electrochemistry and in situ scanning tunneling microscopy, especially in developing this technology to biological molecules and macromolecules. She is the author of about fifty research articles, four patents and several book chapters.

Alexander M. Kuznetsov, professor, graduated in theoretical nuclear physics in 1961 from Moscow Institute of Engineering Physics. He has been affiliated with Institute of Electrochemistry of the Russian Academy of Sciences since 1961 and obtained his D. Sc. Degree in 1971 at this Institute. He was the head of the Theoretical Department of the Institute from 1986−2004 and is presently principal researcher at the A.N. Frumkin Institute of Physical Chemistry and Electrochemistry of the Russian Academy of Sciences. He has published more than 360 scientific papers and 4 books. He is one of the pioneers of the quantum mechanical theory of elementary charge transfer in chemical, electrochemical and biological processes in condensed media. Over the last decade, he has focused on theoretical frames of redox-mediated electron tunneling in electrochemical contacts. He is a member of the Royal Danish Academy of Sciences and Letters and an Editorial Board member for a number of scientific journals.

The boundary-traversing new approaches toward interfacial electrochemistry at the nanoscale and single-molecule levels resemble the earlier transition of physical electrochemistry to the status of new interdisciplinary electrochemical surface science. The electrochemical interface, at the heart of electrochemistry with all its challenges can now be controlled and mapped to the single-molecule and even atomic level.

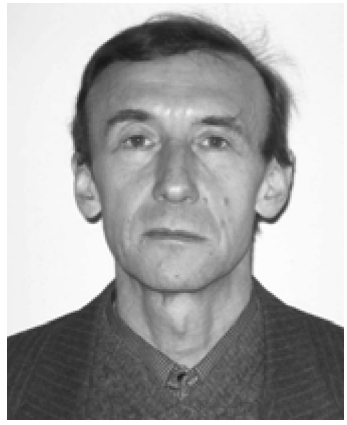

Igor G. Medvedev is a Principal Research Scientist at the A.N. Frumkin Institute of Physical Chemistry and Electrochemistry of the Russian Academy of Sciences where he has worked since 1993. He received his Ph.D. in Solid State Physics in 1982 and his D.Sc. in Theoretical Physics in 1998. His research covers solid state physics, the physics of liquids, theory of adsorption, many-particle physics and the theory of electrochemical electron transfer. His present research is focused on the theory of electron tunneling in bridged electrochemical contacts. He is the author or co-author of more than 60 publications in scientific journals.

Qijin Chi received his Ph.D. degree in analytical and physical chemistry in 1994 from the Changchun Institute of Applied Chemistry, Chinese Academy of Sciences. After having spent one year as a DFG postdoctoral fellow at Tübingen University, Germany, and two years as a JSPS postdoctoral fellow in Tokyo, Japan, he joined the Department of Chemistry at Technical University of Denmark in 1998. He is currently a lektor (associate professor) in chemistry. Qijin Chi also studied molecular biology and biochemistry (2000−2003) at the Johns Hopkins University School of Medicine. His research interests include biological nanomaterials, electrochemistry, surface self-assembled chemistry, and biophysics. He has authored four patents, over fifty research articles, and several book chapters.

Single-molecular interfacial electrochemical ET, directly in aqueous electrolyte solution, has been recorded and disclosed new ET phenomena with no counterparts in classical electrochemistry. To this add at least two other new lines of development. Similarly to the earlier elevation of physical electrochemistry, one line is the introduction of new theoretical notions. Some of these rest on computation of single-molecule conductivity of nonredox[26–33] and redox molecules,[34–38] known from comprehensive studies of single-molecule conductivity in ultrahigh vacuum (UHV). UHV environment enables detailed computational exploration based on methodology such as Green's function, density functional, and molecular dynamics computations. However, theoretical accommodation of the electrochemical environment is in need of new approaches both regarding different concepts,

Tim Albrecht graduated in chemistry at the University of Essen in 2000. He received a Ph.D. with Prof. P. Hildebrandt at the Max-Planck Institute for Radiation Chemistry (now Bioinorganic Chemistry) in Muelheim/Germany for studies on interfacial charge transfer processes of heme proteins using spectroelectrochemistry (SE(R)RS) and electrochemical STM. He held a Marie-Curie fellowship 2004−2006 whilst working in Prof. J. Ulstrup's group and became a lecturer in Physical Chemistry at Imperial College London in 2006. His research interests include (bio)electrochemistry, charge transport through individual molecules, and electrode/nanopore architectures in single-biomolecule sensing. He has published 14 research articles, 2 book chapters, and filed 2 patent applications.

Palle Skovhus Jensen obtained his M.Sc. degree in 2006 at Technical University of Denmark and is presently a Ph.D. student in Prof. J. Ulstrup's group. His research includes interfacial electrochemistry, electrochemical STM and AFM of redox metalloproteins, extending to catalysis of bioelectrochemical processes by molecular scale metallic nanoparticles. He is the co-author of several research articles in these areas.

for example the electrochemical three-electrode configuration, and models particularly for the solvent dynamics and the electrolyte.[33,36–38]

As a second line of development, interfacial pure and applied bioelectrochemistry is emerging out of powerful interdisciplinary efforts.[39–42] These have drawn from all the new state-of-the-art physical electrochemistry introduced into interfacial bioelectrochemistry of redox metalloproteins and DNA-based molecules. Improved voltammetric sensitivity at well-defined electrode surfaces and options for structural and functional mapping of the bioelectrochemical solid−liquid interface at single-molecule resolution are outcomes. It is remarkable that large and fragile redox metalloproteins and metalloenzymes adsorbed on atomically planar electrode surfaces can be mapped to single-molecule resolution in their functional state by a subtle physical phenomenon, the quantum mechanical tunneling effect.[43–45] High-resolution bioelectrochemistry also draws from parallel biotechnology development in protein and DNA-molecular tuning by use

Jens Ulstrup graduated in chemistry in 1964 and obtained a D.Sc. Degree in 1981, both at the University of Copenhagen. He has been affiliated with Technical University of Denmark (DTU) since 1966, from 1984 as a full professor of chemistry. He has been a postdoctoral fellow or visiting scientist at University of Oxford, The A.N. Frumkin Institute of Electrochemistry, Fritz- Haber-Institut/Max-Planck-Gesellschaft, and Utah State University, and a visiting professor at School of Chemistry, University of Sydney. He is a member of the Royal Danish Academy of Sciences and Letters and has received several national and international awards. His research includes chemical rate theory and charge transport in metalloprotein and DNA-based systems which he has tried to combine with notions of single-molecule science. Author or co-author of about 250 research papers, three monographs and many review articles and book chapters.

of mutant proteins,[46,47] de novo synthetic metalloproteins,[48–50] and DNA variability.[51–54] Combination of high-resolution physical bioelectrochemistry with biotechnology and electrochemical surface preparation for electrical signal transfer between molecules and electrodes, for example via biomolecule-size metallic nanoparticles[54,55] has also led to new perspectives for high-resolution biological screening.

We overview here some important parts of these new steps in molecular and biomolecular interfacial electrochemistry. Focus is on recent efforts of several groups including our own group toward structural and functional mapping of single molecules and biomolecules in electrochemical environments. Redox molecules and redox metalloproteins are key target molecules. Electrochemistry, in situ STM at pure and modified single-crystal electrode surface microenvironments, and nanogap electrodes are key experimental approaches, supported by theoretical frames rooted in molecular conductivity and interfacial electrochemical ET theory. In order to place single-molecule electrochemistry in a broader perspective, we overview first briefly in section 2 some systems, environments and ET phenomena associated specifically with single-molecule interfacial molecular electrochemistry. Particular attention is given to single-molecule electrochemistry in the three- and four-electrode configurations of in situ STM and other nanogap electrode configurations. Section 3 overviews theoretical notions needed for single-molecule electrochemistry in the in situ STM and nanogap environment. Key notions are tunneling spectroscopy, the potential distribution in the electrolyte gap in the in situ STM tunnelling gap, spin features, two- and multistep electron hopping, and so-called "Diamond plots" known from single- (or few-)molecule solid state field effect transistors (FET)[56,57] but presently with a novel electrochemical dimension. Sections 4 and 5 overview primary paradigms in nanoscale and single-molecule electrochemical ET. Adsorption, surface lattice formation, and solvation in electrochemical in situ STM imaging are addressed in section 4, with chosen target molecules investigated in some detail. Functionalized organic thiols are in focus and display a remarkable diversity of surface structural patterns and dynamics in the electrochemical environment in spite of their common character as nonredox molecules. Quite a different set of single-molecule electrochemical ET patterns displayed by small redox molecules is overviewed in section 5. These patterns are dominated by two- or multistep ET in which molecular redox centers are electronically populated in bistable but well-defined electronic configurations. Such patterns offer more sophisticated electronic behavior by displaying "amplification", "rectification", and other behavior resembling that of transistors, diodes, and other devices known from microelectronics. These patterns are close to the single-molecule scale and directly caused by the molecular redox centers.

Sections 6 and 7 overview bioelectrochemistry of redox metalloproteins and features of metalloprotein/inorganic hybrid molecular structures at the new levels of resolution. Single-molecule redox metalloproteins/metalloenzymes "in action" is overviewed in section 6 where the blue redox metalloprotein azurin is noted as an emerging paradigm of single-molecule bioelectrochemistry. Some notions of single-molecule ET enzyme function are also noted. Attention in section 7 is on ET phenomena associated with molecular scale "hybrid" objects such as redox molecules and biomolecules bound to metallic nanoparticles and semiconductor nanotubes. Nanoparticles with single-electron charging features (Coulomb blockade) and nanoparticles as catalysts in bioelectrochemistry of redox metalloproteins are particularly addressed and some perspectives noted. Section 8 offers a few suggestions regarding new scientific information and electrochemical and bioelectrochemical "device-like" constructions rooted in the nanoscale and single-molecule nature of the core systems.

2. Single-Molecule Electrochemical Science and Technology: A Brief Overview

2.1. A Primer of Single-Molecule Science

Much recent work on interfacial (bio)electrochemistry has focused on chemical and biological sensing.[49,54,55,58,59] The focus of the present review is on fundamentals of mesoscopic and single-molecule electrochemistry particularly: single-molecule interfacial ET in condensed matter environment at room temperature, as opposed to ultrahigh vacuum and cryogenic temperatures; novel ET phenomena arising from transition from macroscopic ensemble via (well-defined) monolayer to single-molecule behavior, and from semi-infinite electrochemical interfaces to mesoscopic STM and nanogap electrode configurations. New theoretical approaches to stochastic and single-molecule behavior have accompanied the experimental approaches. ET phenomena have a role in broad single-molecule science. To put interfacial single-(bio)molecule electrochemical ET into perspective, we first address single-molecule spectroscopy, chemical dynamics, and other recent single-molecule science.

2.2. Single-Molecule Fluorescence and Chemical Dynamics

Stochastic features of single-molecule fluorescence and other spectroscopy of target molecules at high dilution in optically transparent matrices have disclosed a wealth of details regarding local molecular environments and time

evolution, hidden in ensemble-based probes.[60–70] Systems and data in configurations that resemble single-molecule interfacial ET include[66,67,71–74] bursts of fluorescence ("blinking") after laser illumination; distributions of single-molecule photon emission and excited-state lifetimes; and stochastic time evolution of single-molecule emission spanning time ranges from milliseconds to thousands of seconds, caused by electron hopping or large-amplitude local configurational fluctuations. Such observations also apply to environmentally controlled "on-" and "off-" conductivity states in electrochemically controlled single-molecule conductivity.[71–75]

Real time single-molecule enzyme dynamics in biological environments are other important cases for single-molecule chemical reaction dynamics.[63,64,66–68] As for single-molecule (electronic) spectroscopy, optical excitation is in the μm range but enables single-molecule resolution given adequate matrix dilution. The enzyme cholesterol oxidase with a flavine adenine dinucleotide (FAD) core group fluorescent only in the oxidized state catalyzes O_2-oxidation of cholesterol to ketosteroid.[63,64] As an early example single-molecule turnover by on−off fluorescence of oxidized FAD in the catalytic cycle could be followed in this way.[63,64] Along similar lines more recent efforts by several groups have developed fluorescence-based single-molecule enzyme kinetics to a high degree of detail.[66–68,76,77]

A common denominator in single-molecule enzyme dynamics compared with macroscopic ensemble properties is that large-amplitude conformational fluctuations are convoluted with chemical reaction kinetics in concurring broad time ranges.[66–70] Early[63,64] and recent work by Xie and associates[66,67] has mapped these nontraditional features of enzyme dynamics in great detail based on hydrolytic enzymes and substrates that release a fluorescent reaction product. Enzyme turnover events on a single-molecule basis are intrinsically stochastic, with distributions and large time fluctuations of "waiting times" ("off-states") between individual reaction events. A notable observation is that average waiting times appear to follow the Michaelis−Menten mechanism, thus illustrating equivalence between individual molecular time averaging and ensemble averaging (for a discussion, see 78). Stochastic enzyme dynamics parallel protein dynamics mapped by internal photoinduced ET involving protein complexes with bound fluorescent groups.[66,68] The emerging fluorescence decay patterns have warranted theoretical framing[79] to disclose a wealth of dynamic detail associated with different physical processes in widely different time ranges.[66–68,76,77] Such studies have also added other physical substance to the comprehensive pioneering work by Frauenfelder and associates on the "multi-tier" myoglobin−ligand (CO, O_2) recombination reaction which is so far the case with the most detailed mapping of protein dynamics.[80–82]

Recent reports by Rowan, de Schryver, and associates illuminate single-molecule enzyme kinetics convoluted with internal enzyme dynamics.[76,77] The hydrolytic enzyme, lipase B (*Candida antarctica*) labeled by a fluorescent probe was the key enzyme, combined with an ester substrate yielding a fluorescent product. Single-molecule enzyme turnover showing fluorescent on−off behavior could be followed over long periods of time. The "blinking" events could be ascribed to formation of individual product molecules. The individual catalytic events were both correlated in time and convoluted with large-amplitude enzyme conformational motion notably with most of the conformational states enzymatically inactive.

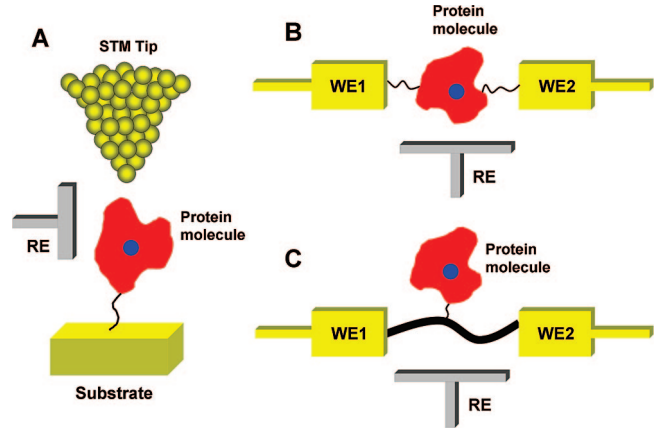

Figure 1. Schematic illustration of three configurations for electrochemical (or bioelectrochemical) approaches to single-molecule charge transfer of redox molecules (particularly for metalloproteins). A protein (or other redox) molecule is assembled in an electrochemical STM gap (A), directly organized in the nanogap between two enclosing electrodes (B), and linked to an inorganic nanowire or nanotube connecting two enclosing electrodes (C). The redox center in the protein molecule is indicated by the blue spot. WE and RE denote working electrode and reference electrode, respectively.

Single-molecule (bio)electrochemical ET has now also been reported, sections 4–6, showing single-molecule electronic behavior and elements of stochastic features,[83–92] but the level of detail has not reached those of fluorescence-based single-molecule enzyme mapping.

2.3. The Scanning Probe Microscopies STM and AFM, and Nanoscale Electrochemical Imaging and Chemical Reactivity

2.3.1. In Situ STM, and Electrochemical Nanogap Electrodes and Nanowires

Two notions have been crucial in developing molecular and biomolecular electrochemistry to molecular-scale resolution. One is the use of single-crystal, atomically planar electrode surfaces to be combined with electrochemical, spectroscopic, and multifarious other surface technology. Well-defined metal and semiconductor surfaces, structurally controlled to the atomic level both offer uniform microenvironments for electrochemical adsorption and interfacial ET and have paved the way for the other notion of true molecular-scale electrochemical technology and for the mapping and control at such levels of resolution[3,4,42,83,92] (Figure 1).

(a) The scanning probe microscopies (SPM), STM and AFM, under electrochemical potential control (in situ STM and AFM) are key single-molecule technologies. Conducting AFM combine both facilities.[94,95] These technologies are reviewed elsewhere.[96–99] (In situ) STM and AFM are complementary in the sense that the former monitors electrical currents through the molecular objects by the tunneling effect under electrochemical potential control of the redox charge state of the target (bio)molecule(s). AFM monitors forces between the molecular-scale targets and the AFM tip. AFM is more directly related to the molecular topography but lateral tip convolution is more important than for STM, and different-range forces (van der Waals, hydration, electrostatic etc.) also convolutes the vertical molecular dimension with specific force dimensions.[100]

(b) Trapping of single molecules between nanometre scale electrochemical electrodes separated by molecular-scale gaps is a second nanoscale configuration with which to approach single-molecule interfacial ET.[101–103] Nanoscale electrochemical electrode pairs can be prepared by the "break junction" principle in which (atomically) thin metallic (say, gold) wires between the electrodes are established, e.g., by electrochemical metal deposition. Subsequent electrochemical metal dissolution can trap molecules from the solution in the gap opened. Similar wiring can be achieved by contacting a gold STM tip with a gold substrate followed by tip retraction and molecular trapping.

(c) Single- or few-molecule electronic mapping can be addressed by a third electrochemical approach. The conductivity of metallic or semiconductor nanowires bound to a pair of enclosing electrodes at given bias voltage between the electrodes can be recorded.[104–110] At the same time the enclosing electrodes can be potentiostatically controlled relative to an electrochemical reference electrode.[108–110] Adsorption of molecules on the wire induces subtle changes in the wire conductivity that can be detected to the level of just a few molecules. The configuration is sensitive enough that even enzyme (glucose oxidase) substrate molecules that change the adsorbed enzyme from its resting state to its active state, can be detected.[108]

All three configurations include two "working electrodes" and a reference electrode. The working electrodes are the substrate and tip in electrochemical STM, or the two nanogap electrodes. A fourth counter electrode is added to in situ STM to monitor Faradaic electrochemical processes. The analogy between nanoscale three-electrode systems and reported single-molecule solid state transistors has long been noted.[84,89] Substrate and tip or the two working electrodes are equivalent to the source and drain electrodes of the transistor, whereas the electrochemical reference electrode is equivalent to the gate electrode of the transistor. Operational differences are, however, that reported single-molecule solid state transistors mostly operate in UHV and at cryogenic temperatures,[57,111,112] whereas electrochemical single-(few-)molecule transistor-like units operate at room temperature in condensed matter environment.[84–92] The latter is, moreover, not restricted to aqueous media but applies also to ionic liquids[113] as a step toward solid state ionic conducting or other media more appropriate for consideration in applied "device-like" function.

The three nanoscale configurations noted will be addressed in sections 3–6, with focus on electrochemical in situ STM of redox molecules and metalloproteins. As a prelude we summarize some observations to be detailed in following sections. "Small" redox target molecules include organic molecules (such as the viologens),[87,88] aniline derivatives[89,90] and other organics,[91,92] Au-nanoparticle molecular hybrids,[114] and transition metal complexes.[83–85] Redox molecules offer more sophisticated conductivity patterns than nonredox molecules, such as negative differential resistance, amplification, and rectification. These effects are becoming understood as new single-molecule interfacial electrochemical ET phenomena with accompanying theoretical chemical frames[34–38] subsequently also picked up elsewhere.[75,115]

Redox metalloproteins as in situ STM target systems were introduced early, section 7. The variety of systems addressed now includes the three major classes of redox metalloproteins, blue copper proteins,[47,116–128] heme proteins,[129–132] and iron−sulfur proteins.[133] These efforts involve not only high image resolution in different microenvironments but also functional mapping[86,125,134] based on the different current/voltage relationships noted.[34–37] Extension to single-molecule metalloenzyme function has been initiated[135–137] but as noted, not reached the level of detail available from single-molecule fluorescence-based studies.

Monolayer, and close to single-molecule resolution of the conductance of molecules immobilized in similar-size gaps between enclosing electrodes (substrate and tip in STM or the working nanoelectrode pairs) has become broadly established and theoretically framed[138–141] Single-molecule electronic mapping with electrochemical potential control is confined to much fewer systems.[142] The electrochemically controlled nanoscale system classes include: nonredox molecules such as pure and functionalized alkanethiols; other larger nonredox biological molecules such as DNA-based molecules; redox molecules such as organic molecules and transition metal complexes; and, redox metalloproteins and metalloenzymes. These systems will be overviewed in sections 3–6.

2.3.2. Some Notions from AFM

Although not in our primary focus, some observations on AFM force microscopy put single-molecule electrochemical STM into another perspective. AFM imaging of adsorbed molecules and biomolecules in contact with aqueous solution does not a priori involve the same requirements regarding electrochemical potential control[25,97] but such requirements are of course needed if electrochemical reactivity is in focus. In some respects image interpretation is even facilitated by the aqueous environment. AFM does not usually reach the same level of adsorbate image resolution as high-resolution STM due to lateral convolution with the tip but atomic and molecular resolution can be achieved for ordered surface molecular and biomolecular adsorbate layers.[99] Other details regarding single-macromolecular structure and dynamic features not accessible by STM are also offered by AFM.[69,143–156] The observations summarized below addressing atomic force spectroscopy can be compared with STM and scanning tunnelling spectroscopy (STS) addressed in sections 4.2–6.

Some analogies and differences in the two scanning probe microscopies can first be noted. Piezoelectric scanner control to subnanometre accuracy and surface scanning of molecular-size objects (and for AFM, larger objects) are at the heart of both. Both technologies operate, moreover, in equivalent spectroscopic modes. AFM can operate in the constant force mode with cantilever (piezo scanner) deflection measured, or in constant height mode with the force measured. These are equivalent to constant current and constant height modes, respectively in STM. Force−distance and force−deflection correlations are analogous to tunneling current/distance and tunneling current/bias voltage spectroscopy, respectively.

Differences between (in situ) STM and AFM are that the primary observable in STM is the tunneling current and the electrical conductivity of the molecular-scale objects. The primary controlling parameters are the bias voltage and the electrochemical potential. The AFM analogues are the cantilever deflection and a range of forces. AFM offers therefore a more direct approach to surface and adsorbate topography ("shape") and applies to a wider range of substrates (i.e., conducting and nonconducting) than STM. With the noted topographic lateral convolution of molecular-scale objects with the geometric tip curvature, lower spatial resolution is, on the other hand expected by AFM which is

therefore better suited to intermediate size, "mesoscopic" objects in the >10 nm size range. Vertical resolution to the molecular level is often achieved but different forces have different spatial extension and observed apparent height may not always accord with the real molecular vertical dimensions.

Single-molecule unfolding of proteins and other macromolecules including mapping of successive domain unfolding,[146–148] macromolecular elastic deformation,[149] and stretching and unwinding of DNA-based molecules,[151,152] have been addressed by AFM. Issues in recent focus have been biological recognition between proteins on a substrate surface and ligand binding groups immobilized on the AFM tip.[153,154] The nature and single-molecule distribution of the forces, parallel single-molecule mapping of recognition and topographic features, and modeling of the free energy landscape of the associated chemical reaction dynamics in the aqueous biological environment are key outcomes.[151–154] In important respects AFM spectroscopy is therefore more advanced than STM spectroscopy.

Combination of AFM-based mechanical forces with optical or electrochemical actuators constitutes other single-molecule AFM development.[155,156] Rational energy conversion in most molecular machine constructs involves at least two steps. The first step is conversion of external (abundantly available) energy such as light energy to locally based mechanical motion, say molecular conformational changes. The second step that should transform the local molecular response to a rational working principle is, however, much more elusive. Recent AFM-based systems offer routes in this direction.[155] One example is light-induced cis−trans isomerization of azobenzene incorporated in a peptide chain linked to an AFM tip.[155a] Light energy is first converted to a structural change in the chain, followed by transduction of the configurational energy change to mechanical energy stored in the AFM cantilever. In a related system the primary energy conversion step is achieved by interfacial electrochemical ET to a ferrocene-based linear polymer.[155b] Oxidation of the ferrocene units induces conformational changes in the polymer, transduced to mechanical energy storage in an AFM cantilever, Figure 2. Other schemes are discussed in refs.156 and 157 and references there.

2.4. Molecular Electronics

Interfacial electrochemistry at the well-defined monolayer level, i.e., in single-crystal surface microenvironment, and at nanoscale and single-molecule levels bears resemblance to the diverse and developing interdisciplinary area known as molecular electronics.[157–160] As in electrochemistry, interfacial ET between metallic source and drain electrodes on the one side and nonredox and redox molecules on the other side is a common denominator of molecular electronics. Commonly noted differences are that the molecular environments of working molecular electronics as commonly understood are mostly UHV and cryogenic temperatures, whereas interfacial electrochemistry toward the single-molecule level operates at ambient temperatures in condensed matter environments. The latter represent different physical properties ranging from nonconducting organic liquids via polar, protic, and ionic liquid media, ultimately to solid ionic and conducting media.

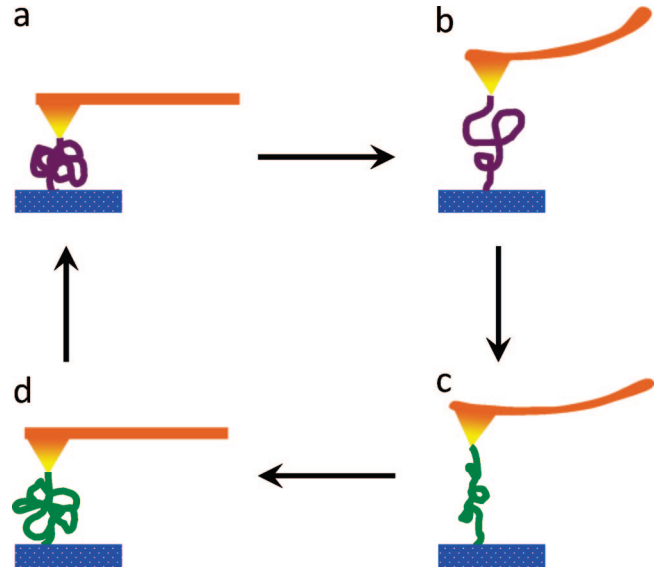

Figure 2. An AFM-based single-molecule mechanical device. (a) A ferrocene-based polymer is enclosed between a conducting substrate and a conducting AFM tip. (b) Electrochemical oxidation or reduction of the ferrocene unit from the substrate electrode causes a conformational change in the polymer. (c) The conformational energy change is transmitted to the cantilever and stored as mechanical energy. (d) Reoxidation or rereduction returns the ferrocene units and the cantilever to the initial state. Adapted from ref 155b. A similar principle based on light-induced cis−trans isomerization of a protein azobenzene derivative was introduced in ref 155a.

2.4.1. Notions of Single-Molecule Electronic Conductivity of Nonredox Molecules

Molecules which are by normal chemical notions redox inactive in accessible electrochemical potential ranges, in the molecular-scale confinements of STM and nanogap electrode pairs are expected to exhibit simple current/voltage features. The LUMO and HOMO levels of, say some of the key molecular targets, pure and functionalized alkane (di)thiols, are strongly off-resonance with respect to the Fermi levels of the enclosing electrodes. Superexchange dominates the conductivity with current/bias voltage and current/overpotential effects reflected largely in the molecular HOMO and LUMO energies, i.e., tunneling barrier features, with featureless current/voltage relations.[26–32,138–141,158–163]

The off-resonance energy features have favored nonredox molecules as main targets for evolving state-of-the-art electronic structure and electronic transport computations that reach the level where not only current/voltage correlations but also absolute molecular conductivity values that warrant direct comparison with experimental data can be addressed.[164] The present status is overviewed in recent review and feature articles.[138–142] We presently note some issues of importance to the electrochemical environments which we elaborate in section 4.2.

Nonredox molecules represent barriers to electronic conductivity and are perhaps not to be considered as primary molecular electronics elements. Understanding of the relatively simple conductivity mechanisms of nonredox molecules is, however, important. At the same time, combined experimental and theoretical efforts in nonredox single-molecule conductivity has enabled crucial features of interfacial single-molecule electrochemical ET to be addressed. These include the molecule−electrode contacts, dynamics of the molecule/electrode binding, and dynamics of the

molecular structure itself reflected in temperature dependence and "gating" of the molecular conductivity.[39,87,160–163]

Up to 5 orders of magnitude discrepancy between measured and computed single-molecule conductivities were common a few years ago.[164] Many reports over the past few years have, however, pointed to the importance of the physical molecule/electrode contacts. Improved technology based on break-junction and single-molecule "catching" where the molecule/electrode contacts are much better controlled has improved the accordance tremendously, perhaps leaving the conclusion that the discrepancy was inherent in experimental rather than theoretical and computational problems.[141,164]

Once on the way toward correspondence between experimental binding configurations and theoretical models, other binding properties come into focus. Contacting of strongly chemisorbing molecules such as thiols and dithiols on different metallic hollow, bridge, atop, and conical Au-surface sites evoke rather different electronic charge distributions in the Au−S bonding region.[140,165–168] In turn this is reflected both in the absolute conductivity values and in the bias voltage, temperature, and molecular length dependence of the molecular conductivities. Switching between different binding modes can also be induced by these external factors. Observed molecular tunneling current switching should therefore be assessed with consideration of such effects.[140,164] We address some specific case studies along these lines extended to electrochemical environments in section 4.2. It is noted that solvation effects can be crucially important both for conductivity and for in situ STM patterns as well as for the packing of even strongly chemisorbed molecules on the electrochemical electrode surface in contact with aqueous electrolyte.[33]

2.4.2. Molecular Rectification and Amplification

Single- (and few-)molecule and -biomolecule interfacial electrochemical ET in nanoscale confinements will be in focus in sections 5–7 with redox target systems fundamentally different from nonredox systems. In contrast to the long-range superexchange molecular conductivity mechanism of nonredox molecules,[138–141] the presence of (a) low-lying molecular redox level(s) evokes a quite different mechanistic pattern, namely two- or multistep electron or hole "hopping" among well-defined molecular redox centers. In the context of electrochemical in situ STM, this notion was introduced in refs 34, 169, and 170. The electron hopping mechanism offers a greater variety of electronic functions such as current rectification, negative differential resistance, switching, and amplification, which cannot be reconciled with tunneling current/voltage correlation patterns for nonredox molecular junctions. Other more sophisticated correlations emerge when tunneling current/voltage correlations are taken from two- to three-terminal configurations, such as in interfacial electrochemical ET.

As the accessible redox level(s) of confined redox molecules are brought into the energy window between the Fermi energies of the enclosing electrodes, more efficient conductivity channels than off-resonance superexchange open. These mechanisms cause new spectroscopic features in the current/voltage relationships and make redox molecules much more versatile as active molecular-scale electronic elements. The molecular conduction mechanisms accord with different physical patterns, of which the following are important in our present context:

(a) Coherent resonance electron tunneling across the junction through the molecular redox level. The latter is in resonance with vacant and occupied electronic levels in the enclosing electrodes and broadened by electronic coupling to the electrodes or by other decay channels. The bias voltage is the sole controlling external parameter in two-terminal junctions while the gate electrode potential is an additional important controlling parameter in three-electrode junctions. Most theoretical efforts have focused on the two-terminal limit.[26,138–141,164]

(b) Resonance tunnelling accompanied by weak vibronic effects in which the transmitting electron interacts with local vibrational modes. This mechanism is the basis of inelastic tunnelling spectroscopy (IETS) discovered early[171,172] and now broadly applied.[173–178] IETS adds vibrational fine-structure to the current/voltage relationships but does not affect the coherent nature of the transition. Coherent or weakly vibrationally affected resonance tunnelling is a likely transport mechanisms in UHV-based two- and three-terminal solid state junctions bridged by different molecules such as organic redox molecules,[176–178] C_{60},[111] and transition metal complexes.[179–181] In view of the large bias or gate voltage range often needed, a broader variety of molecules and electronic LUMO and HOMO levels than commonly associated with electrochemical redox processes appear to follow these patterns. Most reported cases of molecular-scale electronic diode,[182] transistor, and switch function in solid state environments accord with these notions.[57,110–112,178,179]

(c) Different patterns emerge in the opposite limit of strong electronic-vibrational coupling of the confined target molecules, leading now to excess electron or hole trapping at the molecular site. Tunneling conductivity then changes from coherent (resonance) tunnelling to hopping, i.e., two- or multistep electron or hole transfer between well-defined molecular orbitals with full or partial vibrational relaxation between successive molecular ET events.[34–37] These are multiphonon charge transfer mechanisms, conspicuous for redox molecules in electrochemical STM[83–92,113] in contact with aqueous electrolyte solution or ionic liquids. These patterns are in focus in the following sections.

The nontrivial distinction between single-molecule conductivity in two- and three-terminal junctions as under UHV and cryogenic temperature conditions is no less crucial for redox molecular conductivity when the molecules are coupled to an environmental vibrational continuum. Transition metal complexes,[183] metalloporhyrins,[184] heteropolytungstates,[185] organic redox molecules such as viologen-based molecules,[88,186] and redox metalloproteins such as cytochrome c[187] and azurin[126–128] have been characterized in two-electrode environments. Imaging has been at single-molecule resolution, with features such as negative differential resistance and bias voltage controlled reversible height variation observed.

Redox molecules and biomolecules in three-electrode condensed matter electrochemical in situ STM and nanoelectrode confinement are, however, in our focus here. The charge state of the target molecules can here be controlled precisely by the electrochemical potential relative to a reference electrode (the overpotential). Tip coating further reduces spurious Faradaic currents through the tip, leaving pure tunneling currents through the molecule and the tip, Figure 3. As for three-electrode solid state junctions, two kinds of molecular tunneling spectroscopy emerge in condensed matter environment at room temperature. The molecular tunneling current variation with the bias voltage can

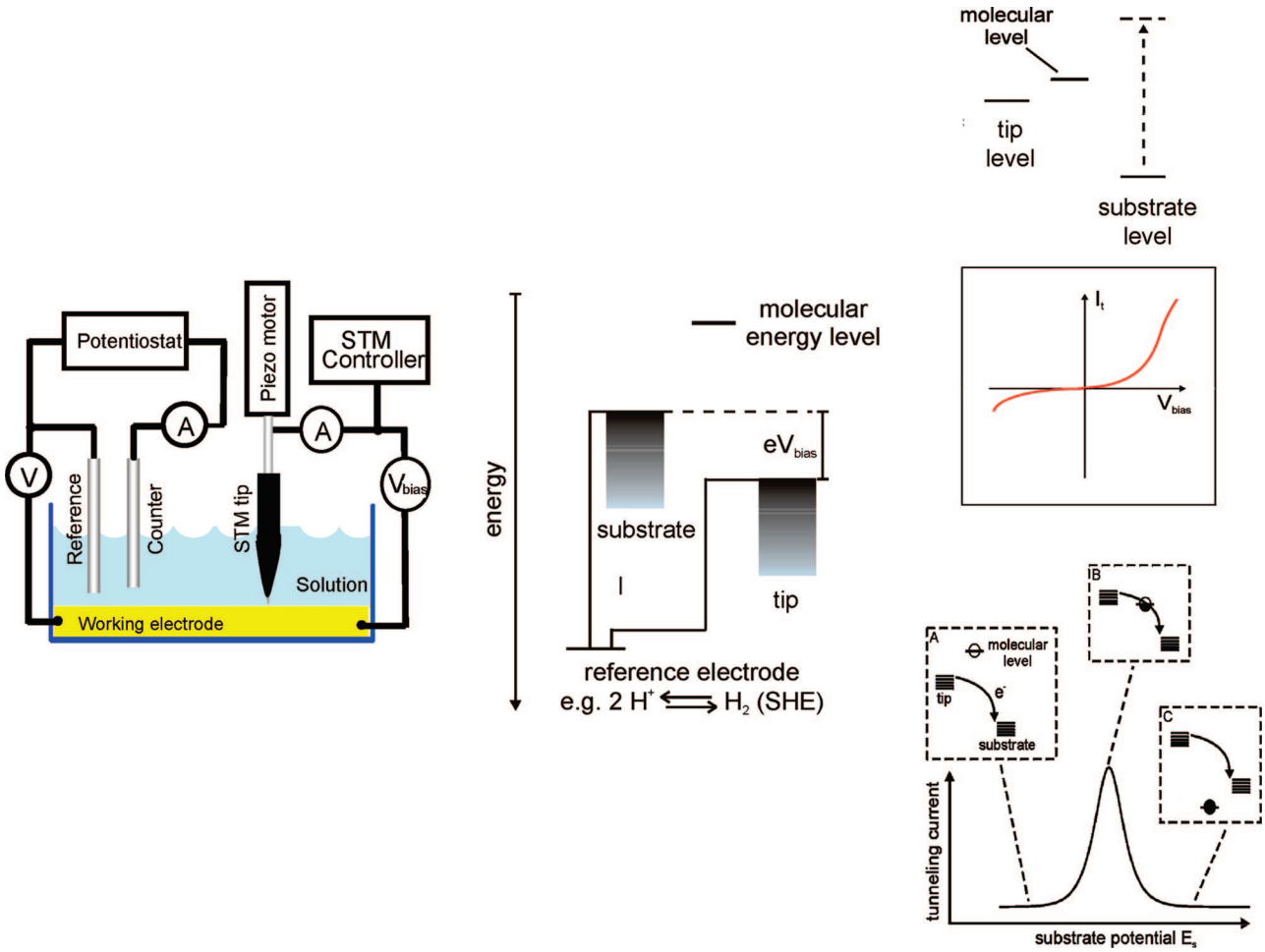

Figure 3. Left: Schematic view of in situ STM with independent electrochemical potential control of the substrate working electrode and the tip relative to a common reference electrode. Reprinted with permission from ref 37. Copyright 2001 American Chemical Society. Middle: Energy diagram of tip, substrate and redox level in the in situ STM configuration. Right: Energy diagram and expected schematic tunneling current dependence on the bias voltage at fixed overpotential and on the overpotential at fixed bias voltage, schematic. Further discussion in section 5.

be recorded, Figure 3. The difference from such correlations in two-terminal junctions is that the electrochemical overpotential is fixed and controls the charge state of the molecule. Alternatively, the tunneling current/overpotential correlation at fixed bias voltage, i.e., for parallel variation of the electrochemical substrate and tip potentials, can be recorded. This is equivalent to the current/gate voltage relation in solid state transistor-like junctions.

Electrochemical in situ STM was introduced by Kolb,[4,22] Siegenthaler,[21] Nichols,[23] and Itaya[188] and their associates in the late 1980s. Concepts and theoretical formalism of molecular ET behavior in electrochemical in situ STM were introduced in the early 1990s[34,169,170] and developed until presently[35–38,189] (section 3). Following a pioneering report on single-molecule electrochemical in situ STM current/overpotential correlation of Fe-protoporphyrin IX by Tao[83] with the first clear spectroscopic feature, later to be accommodated by theoretical notions,[35–37] this area has developed in parallel with accompanying theoretical notions.

2.4.3. Electrochemical Switching, Molecular Wiring, and Electronic Circuits

To put single-molecule electrochemistry into still another perspective, comparison with a class of electrochemically triggered monolayer systems with potential for reaching the molecular scale is appropriate. Transition metal complexes with large interlocked ligand systems or interlocked organic supramolecular structures are system classes where electronic structure changes induce drastic molecular conformational changes. "Bursts" of mechanical energy resembling that observed in the single-molecule AFM-based mechanical energy storage device, Figure 2, are induced by the altered subtle balance between noncovalent intramolecular interactions, coordinative and hydrogen bonding, and electrostatic forces caused by the external stimuli. There are many such molecular architectures that have led to replicas of electronically triggered "rotors", "gears", "paddle wheels", "tweezers", "harpoons", etc. now comprehensively reviewed.[157] The rotaxanes and catenanes are broadly studied classes where electrochemical redox stimuli trigger rotational and translational intramolecular conformational transitions. Catenane and rotaxane monolayers show different electronic (tunneling) conductivity in the different molecular charge states,[190–193] suggesting a molecular basis for electrochemically induced conductivity switching between conducting "on" and nonconducting "off" states. Due to the large configurational difference between the "on" and off" states, interconversion between the two states, is thermally activated and is therefore a slow process offering to the class properties possibly suitable for a molecular information storage principle. Rotaxanes and catenanes are further of interest because they are examples where attempts to incorporate molecular-

scale switching elements into larger electronically working structures such as logical gates and even "electronic circuits" have been reported[190–193] (see also report by Feringa and associates[194]).

The rotaxanes and catenanes offer at the same time an electrochemically controlled electronic and mechanical switch. Rotaxanes and catenanes have been characterized all the way from bulk solution via both three-electrode electrochemical and two-electrode monolayers in contact with solution or solid electrolyte media, to solid state three-electrode configurations. Most focus has been on monolayer on−off hysteretic electronic properties of "writing" and "reading" caused by thermally activated interconversion. Rotaxane junctions have been target molecules also in combinations into "logical circuits", at ultrasmall scales, although not to the level of the single molecule.[190]

The rotaxanes and catenanes have shown molecular-scale working principles but the low on−off current ratios and need for high voltages to induce the changes in the molecular charge states may constitute problems toward working devices. The amplification on−off ratios and the diode rectification ratios of the Os-complexes[84,85] in the electrochemically controlled three-electrode in situ STM configuration, section 5, thus exceed significantly most two-terminal rotaxane and catenane on−off ratios.[190] The use of three-terminal junctions, with an additional gate electrode as in electrochemical configurations, could improve this.

3. Theoretical Frames of Interfacial Electrochemical ET at Macroscopic and Molecular Scales

In this section we provide first a brief overview of some elements of the formal theory of interfacial electrochemical ET processes. Emphasis is on elements central for approaches to single-molecule electrochemical ET as encountered in electrochemical in situ STM and other nanogap electrode configurations. This will be followed by an overview of recent theoretical efforts in these areas of molecular-scale electrochemical ET. We shall use these concepts as a reference in the discussion of a variety of new nanoscale nonredox and redox molecular-scale electrochemical systems in sections 4.2 and 5, respectively. The theoretical frames offer clues also to macromolecular bioelectrochemistry which, however, poses other challenges detailed in sections 6 and 7. A comprehensive discussion of condensed matter ET systems in homogeneous solution and at electrochemical interfaces in general is obviously by far beyond the scope of this overview. As noted, our present focus is the combination of interfacial electrochemical ET processes with the nanoscale and single-molecule perspectives, such as encountered most clearly in electrochemical in situ STM and nanoelectrode configurations.

3.1. Elements of the Formal Theory of Interfacial Electrochemical ET

Following early reports by Hush,[195] Marcus,[196] and Gerischer,[197] the line of quantum mechanical theory of interfacial electrochemical ET processes that has continued until the present time started with nonadiabatic processes and the Fermi golden rule[198] subsequently generalized to adiabatic electrochemical ET.[199] For overviews of this early phase, see refs 195d,e and 200. Comprehensive overviews of the wealth of facets of the present status of theoretical ET science are also available.[138,139,164,195d,e,201–207] Such reviews are clearly not within the scope of the present report where focus is on new nanoscale and single-molecule aspects of interfacial electrochemical ET. The following recent notions in general theoretical interfacial ET science are, however, also central in relation to the nanoscale and single-molecule aspects and will be used below. These notions refer mostly to the electronic coupling between the target molecules and the electrochemical surface. We shall show in section 3.4 that the coupling features acquire a new importance in nanoscale double-contacts such as in situ STM and here even leads to interfacial ET phenomena with no immediate analogue in macroscopic electrochemistry.

The introduction of the Anderson model[208] was an important step in the description of the electronic coupling, bridging the gap between the nonadiabatic weak-coupling and adiabatic strong-coupling limits. Electrochemical Landau−Zener formalism is an alternative approach to this important issue.[209] Attention to the electronic density of states of the metal electrode is another issue relating to the electronic factor.[210] While of first immediate importance for the weak-coupling limit the density also determines crucially both electrochemical potential energy surfaces and the molecular conduction mechanisms in the strong-coupling adiabatic limit. The incorporation of electron correlation and spin effects are other important recent elements of interfacial electrochemical ET.[211] Electron tunneling through molecular barriers is finally a theoretical notion to which molecular detail can now be added[212,213] and is warranted by a wealth of experimental data, cf. discussion in sections 4.2–7 and reviews.[138,139,201–207]

3.1.1. Nonadiabatic Electrochemical ET Reactions

Most work on nonadiabatic electrochemical ET has used so-called spin-less models where the degeneracy of the electronic energy levels in the metal due to the electron spin was ignored. A similar approximation was used in reports on adiabatic electrochemical ET reactions[198,199,208,209] and in work on electron tunneling in electrochemical STM contacts[34,36,214–218] This model is reasonable for single-electrode outer-sphere ET reactions in the absence of a magnetic field and implies that the Coulomb repulsion between the electrons in the valence orbital of the redox group is infinitely large. Only single occupation of this orbital may therefore be taken into account. However, recent experimental studies of redox-mediated electron tunneling in the in situ STM configuration[83–86,121,125,219] and theoretical results based on the Anderson model beyond the spin-less approximation[220–222] has warranted analysis of the electron spin problem in electrochemical kinetics in detail. Such an approach was introduced in[223] where the electron spin effect was included from the very beginning.

The calculation of the probability (per unit time) of the transition of one electron from the metal to the reactant should take into account ET from different electronic energy levels, ε, in the metal. Every energy level in the metal may be occupied by two electrons with opposite spin. The probability of occupation is determined by the Fermi distribution function $f_L(\varepsilon)$. As for reacting molecular species the occupation of a one-electron energy level depends on the value of the repulsion energy U between two electrons with opposite spin. Depending on the properties of the reactants, the reaction may have one- or two-electron character. One-electron ET to a vacant energy level in the

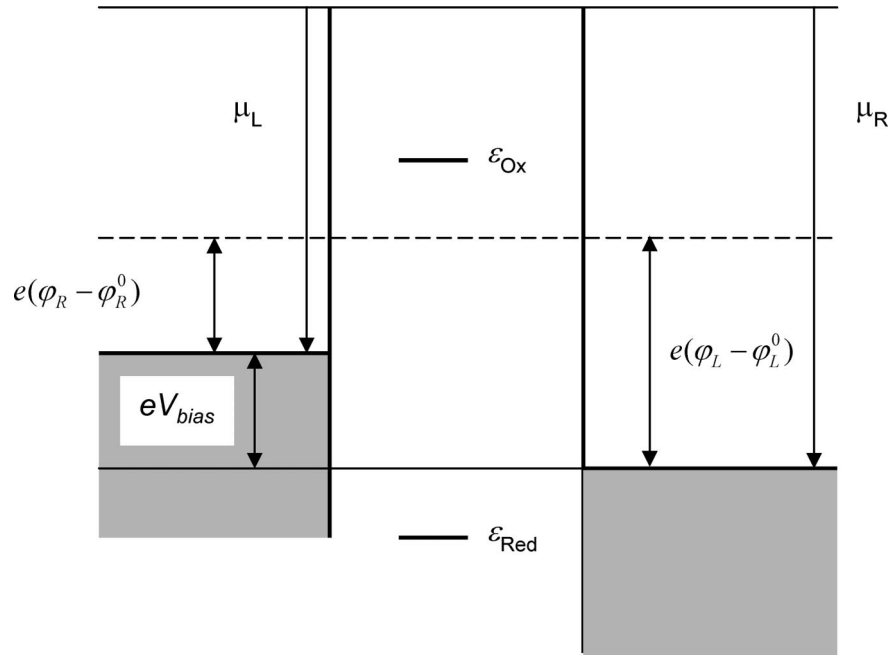

Figure 4. Energy diagram for tunneling through a redox molecule. The dashed line shows the position of the electrochemical potentials at equilibrium. The equilibrium potentials are defined by eqs 39 and 40, cf. also Figure 3.

reactant formally corresponds to a very large value of the repulsion energy U ($U \rightarrow \infty$). Two-ET reactions correspond to small values of U. However, unlike processes in vacuum or in nonpolar matrices, two-ET reactions in polar solvents usually proceed in two sequential steps due to strong interaction with the solvent polarization (phonons). The solvent reorganization free energy for the simultaneous transition of two electrons is four times the reorganization energy, E_{rL}, for the transition of a single electron (the subscript L (left) is used here since the substrate electrode will be considered as the left electrode in the STM systems discussed below while the right electrode (R) is represented by the STM tip (see Figure 4). Sequential one-electron transitions are therefore more probable than simultaneous transition of two electrons and only a single electron transferred in each step.

In one-ET reactions or in the first step of two-electron reactions, only one electron occupies the energy level in the reactant. This results in the following transition probabilities for the forward k_{LB} (from the electrode L to the reactant B) and reverse k_{BL} reactions

$$k_{LB} = 2k_L^0 \int \frac{d\varepsilon}{k_B T} f_L(\varepsilon) \exp\{-[E_{rL} - \Delta G_{BL} - (\varepsilon - \varepsilon_{FL})]^2/4E_{rL}k_B T\} \quad (1)$$

$$k_{LB} = 2k_L^0 \int \frac{d\varepsilon}{k_B T} [1 - f_L(\varepsilon)] \exp\{-[E_{rL} + \Delta G_{BL} + (\varepsilon - \varepsilon_{FL})]^2/4E_{rL}k_B T\} \quad (2)$$

ΔG_{BL} is the free energy of transition from the Fermi level of the metal ε_{FL} to the energy level in the reactant ε_B while k_B is Boltzmann's constant, and T the temperature. ΔG_{BL} is

$$\Delta G_{BL} = \varepsilon_{FL} - \varepsilon_B - \Delta G_{solv} - e\phi_L + e\psi \quad (3)$$

where ΔG_{solv} is the difference of the solvation free energies of the reduced and oxidized forms, φ_L the electrode potential with respect to the potential in the bulk solution (taken to be zero), and ψ the potential at the site of the reactant (the Frumkin correction).

The factor k_L^0 is[202]

$$k_L^0 = \frac{\omega_{eff}}{2\pi} 2\kappa_L \rho_L k_B T \exp(-\sigma) \quad (4)$$

where ω_{eff} is the effective frequency of the whole vibrational subsystem, $\rho_L$the density of electron states in the metal disregarding the spin degeneracy, κ_L the electronic transmission coefficient for single passage through the crossing of two diabatic free energy surfaces and the exponential represents the Franck - Condon factor for the high-frequency quantum degrees of freedom of the solvent and the reactant. The corresponding Franck - Condon factor for the classical degrees of freedom is represented by the exponentials under the integral signs in eqs 1 and 2. General expressions for the transition probability for arbitrary frequency spectrum of the vibrational subsystem can be found elsewhere.[202,203]

It follows from eqs 1 and 2 that the transition probabilities for forward and reverse reactions are related to each other by the principle of detailed balance

$$k_{BL} = k_{LB} \exp\left(-\frac{\Delta G_{BL}^{(2)}}{k_B T}\right) \quad (5)$$

where $\Delta G_{BL}^{(2)}$ is defined as

$$\Delta G_{BL}^{(2)} = \Delta G_{BL} + k_B T \ln 2 \quad (6)$$

This quantity differs from the free energy of the transition in the spin-less model by the last term which takes into account the degeneracy of the electronic energy levels in the metal. This term results in a shift (ca. $0.7 \times k_B T$) of the equilibrium potential φ_L^0 compared to the spin-less model. The equilibrium potential is defined by the equation

$$\Delta G_{BL}^{(2)} + k_B T \ln \frac{C_{Ox}}{C_{Red}} = \Delta G_{BL}^{(0)} + k_B T \ln 2 + k_B T \ln \frac{C_{Ox}}{C_{Red}} = 0 \quad (7)$$

where C_{Ox} and C_{Red} are the concentrations of the oxidized and reduced forms of the reacting species and the superscript (0) means that the electrical potential involved in the free energy is the equilibrium potential. In the following we consider the "cathodic" overpotential η

$$\eta = \phi_L^0 - \phi_L \quad (8)$$

In the general case eq 1 can be rewritten in the form

$$k_{LB} = 2k_L^0 \exp\{-[E_{rL} - \Delta G_{BL}]^2/4E_{rL}k_B T\} \times \int 2\frac{dx \exp[x(1 - \Delta G_{BL}/E_{rL} - k_B Tx/E_{rL})]}{1 + \exp(2x)} \quad (9)$$

The exponential factor in front of the integral in eq 9 represents the usual quadratic free energy form of the rate constant.[202,203] If the values of the reorganization energies in the integral terms are formally increased to infinity, eq 9 takes the well-known quadratic form

$$k_{LB} = 2\pi k_L^0 \exp\{-[E_{rL} - \Delta G_{BL}]^2/4E_{rL}k_B T\} \quad (10)$$

This equation includes the inverted free energy region at large overpotentials and bias voltages. However, the exact expressions have no inverted region because the integral factors suppress the increase of the activation free energies.[202,203]

At small overpotentials (compared to the reorganization free energy), the current (neglecting the Frumkin correction) is described by the Tafel equation where, however, the exchange current i_0 is $\sqrt{2}$ times larger than the exchange current in the spin-less model.[197–205] In the case of nonadiabatic reactions the effect of spin degeneracy thus reduces to a renormalization of the equilibrium potential and exchange current.

3.1.2. Adiabatic Electrochemical ET Reactions

Calculation of rate constants for adiabatic ET reactions is more complicated than for nonadiabatic reactions. Most attention has been given to the spin-less model for which relatively simple expressions can be obtained.[198,199,208,209,214–217] It was implicitly believed that the spin-less model is equivalent to the model with infinitely large Coulomb repulsion between the electrons on the same valence orbital of which a more detailed study has been reported.[223]

Due to strong electronic coupling of the reactant with the electrode in the adiabatic limit,[202,203] multiple electronic transitions take place during passage of the reactant electronic energy level through a region near the Fermi level of the electrode.[36,202,203,209,219–224] The electronic transmission coefficient in the rate constant is unity independent of the spin degeneracy. For example for k_{LB}

$$k_{LB} = \frac{\omega_{eff}}{2\pi} \exp(-G_a/k_B T) \quad (11)$$

where the activation Gibbs free energy G_a is determined by the form of the adiabatic Gibbs energy surface (AGES) $U_{ad}(q)$ where q is an effective dimensionless coordinate of the slow solvent subsystem. The strong interaction of the valence electrons of the redox group with the electrode along with the Coulomb repulsion energy U affects the shape of the AGES and, in turn, the values of ω_{eff} and G_a. The effect of U on the shape of the AGES, the Gibbs activation free energy G_a, as well as on ω_{eff} for finite values of U was studied in refs 209, 220–223, 225, and 226 within the framework of an exactly solvable model. It was found that the electron correlation effects are important and lead to a lowering of the activation Gibbs energies compared with AGES calculated within the Hartree−Fock approximation. In order to check the validity of the commonly used assumption that ω_{eff} and G_a obtained in the spin-less model do not differ from those obtained with large values of U it is sufficient to consider infinitely large U. The values of ω_{eff} in the wide-band approximation for the electronic structure of the electrode at $\eta = 0$ in the spin-less model[220]

$$\tau_L \omega_{eff} \approx \left(\frac{2E_{rL}}{\pi\Delta} - 1\right)^{1/2} \quad (12)$$

and in the limit $U \rightarrow \infty$

$$\tau_L \omega_{eff} \approx \left(\frac{E_{rL}}{\pi\Delta} - 1\right)^{1/2} \quad (13)$$

indeed only differ insignificantly (approximately by the factor $2^{1/2}$). Δ is here the width of the valence orbital and $\tau_L$the longitudinal relaxation time of the solvent.

However, the difference in G_a can be more pronounced. $U_{ad}(q)$ is given by refs 208, 220, 221, and 225

$$U_{ad}(q) = E(q) + E_r q^2 \quad (14)$$

where $E(q)$ is the energy of the electronic subsystem, and E_r the reorganization Gibbs energy, cf. eqs 1 and 2. The AGES for the spin-less model has been studied in detail.[208] An approximate solution for $E(q)$[228] for the mixed valence regime (see eq III.12 of ref [228]) was used for the calculation of AGES and G_a in the case when $U \rightarrow \infty$[220,223]

$$E(q) \approx \varepsilon_a(q)\, n_a(q) + \frac{(2j+1)\Delta}{2\pi} \ln\{\varepsilon_a^2(q) + [(2j+1)\Delta]^2\} \quad (15)$$

with

$$\varepsilon_a(q) = E_{rL} - 2E_{rL}q - e\eta \quad (16)$$

being the electron energy level in the redox group, and

$$n_a(q) = \frac{1}{2} - \frac{1}{\pi} \arctan \frac{\varepsilon_a(q)}{(2j+1)\Delta} \quad (17)$$

the occupation number of this energy level. j is the total angular momentum of the electronic state in the redox group. $j = 0$ for the spin-less model and $j = 1/2$ in the limit $U \rightarrow \infty$ so that the difference between these two cases reduces to renormalization of the parameter Δ. The activation Gibbs free energy is given then by

$$G_a = [(1 - n_t - e\eta)n_t - (1 - n_i - e\eta)n_i]E_r + \frac{(2j+1)\Delta}{2\pi} \ln \frac{(1 - 2n_t - e\eta)^2 + [(2j+1)\Delta/E_r]^2}{(1 - 2n_i - e\eta)^2 + [(2j+1)\Delta/E_r]^2} \quad (18)$$

n_t and n_i are the occupation numbers of the redox level in the transition and initial state, respectively. Equation 18 coincides with eq 18 of ref[208] only when $j = 0$ and $\eta = 0$. To compare the spin-less model and the limit $U \rightarrow \infty$, we consider the case when $\Delta = 4k_B T = 0.1$ eV, $E_r = 1$ eV, and $\eta = 0$. Equation 18 then yields $E_a = 5.9k_B T$ and $3.5k_B T$ for the spin-less model and the limit $U \rightarrow \infty$, respectively. The

ET rates can thus differ by an order of magnitude.

The analytical calculations of the adiabatic transitions usually reduce the problem to the calculation of a one-dimensional potential profile along a single reaction coordinate and subsequent calculation of the rate constant within the transition state method. The dynamics of the motion along this reaction coordinate is usually not considered. Stochastic motion along the reaction coordinate has been addressed by computer simulations. In one of the methods, random motion of the system along the adiabatic Gibbs energy surface was considered.[227] The system involved a single effective reactive mode interacting with the heat bath. Both subsystems were considered as particles and a stochastic collision model was used for the interaction between the systems.[229,230] The form of the system trajectories near the potential barrier top was studied and the transmission coefficient calculated. It was found that the higher the friction the larger is the probability of barrier recrossing, in qualitative accordance with the predictions of Kramers theory.

3.1.3. The Intermediate Region

Analytical theory has so far been elaborated only for the two limiting cases discussed. Attempts to construct an analytical theory in the region of intermediate electronic interaction between the reactant and the electrode have not been successful. Based on available methodology,[231,232] an "exact" method for the calculation of the electrochemical ET rate was suggested.[233,234] It was, however, recognized[235] that this method is exact only when a single electron is present so that the presence of the Fermi sea of the electrode is ignored. This method thus leads to correct results only in the nonadiabatic limit.

Increasing interest over the last few years was given to approximate descriptions that embrace the whole range of interactions. Such attempts[209] are usually based on two mutually exclusive approximations. On the one hand, the integration of the Franck−Condon factor over the electronic energy spectrum in the metal electrode is undertaken with due account of the Fermi distribution function. On the other hand, the electronic transmission coefficient is calculated by the Landau−Zener formula for two discrete energy levels (one for the initial state in the reactant molecule, the other one for an effective energy level of the metal for the final state).

A consistent numerical approach with multiple transitions between various energy levels in the metal and in the reactant along the motion on the reaction coordinate is available.[236] This system is characterized by a large number of Gibbs free energy surfaces for the initial and final states. Linear Gibbs free energy surfaces and a Monte Carlo method for the probabilities of transitions between the manifold of energy surfaces were considered.[225] This approach was generalized to parabolic surfaces and the dependence of the transition probability on the Landau−Zener parameter. Simple interpolation formulas for this dependence in the whole interval of the variation of the Landau−Zener parameter for variable overpotential were also considered.

3.2. Electrochemically Controlled Single-Electron Transitions

Intensive theoretical studies of single-electron transitions in the 1980s[237–240] and subsequent experimental investigations in solid-state contacts are now being extended to electrochemical systems.[241–246] The physical mechanism of these phenomena is rooted in the fact that when the size of the electron-donor and/or the electron-acceptor is small, the transition of an electron changes considerably the energetic conditions for the transition of a second electron. The transition free energy becomes unfavorable and the transition is blocked until either the electron leaves the acceptor (if this is an electrode) or the acceptor itself (if this is a molecule) diffuses into the bulk solution, enabling a new acceptor molecule to approach the electrode. The current would then fluctuate in time. The observation of such fluctuations is, however, a great challenge. A simpler system is represented by a metal electrode and solute coated metallic nanoparticles.[241–244] The transfer of an electron from the Fermi level of the electrode increases the electrostatic energy of the nanoparticle by $e^2/2C$ where e is the electronic charge and C the capacitance of the particle. The electrode potential must therefore be increased successively by e/C for the transition of each additional electron. Such Coulomb blockade effects are long known in electrode processes of multivalent reactants, e.g. $[Ru\text{-}(bpy)_3]^{3+/2+/1+/0}$ (bpy = 2,2′-bipyridine).[242] Steps in the current/voltage dependence appear when the electrode potential exceeds the value corresponding to the next oxidation (or reduction) stage. The difference is expressed by the following sequence of formal potential steps for successive charging $ze \rightarrow (z-1)e$

$$E^0_{zz-1} = E_{pzc} + \frac{(z-1/2)e}{C} \tag{19}$$

where E_{pzc} is the zero charge potential determined by the capacitance of the particle.[242] If the capacitance is independent of the charge state of the nanoparticle, the steps should be evenly spaced for monodisperse nanoparticles. This was observed experimentally[242–245] also at the level of the single (1.6 nm) nanoparticle in the in situ STM configuration.[246]

3.3. ET Concepts and Formalism at the Molecular Scale: Nonredox Molecules

Nanojunctions mediated by single molecules attract attention per se and for their potential future applications in nanoelectronics. In general these molecules are of a complex structure and involve various functional groups. The simplest case of a molecular scale junction is represented by a single stretched chain molecule consisting of identical molecular fragments without any redox groups. Three mechanisms of electron transport through such a molecule may be distinguished: (i) tunneling, (ii) superexchange, and (iii) hopping. In the first mechanism, the bridge molecule simply represents a barrier for ET which tunnels deep under the barrier. The term superexchange (for the second mechanism) also implies tunneling but in a system with vacant electronic energy levels higher than the energy of the tunneling electron (nonresonance tunneling), mediating virtually the ET process. Slow nuclear degrees of freedom do not follow these virtual transitions and stay tuned at their transition configuration matching the energy levels of the donor and acceptor states.

The hopping mechanism entails sequential ET between neighboring localization sites with full energy relaxation in each elementary act. In a polar environment, this mechanism is sometimes called the polaron mechanism, due to its resemblance to the electron transport in doped polar semiconductors or ET reactions in polar solvents. Unlike "real" redox hopping, the temporarily occupied electronic level(s) remains located far above the fermi levels of the electrodes.

This implies that the interaction with the environment is weak. The hopping mechanism for "real" redox molecules prevails when the energy levels lie near the Fermi level in the donor metal and the interaction with the medium is strong; occupation of these levels is then assisted by slow mode fluctuations. Superexchange corresponds to the opposite limit, when energy levels are well above the donor Fermi level and interactions with the medium are weak. Simple under-barrier tunneling prevails when these energy levels are located far above the Fermi energy of the donor with no virtual transitions contributing to the conductance.

Direct in situ tunneling systems were explored theoretically in refs 247–249. A main new element of the theory was the introduction of conformational fluctuations of the molecular fragments in an attempt to explain experimentally observed Arrhenius-type temperature dependence of the current.[249] Another important point was the incorporation of Debye screening of the electric potential in the tunneling gap. The incorporation of conformational fluctuations resulted in explicit dependence of the current on the characteristics of the random process and on the length of the molecule. In the high temperature limit for soft molecules, the current exhibits Arrhenius temperature dependence with an apparent activation energy that increases with the length of the molecule.[248] The current is practically independent of the temperature in the low temperature limit.

A new effect is caused by the Debye screening of the electrode potentials. Rectification of the current emerges when screening is strong even in intrinsically symmetric system.[247] Qualitatively similar results were obtained for the superexchange mechanism under the assumption that the electronic energy level of each molecular fragment is coupled with its own vibrational "gating" mode.[247,249]

The origin of the rectification is as follows. At Debye screening lengths shorter than the length of the bridge (i.e., for high electrolyte concentration), the potential variation affects mainly the bridge group energy levels (or the height of the potential barrier) adjacent to the electrodes. The levels (and the potential barrier) in the rest of the bridge remain unaffected. Consider, e.g., the potential of the substrate electrode fixed and the potential of the tip varying. The distance between most of the levels (the top of the barrier) of the bridge and the Fermi level (which mainly affect the current) then remains constant at positive bias, i.e. when the Fermi level of the left electrode is located higher than that of the right electrode, but decreases at negative bias. This effect can increase the current dramatically.

The hopping mechanism for in situ STM[207] and for ET in homogeneous solution has been addressed in a number of reports.[250–256] The in situ STM current/voltage dependence for the molecule itself (i.e., excluding the potential dependence of the rate constant for electron exchange between the edges of the molecule and the electrodes) is mainly Ohmic with the resistance roughly proportional to the length of the molecule.[207]

3.4. ET Concepts and Formalism at the Molecular Scale - Redox Molecules

In situ tunneling through redox molecules with low-lying accessible electronic levels inserted between the substrate and tip electrodes in electrochemical in situ STM or between a pair of electrochemical nanogap electrodes offer particular perspectives in molecular scale electronics. The redox level(s) can bring the molecule to display rectification, amplification, negative differential resistance, and other properties of possible importance in molecular scale electronics. In contrast to most reported cases of single-molecule electronics, the electrochemical bridge group tunneling contacts, moreover operate in condensed matter environment (as opposed to ultrahigh vacuum) and at room temperature (as opposed to cryogenic temperatures).

The system consists of two metal electrodes (left, L, and right, R) immersed into the electrolyte solution and a molecule with a redox group, B, confined in the gap between the electrodes, Figure 4. Two potential differences can be controlled independently: the bias voltage between the metals, V_{bias} and the potential of the left (φ_L) or right (φ_R) electrode with respect to the potential in the bulk of the solution (φ_s). The latter will be taken to be zero ($\varphi_s = 0$) throughout. Positive bias voltage will be specifically considered. Extension to negative bias voltages is straightforward.

The theory of these processes goes back to the first theoretical reports in the 1960s and 1970s on bridge-assisted ET in bulk polar media and at electrodes.[257–263] For reviews of later work in this large area, see for example refs 201–207. A crucial factor controlling these processes is strong interaction of the electron with the polar environment (phonons) and/or local vibrational modes. This interaction is decisive also in electron tunneling between two metals through a bridge molecular redox-group. The mere existence of two valence states of the redox group at fixed electric potential (a bistability property) is a result of strong interaction of this group with the vibrational subsystem. This was recognized in the early theoretical studies of electron tunneling through a single-molecule redox group[34,214] where one of the electron tunneling mechanisms was described, viz. stepwise sequential ET through a relaxed intermediate state when the coupling of the bridge group with both electrodes is weak (subsequently further elaborated[265]). The current was expressed through the rate constants (transition probabilities) for the individual ET steps, and the limit of diabatic ET (employing the Fermi golden rule[202,203]) and the high-temperature limit were in focus. The strong interaction of the redox group with the vibrational subsystem results in the appearance of the Franck−Condon factor in the transition probabilities. By its physical nature and methods of description, this phenomenon is not the prerogative solely of electrochemical systems but applies also to tunneling contacts in condensed matter of different nature, in particular solid state junctions. In fact essentially the same approach was used much later in theoretical analysis of stepwise sequential electron tunneling through solid state contacts in the low-temperature limit.[266] The notion of "Franck−Condon blockade" of the tunneling process invoked[266] is thus completely identical to the Franck−Condon factor in the much earlier reports. A similar mechanism, viz. inelastic electron tunneling accompanied by multiphonon excitation has also been addressed[217,268,269] and expansion in powers of the coupling constant characterizing the interaction of the electrons with phonons used. This representation is useful in the weak coupling limit when the oxidized state is the only state of the bridge group. The weak tunneling limit was subsequently also addressed in detail by Sumi,[218,267] who studied the dependence of the tunneling current on the bias voltage and suggested a method for estimation of the solvent reorganization free energy.

Experimental investigations of single-molecule electrochemical redox switches were initiated by Tao's report[83] that

disclosed tunneling current features of a single redox molecule (iron protoporphyrin IX) with a maximum in the apparent height vs overpotential dependence at the equilibrium potential. A theoretical explanation of these data was offered using concepts of resonant electron tunneling averaged over the distribution function of free phonons.[217] Electron tunneling through a single, i.e., the oxidized state of the redox group was thus considered, with emphasis on the inverted free energy region. Further studies[35] and later reports[36,119,134,216] have shown that the incorporation of both valence states is of principal importance in a full theoretical formalism for the dynamic nature of the process; see sections 3.5, 3.7, and 5.

A new mechanism of electron tunneling, even a new ET phenomenon, in the in situ bridge contacts when the interaction of the redox group with both metals is strong (the adiabatic limit), was reported early.[216,268] A "boost" of electrons, i.e., up to hundred(s) of electrons can then be transferred between the metals via the redox molecule in a single in situ STM event, while the bridge group redox level passes through the energy window between the Fermi levels of the metals. This ET mechanism was fully rationalized[35] and subsequently experimentally substantiated, cf. section 5.

One of the most important theoretical outcomes was the prediction of a maximum in the tunneling current/overpotential dependence near the equilibrium potential of the redox group at fixed bias voltage.[35] This expectation has been supported by recent experimental studies,[87,89,91,121,124,219,269,270] discussed in section 5. Not only the maximum itself has been clearly observed but the dependence of the maximum current and the position of the maximum on the bias voltage has also been studied[35,125,269] and analyzed.[269,271] The application of the theory to new experimental data also disclosed a need to include other features in a more detailed analysis. In particular, the Debye screening of the electric potential in the tunneling gap has to be considered. As shown,[247,249,271,272] this is likely to disclose a number of new effects, cf. section 3.3. Particularly, a transparent analytical theory was developed for the limits of weak and strong electronic coupling between the bridge molecule and the electrodes. The theoretical description of intermediate interactions must, however, be approached by computer simulation methods as noted, section 3.1.3. We therefore start from the limit of weak electronic coupling of the redox molecule with the metals.

3.4.1. Totally Nonadiabatic Transitions

We consider first the case where the interaction of the redox group with both metals is weak, corresponding to totally nonadiabatic electronic transitions. The electron tunneling mechanism in this case is of a stepwise character. We start from the state where the redox group is, e.g., in the oxidized state. ET from the left metal to the redox group B, i.e., reduction of the redox group, is then the first step. In the high-temperature limit the thermal fluctuations of the molecular environment are crucial and take the electronic energy level ε_B toward the Fermi level of the left metal ε_{FL}. Following the first ET step, the molecular level relaxes fully to a new position below the Fermi level of the right metal ε_{FR}. However, at room temperature, due to renewed thermal fluctuations of the molecular environment the occupied electronic energy level will approach resonance with unoccupied energy levels of the right metal. ET to these levels will then reoxidize the redox group completing the ET cycle with overall ET from the left to the right metal (Figure 4)

The electric current through the contact following this mechanism can be given as[35,218]

$$j = e\frac{k_{LB}k_{BR} - k_{BL}k_{RB}}{k_{LB} + k_{BL} + k_{RB} + k_{BR}} \tag{20}$$

where k_{LB} and k_{BR} are the rate constants for ET from the left metal to the redox group and from the redox group to the right metal, respectively. k_{BL} and k_{RB} are the rate constants for the reverse transitions. The method of kinetic equations which leads in fact to the same equation has also been used later.[266,272–276]

The equation for ET to the right electrode analogous to eq 5 takes the form

$$k_{RB} = 2k_{BR}\exp\left(-\frac{\Delta G_{RB}}{k_B T}\right) \tag{21}$$

where ΔG_{RB} is the reaction free energies of the electronic transition from the Fermi level of the right metal (STM tip) ε_{FR} to the redox group with spin degeneracy disregarded and

$$k_{BR} = 2k_R^0\int \frac{d\varepsilon}{k_B T}[1 - f_R(\varepsilon)]\exp\{-[E_{rR} - eV_{bias} + \Delta G_{BL} + (\varepsilon - \varepsilon_{FR})]^2/4E_{rR}k_B T\} \tag{22}$$

with V_{bias} being the bias voltage, i.e. the difference of electrochemical potentials of the two metals, eq 22 also can be rewritten in the form

$$k_{BR} = k_R^0\exp\{-[E_{rR} - eV_{bias} + \Delta G_{BL}]^2/4E_{rR}k_B T\}\times \int \frac{dx\exp\{x[1 - (\Delta G_{BL} - eV_{bias})/E_{rR} - k_B Tx/E_{rR})]\}}{1 + \exp(2x)} \tag{23}$$

The reaction free energies are related to each other as

$$\Delta G_{RB} = eV_{bias} - \Delta G_{BL} \tag{24}$$

Using eqs 21 and 24, the expression for the current can be transformed to[38]

$$j_{nad} = e\left[2k_{LB}k_{BR}\sinh\frac{eV_{bias}}{2k_B T}\right]\Bigg/\left\{k_{LB}\left[\exp\left(\frac{eV_{bias}}{2k_B T}\right) + \exp\left(\frac{eV_{bias}/2 - \Delta G_{BL}^{(2)}}{k_B T}\right)\right] + k_{BR}\left[\exp\left(\frac{eV_{bias}}{2k_B T}\right) + \exp\left(-\frac{eV_{bias}/2 - \Delta G_{BL}^{(2)}}{k_B T}\right)\right]\right\} \tag{25}$$

where $\Delta G_{BL}^{(2)} = \Delta G_{BL>} + k_B T\ln 2$.

The reaction free energy ΔG_{BL} depends on the electrode potentials

$$\Delta G_{BL} = \varepsilon_{FL} - \varepsilon_B - \Delta G_{solv} - e[\phi_L - \phi_s] + e[\psi(z;\phi_L - \phi_L^{pzc}, \phi_R - \phi_R^{pzc}) - \phi_s] \tag{26}$$

where the Fermi levels $\varepsilon_{FL}$and ε_{FR} are counted from the energies $-e\varphi_L$ and $-e\varphi_R$ (φ_L and φ_R are the Galvani potentials of the left and right electrodes respectively), ε_B is the electronic energy in the bridge group counted from the energy $-e\varphi_s$, where φ_s is the potential in the bulk of the solution. As noted, we shall take the potential φ_s to be zero throughout. ΔG_{solv} is the difference of the solvation free energies of the redox group in the reduced and oxidized states

and $\psi(z;\varphi_L - \varphi_L^{pzc}, \varphi_R - \varphi_R^{pzc})$ the potential at the site of the redox group. This potential depends on the Galvani potentials φ_L and φ_R and on the potentials of zero charge φ_L^{pzc} and φ_R^{pzc} of the corresponding electrodes.

As seen from eq 26, the behavior of the current depends on the potential distribution in the tunneling gap. Analysis of the equations shows that the current as a function of the electrode potential at fixed bias voltage V_{bias} has a maximum close to the equilibrium potential. Approximate expressions describing the current in the neighborhood of the maximum can be derived using approximate expressions for the rate constants which emerge from eqs 1 and 22 at small absolute reaction free energy values of the transitions

$$k_{LB} \approx 2\pi k_L^0 \exp(-E_{rL}/4k_BT) \exp(\Delta G_{BL}/2k_BT)$$
$$k_{BR} \approx \pi k_R^0 \exp(-E_{rR}/4k_BT) \exp[(eV_{bias} - \Delta G_{BL})/2k_BT] \quad (27)$$

where E_{rL} and E_{rR} are the reorganization free energies of the molecular environment and

$$k_R^0 = 2\frac{\omega_{eff}}{2\pi}\kappa_R\rho_R k_BT \quad (28)$$

The factor π appears from the integration over the electronic energy spectrum. Equation 27 is valid when the absolute values of the reaction free energies are much smaller than reorganization energies. The approximate expression for the electric current obtained with the use of eqs 27 and 28 then takes the form

$$j_{nad} = j_0\left[\sinh\frac{eV_{bias}}{2k_BT}\right]\Bigg/\left\{\exp\left(\frac{eV_{bias}}{4k_BT}\right)\times \cosh\left[\frac{eV_{bias}/2 - \Delta G_{BL}^{(2)}}{2k_BT} - a\right] + \exp\left(-\frac{eV_{bias}}{4k_BT}\right)\cosh\left[\frac{eV_{bias}/2 - \Delta G_{BL}^{(2)}}{2k_BT} + a\right]\right\} \quad (29)$$

where

$$j_0 = 4e\frac{\omega}{2\pi}\sqrt{2\kappa_L\rho_L\kappa_R\rho_R}k_BT\exp(-\bar{E}_r/4k_BT) \quad (30)$$

$$a = \ln\left\{\sqrt{\frac{\kappa_L\rho_L}{\kappa_R\rho_R}}\exp\left[\frac{E_{rR} - E_{rL}}{8k_BT}\right]\right\} \quad (31)$$

$$\bar{E}_r = \frac{1}{2}(E_{rL} + E_{rR}) \quad (32)$$

For a symmetric contact ($\kappa_L = \kappa_R = \kappa$; $E_{rR} = E_{rL} = E_r$; $\rho_L = \rho_R = \rho$) $a = 0$ and thus

$$j_{nad} = e\frac{\omega_{eff}}{2\pi}2\sqrt{2}\pi\kappa\rho k_BT \times \exp(-E_r/4k_BT)\frac{\sinh\dfrac{eV_{bias}}{4k_BT}}{\cosh\dfrac{eV_{bias}/2 - \Delta G_{BL}^{(2)}}{2k_BT}} \quad (33)$$

The expression for the tunneling current in the general case is formally identical to eq 29 but with different values for the parameters j_0 and a:

$$j_0 = e\frac{\omega_{eff}}{2\pi}2\pi\sqrt{2\kappa_L\rho_L\kappa_R\rho_R I_L I_R}k_BT\exp(-\bar{E}_r/4k_BT) \times \exp\{-(\Delta G_{LB}^{(2)} - k_BT\ln 2)^2/(8k_BTE_{rL}) - (eV_{bias} - \Delta G_{LB}^{(2)} + k_BT\ln 2)^2/(8k_BTE_{rR})\} \quad (34)$$

$$a = \ln\left\{\sqrt{\frac{\kappa_L\rho_L I_L}{\kappa_R\rho_R I_R}}\exp\left[\frac{E_{rR} - E_{rL}}{8k_BT}\right]\right\} - \frac{(\Delta G_{LB}^{(2)} - k_BT\ln 2)^2}{8E_{rL}k_BT} + \frac{(eV_{bias} - \Delta G_{LB}^{(2)} + k_BT\ln 2)^2}{8E_{rR}k_BT} \quad (35)$$

where I_L and I_R are the integrals on the right-hand-side of eqs 9 and 23. Equations 29 and 33 are still rather complex since the dependence of the reaction free energy of transition $\Delta G_{BL}^{(2)}$ on the electrode potentials in general may be complicated. The parameter a also in general depends on the bias voltage. The relation of $\Delta G_{BL}^{(2)}$to the electric potentials is discussed in the next subsection.

In the limit $\Delta G_{BL} \gg E_{rL}$ and $eV_{bias} - \Delta G_{BL} \gg E_{rR}$ the integrals I_L and I_R behave as

$$I_L \approx \left(\frac{\pi E_{rL}}{k_BT}\right)^{1/2}\exp\{[E_{rL} - \Delta G_{BL}]^2/4E_{rL}k_BT\} \quad (36)$$

$$I_R \approx \left(\frac{\pi E_{rR}}{k_BT}\right)^{1/2}\exp\{[E_{rR} - eV_{bias} + \Delta G_{BL}]^2/4E_{rR}k_BT\} \quad (37)$$

It then follows from eqs 9 and 23–25 that for the symmetric contact and positive bias voltage

$$j_{n.ad.} = e\left[4k^0(\pi E_r/k_BT)^{1/2}sh\frac{eV_{bias}}{2k_BT}\right]\Bigg/\left\{2\left[\exp\left(\frac{eV_{bias}}{2k_BT}\right) + \exp\left(\frac{eV_{bias}/2 - \Delta G_{BL}^{(2)}}{k_BT}\right)\right] + \exp\left(\frac{eV_{bias}}{2k_BT}\right) + \exp\left(-\frac{eV_{bias}/2 - \Delta G_{BL}^{(2)}}{k_BT}\right)\right\} \quad (38)$$

3.4.2. Reaction Free Energy of the Transition and the Electrode Potentials

The general relationship between the reaction free energy of the transition and the electrode potential is given by eq 26. It is convenient to introduce the "equilibrium" potentials φ_L^0 and φ_R^0 determined by the condition that the currents through each electrode and the reaction free energies of the transition $\Delta G_{BL}^{(2)}$ and $\Delta G_{RB}^{(2)}$ vanish at zero bias voltage.[35,36] This gives

$$e\phi_L^0 - e\psi^0(z;\phi_L^0 - \phi_L^{pzc}, \phi_R^0 - \phi_R^{pzc}) - e\varphi_L^0 = 0 \quad (39)$$

$$e\phi_R^0 - e\psi^0(z;\phi_L^0 - \phi_L^{pzc}, \phi_R^0 - \phi_R^{pzc}) - e\varphi_R^0 = 0 \quad (40)$$

where the standard redox-potentials are

$$e\varphi_L^0 = \varepsilon_{FL} - \varepsilon_B - \Delta F_{solv} + k_BT\ln 2; \quad e\varphi_R^0 = \varepsilon_{FR} - \varepsilon_B - \Delta F_{solv} + k_BT\ln 2 \quad (41)$$

The last terms on the rhs of eq 41 take into account the spin degeneracy of the Fermi levels in the metals. Equations 39 and 40 give the following equation for determination of the "equilibrium" potential φ_L^0

$$\phi_L^0 - \psi^0(z;\phi_L^0 - \phi_L^{pzc}, \varphi_R^0 - \varphi_R^{pzc} + \phi_L^0 - \varphi_L^0) = \varphi_L^0 \quad (42)$$

As seen from eq 42, φ_L^0 does not in general coincide with the standard redox potential and differs from the latter by

the potential at the site of the redox group ψ^0. We also introduce the "cathodic" overpotential

$$\eta = \phi_L^0 - \phi_L \tag{43}$$

Positive values of η mean that the potential of the left electrode is lower than the corresponding "equilibrium" potential, taking into account the relationship between the bias voltage and the electrode potentials..[247]

Using

$$V_{bias} = \phi_R - \phi_R^0 - (\phi_L - \phi_L^0) \tag{44}$$

we obtain for the reaction free energy[202]

$$\Delta G_{BL}^{(2)} = e\{\eta + \psi(z;\phi_L^0 - \phi_L^{pzc} - \eta;\phi_R - \phi_R^{pzc}) - \psi^0(z;\phi_L^0 - \phi_L^{pzc};\phi_R^0 - \phi_R^{pzc})\} \tag{45}$$

The quantities ψ and ψ^0 as well as the "equilibrium" potentials φ_L^0 and φ_R^0 should be calculated as the solution of the corresponding electrostatic problem. At small values of V_{bias} and η eq 45 can be recast approximately as

$$\Delta G_{BL}^{(2)} \approx e(\xi\eta + \gamma V_{bias}) \tag{46}$$

where

$$\gamma(z) = \left.\frac{\partial\psi}{\partial\phi_R}\right|_{\phi_R=\phi_R^0}; \quad \xi(z) = 1 - \left.\frac{\partial\psi}{\partial\phi_L}\right|_{\phi_L=\phi_L^0} - \gamma(z) \tag{47}$$

Equations 46 and 47 are exact only when the response of the double layer to the electrode potentials is linear.

We consider a narrow tunneling gap with a small redox group the effect of which itself on the potential distribution may be neglected. The Poisson - Boltzmann equation is nonlinear when the potential exceeds k_BT/e. A number of other effects such as dielectric saturation and spatial dispersion of the dielectric properties of the solvent, ion transfer from the bulk of the solution, "lattice saturation" effects etc. could also be important.[277] However, as shown,[277] most of these effects compensate almost completely each other in a narrow gap. The potential distribution is therefore very close to that obtained as the solution of the linearized Poisson−Boltzmann equation. The solution has the following form for a system with planar geometry[277]

$$\psi(z;\phi_L;\phi_R) = \gamma(L - z;L_d)(\phi_L - \phi_L^{pzc}) + \gamma(z;L_d)(\phi_R - \phi_R^{pzc}) \tag{48}$$

where L is the width of the tunneling gap, L_d the Debye length, and

$$\gamma(z;L_d) = \frac{\exp(z/L_d) - \exp(-z/L_d)}{\exp(L/L_d) - \exp(-L/L_d)} \tag{49}$$

We obtain for ξ and γ in eq 47

$$\xi(z) = 1 - \gamma(L - z, L_d) - \gamma(z, L_d); \quad \gamma(z) = \gamma(z, L_d) \tag{50}$$

In this case the relationship between ϕ_L^0 and the standard potentials φ_L^0 and φ_R^0 can be derived

$$\phi_L^0 = \{[1 - \gamma(z)]\varphi_L^0 + \gamma(z)\varphi_R^0 - \gamma(L - z)\phi_L^{pzc} - \gamma(z)\phi_R^{pzc}\}/\xi(z) \tag{51}$$

Equations 50 and 29 give a simple approximate current expression for $eV_{bias} < E_r$

$$j_{nad} = j_0 \sinh\frac{eV_{bias}}{2k_BT}\left\{\exp\left(\frac{eV_{bias}}{4k_BT}\right) \times \cosh\left[\frac{e(0.5 - \gamma)V_{bias} - e\xi\eta}{2k_BT} - a\right] + \exp\left(-\frac{eV_{bias}}{4k_BT}\right) \times \cosh\left[\frac{e(0.5 - \gamma)V_{bias} - e\xi\eta}{2k_BT} + a\right]\right\}^{-1} \tag{52}$$

a and j_0 are given by eqs 30–32. The factor a describes possible asymmetry of the contact due to nonsymmetric location of the redox group and different electronic interactions of the redox group with the electrodes. This equation is formally exact if eqs 34 and 35 are used.

The current as a function of overpotential η has a maximum at $\eta = \eta_{max}$. η_{max} depends on the bias voltage and tends to $\eta_{max} = 0$ when $V_{bias} \to 0$. The dependence of η_{max} on V_{bias} can be recast in parametric form as follows:

$$\frac{e\xi\eta_{max}}{2k_BT} = \left(\frac{1}{2} - \gamma\right)\ln\frac{\sinh(a + u)}{\sinh(a - u)} - u; \quad \frac{eV_{bias}}{2k_BT} = \ln\frac{\sinh(a + u)}{\sinh(a - u)}, \quad a \neq 0 \tag{53}$$

where the running variable u varies within the interval $|u| \leq |a|$. The dependence of η_{max} on V_{bias} can be found in the explicit form for large $|V_{bias}|$ ($E_r > |V_{bias}| \gg k_BT$)

$$\frac{e\xi\eta_{max}}{2k_BT} = \left(\frac{1}{2} - \gamma\right)\frac{eV_{bias}}{2k_BT} \mp a \tag{54}$$

where + and − correspond to negative and positive values of V_{bias}, respectively. Equation 54 holds also in the case when $a = 0$. In this case it takes the form $\eta_V = 0$ where

$$\eta_V = \xi\eta_{max} + (\gamma - 1/2)V_{bias} \tag{55}$$

According to eq 54, the slope of the line η_{max} (V_{bias}) is

$$S(z, L_d) = \frac{1 - 2\gamma(z, L_d)}{2[1 - \gamma(L - z, L_d) - \gamma(z, L_d)]} \tag{56}$$

If the redox group is located symmetrically in the tunneling gap ($z = 1/2$), then $\gamma(z,L_d) = \gamma(L - z,L_d)$. The slope is therefore $S = 1/2$ and independent of the Debye length. The quantity $|a|$ in this case is small or zero.

The width of the maximum (at half-height) is

$$\frac{\Delta_\eta}{k_BT} = \frac{4\ \text{arccosh}\ 2}{1 - \gamma(L - z, L_d) - \gamma(z, L_d)} \tag{57}$$

Unlike the slope, Δ_η depends on the Debye length even for a symmetric contact. It should be noted, however, that Δ_η is independent of E_r and V_{bias} in the weak coupling limit for $eV_{bias} < E_r$. It is shown below that the width can be rather large depending on the value of L_d.

When $eV_{bias} > E_r$ and η_V= const, it follows from eq 38 that the tunnel current goes to a constant value. When η_V is of the order of $V_{bias}/2$, eq 36 can be used for I_L and eq 21 for k_{RB}. It can be shown that the width $\Delta_\eta \approx V_{bias}$ in this case.

The general equations allow calculating the current in the nonadiabatic limit in the whole range of the bias voltage and overpotential, Figures 5 and 6. Figure 5 shows the dependence of the current (normalized to $j_{norm} = ek^0(\pi E_r/2k_BT)^{1/2}$ at large bias voltage) on the bias voltage for a nonadiabatic process calculated with the use of eqs 1, 20–23, 25, 34, 35, and 54 and of the approximate eqs 29–32. The

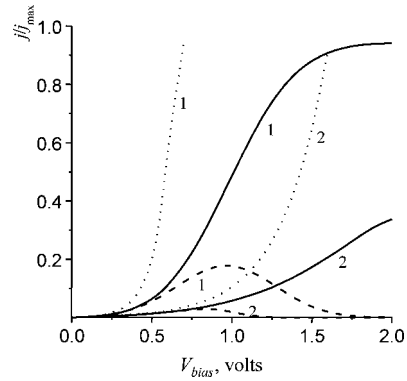

Figure 5. Dependence of the tunneling current through a redox molecule on the bias voltage at $\eta = 0$: 1. $L_d/L = 1.5$; 2. $L_d/L = 0.3$. The solid curves are calculated according to the exact equations, (1), (20–22), (25), (34), and (35), the dotted curves with the use of eqs 30–32 and 52, and the dashed curves by eqs 10, 20, and 21 and similar equations for k_{BR}. $z/L = 0.5$.

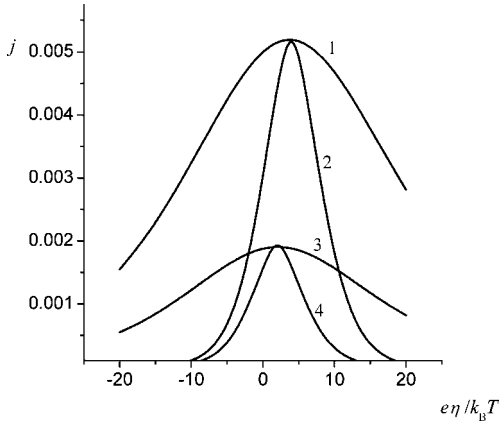

Figure 6. Dependence of the tunneling current on the overpotential. The current is normalized to $k^0\sqrt{4\pi E_r}$ (see text), $E_r = 0.5$ eV; $z/L = 0.5$. 1: $eV_{bias} = 0.2$ eV; $L_d/L = 0.8$; 2: 0.2 eV; 0.3; 3: 0.1 eV; 0.8; 4: 0.1 eV; 0.3.

correlations calculated with the use of the simple quadratic ("Marcus-type") expression for the rate constants of the type of eq 10 are also shown. The comparison shows that the simple approximate equation (dotted curves) works well for $eV_{bias} < E_r$ as expected. The dependences based on the quadratic rate constant expressions (dashed curves) extend to a slightly wider region. However, they also deviate strongly from the exact solution (solid curves) at large bias voltage, showing a maximum and subsequent fast decay. The exact current/voltage curve reaches instead a plateau rather rapidly at large L_d/L whereas the current dependence on the bias voltage is much weaker at small L_d/L values. The latter is due to strong screening of the potential by the electrolyte, resulting in small values of γ (e.g., $\gamma = 0.47$ and 0.2 for $L_d/L = 1.5$ and 0.3, respectively) and therefore, in a weak dependence of the electronic energy level of the redox group on V_{bias}.

Figure 6 shows the dependence of the current (normalized to $k^0\sqrt{4\pi E_r}$ where $k^0 = k_L^0 = k_R^0$ and $E_r = E_{rL} = E_{rR}$) on the overpotential calculated with the use of the exact equations. It is seen that the current passes a maximum near the equilibrium potential. The maximum is narrower when the screening is stronger. A more detailed analysis of the current behavior in the neighborhood of the maximum can be performed with the use of the approximate equations obtained within linear electrostatics (eqs 54–57). These involve the overpotential and bias voltage in the combination $\eta_v = \xi\eta + (\gamma - 0.5)V_{bias}$, where the quantities ξ and γ depend both on the position of the redox group z and on the Debye length L_d (eq 49). Typical $\xi(z)$ and $\gamma(z)$ curves are shown in Figure 7A. The quantity γ quantifies the effect of variation of the potential of the right electrode on the potential at the site of the bridge group and therefore increases monotonously with increasing z. The quantity ξ quantifies the effect of variation of the potentials of both electrodes and therefore passes through a maximum. Typical dependences of the position of the maximum of the tunneling current on the bias voltage are shown in Figure 7B. All curves cross at the point $\eta_{max} = 0$, $V_{bias} = 0$. The slope is well described by the approximate eq 56 at small a values whereas it reaches a limiting value at larger bias voltages when a is large.

The dependence of the slope on the position of the redox group is shown in Figure 8A. The slope is close to 1/2 for small values of the Debye length (strong screening) and practically independent of the position of the redox group within the interval between $0.3L$ and $0.7L$. The dependence is stronger at larger values of the Debye length. The slope is also larger if the redox group is located closer to the left electrode. This asymmetry is caused by the choice of the

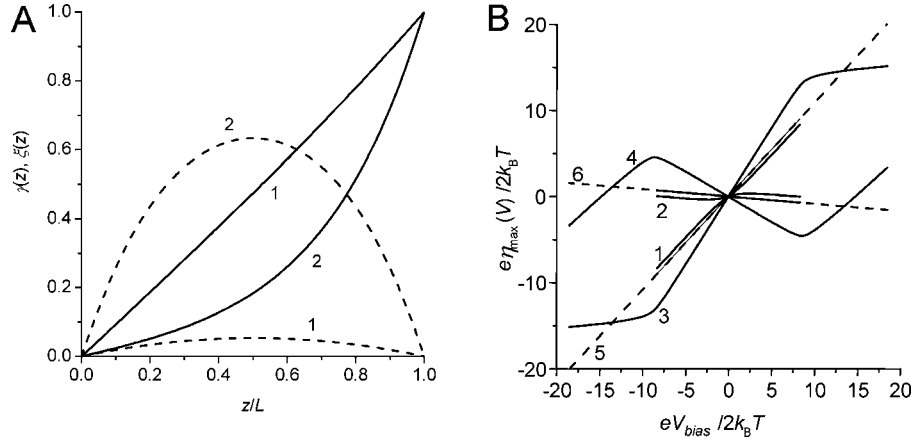

Figure 7. (A) Dependence of the coefficients $\gamma(z)$ (solid lines) and $\xi(z)$ (dashed lines) on the position of the redox group in the tunneling gap at different values of the Debye length L_d.1: $L_d/L = 1.5$, 2: $L_d/L = 0.3$. (B) Dependence of the position of the maximum of the tunneling current/overpotential relation on the bias voltage at different positions of the redox group z and the parameter a calculated according to eq 53 (solid lines). Dashed lines calculated according to eq 54 at corresponding positions of the redox group and $a = 0$. $L_d/L = 0.5$. (1) $z/L = 0.3$, $a = 0.2$; (2) $z/L = 0.7$, $a = -0.2$; (3) $z/L = 0.3$, $a = 5$; (4) $z/L = 0.7$, $a = -5$.

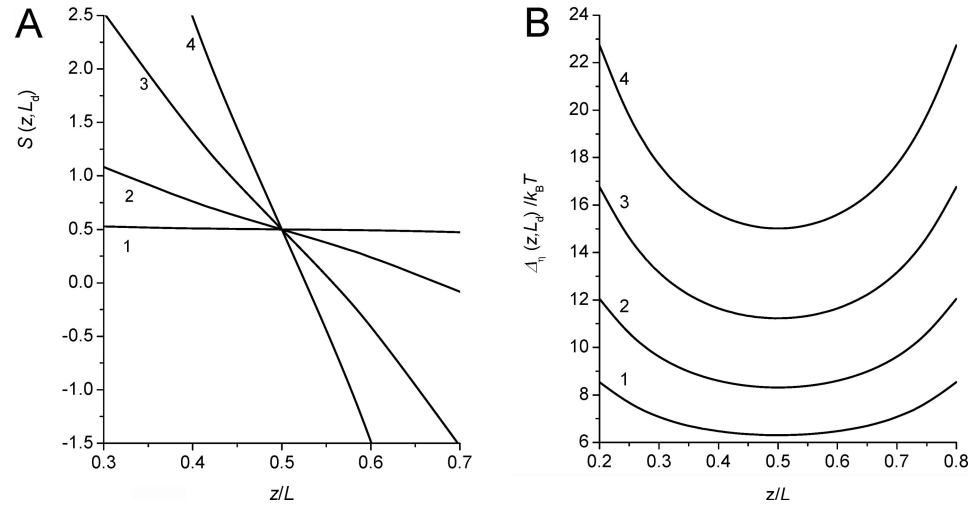

Figure 8. (A) Dependence of the slope of the line η_{max} (V_{bias}) on the position of the redox group at different values of the Debye length. $L_d/L = 0.1$ (1); 0.5 (2); 1 (3); 1.5 (4). (B) Dependence of the width of the tunneling current/overpotential maximum on the position of the redox group at different values of the Debye length. $L_d/L = 0.2$ (1); 0.3 (2); 0.4 (3); 0.5 (4).

left electrode as the substrate (with corresponding consequences for the potential variations).

The slope depends on two quantities, $\gamma(z; L_d)$ and $\gamma(L - z; L_d)$, eq 56. In order to determine these separately from experimental data we need an additional relationship, determined by the width of the maximum Δ_η, eq 57, Figure 8B. As seen from Figure 8B, the width increases with increasing Debye length. Within the approximations used the width is independent of the bias voltage and determined by the same quantities as the slope. The use of experimental data for the slope and the width of the maximum therefore allows determining $\gamma(z; L_d)$ and $\gamma(L - z; L_d)$

$$\gamma(z, L_d) = \frac{1}{2} - \frac{4S}{\Delta_\eta} \operatorname{arccosh} 2; \quad \gamma(L - z, L_d) = 1 - \frac{1}{2S} - \left(1 - \frac{1}{S}\right)\gamma(z, L_d) \quad (58)$$

The use of the $\gamma(z; L_d)$ and $\gamma(L - z; L_d)$ dependence on z and L_d (eq 49) allows in turn in principle estimating the position of the redox group in the tunneling gap.

3.4.3. The Strong-Coupling Limit and Coherent Transitions in Electrochemical in Situ STM

When the interaction of the redox group with both metals is strong the mechanism of the electronic transition changes its character entirely. A "boost" of a large number of electrons n now tunnel through the energy level of the redox group as it relaxes through the energy window between the Fermi levels of two metals at each reaction step (reduction and oxidation), cf. above and refs 216, 268, 269, and 278. The exact expression for the current can be obtained by averaging the partial tunneling current (at a given position of electronic energy of the redox group) over the thermal distribution of the vibrational coordinates in the adiabatic double-well potential.[273] The derivation is based on the Born - Oppenheimer scheme: a partial tunneling current, $j(q_k)$ at fixed position q_k of the nuclei constituting the slow vibrational subsystem may first be calculated. This current is then averaged over the distribution of the coordinates q_k in the potential formed by the adiabatic free energy surface $U_{ad.}(q_k)$[215,223,226,271,278]

$$U_{ad}(\{q_k\}) = E(\{q_k\}) + \frac{1}{2}\sum_k \hbar\omega_k q_k^2 \quad (59)$$

where $E(\{q_k\})$ is the ground-state energy of the electronic subsystem including the electrons of both electrodes and the electrons in the valence orbital of the bridge group.

The dependence of $E(\{q_k\})$ on the vibrational coordinates is due to the electronic energy level dependence in the redox group

$$\varepsilon_B(\{q_k\}) = \varepsilon_B - \sum_k \gamma_k q_k + e[\phi_L - \psi(z;\phi_L - \phi_L^{pzc};\phi_R - \phi_R^{pzc})] \quad (60)$$

where γ_k are the coupling constants and the energy level of the redox group is counted from the Fermi level of the left electrode.

Since eq 60 (and hence the energy $E(\{q_k\})$ involves the vibrational coordinates only in the combination $\sum_k \gamma_k q_k$, a single dimensionless coordinate may be introduced

$$q = \sum_k \gamma_k q_k / 2E_r; \quad E_r = \frac{1}{2}\sum_k \frac{\gamma_k^2}{\hbar\omega_k} \quad (61)$$

The averaging over the vibrational coordinates may be then reduced to[271]

$$j(\Delta_L, \Delta_R, \eta, V_{bias}) = \frac{\int_{-\infty}^{\infty} j(q, \Delta_L, \Delta_R, \eta, V_{bias}) \exp[-U_{ad}(q, \Delta_L, \Delta_R, \eta, V_{bias})/k_BT]\, dq}{\int_{-\infty}^{\infty} \exp[-U_{ad}(q, \Delta_L, \Delta_R, \eta, V_{bias})/k_BT]\, dq} \quad (62)$$

where for the spin-less model

$$U_{ad}(q, \Delta_L, \Delta_R, \eta, V_{bias}) = \varepsilon_B(q) n_L(q) + \frac{\Delta_L}{2\pi} \ln[\varepsilon_B^2(q) + \Delta^2] + [\varepsilon_B(q) + eV_{bias}] n_R(q) + \frac{\Delta_R}{2\pi} \ln\{[\varepsilon_B(q) + eV_{bias}]^2 + \Delta^2\} + E_r q^2 \quad (63)$$

$$j(q,\Delta_L,\Delta_R,\eta,V_{bias}) = \frac{2e\Delta_L\Delta_{tR}}{\pi\hbar\Delta}\left[\arctan\frac{eV_{bias}+\varepsilon_B(q,\eta,V_{bias})}{\Delta} - \arctan\frac{\varepsilon_B(q,\eta,V_{bias})}{\Delta}\right] \quad (64)$$

$$n_L(q) = \frac{\Delta_L}{\Delta}\left[\frac{1}{2} - \frac{1}{\pi}\arctan\frac{\varepsilon_B(q)}{\Delta}\right] \quad (65)$$

$$n_R(q) = \frac{\Delta_R}{\Delta}\left[\frac{1}{2} - \frac{1}{\pi}\arctan\frac{\varepsilon_B(q)+eV_{bias}}{\Delta}\right] \quad (66)$$

Δ_L and Δ_R are here the widths of the electronic energy level of the redox group due to the interaction with the corresponding electrode ($\Delta = \Delta_L + \Delta_R$) and

$$\varepsilon_B(q,\eta,V_{bias}) = E_r - 2E_rq - \xi e\eta - \gamma eV_{bias} = E_r - 2E_rq - e\eta_V - eV_{bias}/2 \quad (67)$$

It can be shown that if at $\Delta_R = \Delta/2$ and $\eta_V = 0$ the AGES has two potential wells then their depths are the same even under the condition when the stationary tunneling current flows across the contact electrode-redox molecule-tip of the STM. The parameter η_V defined by eq 67 therefore has the physical meaning of the effective overpotential.[271]

In the limit of small Δ, bias voltage and overpotential ($\Delta < eV_{bias}, eV_{bias}, e\eta \ll E_r$) eq 62 is reduced to the approximate equations similar to those in the foregoing section. This equation can also be obtained using the simple kinetic model. The reverse transitions may be neglected in the adiabatic limit when $eV > k_BT$ and the current given by eq 62 is[37]

$$j = 2en\frac{k_{LB}k_{BR}}{k_{LB}+k_{BR}} \quad (68)$$

where

$$n \approx eV_{bias}\left(\frac{1}{2\kappa_L\rho_L} + \frac{1}{\kappa_R\rho_R}\right)^{-1} \quad (69)$$

We note that the degeneracy of the energy levels in the metal affects the number of electrons transferred in each reduction or oxidation step in this limit. The origin of the factor 2 in the first term in the parenthesis is due the fact that the energy interval for the transition of one electron from the left metal to the redox group, $\Delta\varepsilon_{LB} \sim 1/(2\kappa_L\rho_L)$ is one-half of the corresponding energy interval calculated with the neglect of double occupation of a given electronic state in the metal by electrons with opposite spin. In the case of negative bias voltage (opposite direction of the current) the factor 2 is moved from the first to the second term in the parenthesis.

An expression for the current similar to eq 52 can be derived using eq 68 at small overpotential and bias voltage. The expression differs from eq 52 by the form of the constants j_0 and a. A quite simple current expression is obtained, if a weak dependence of the reorganization energy on the position of the redox group within the tunnel gap may be neglected[268]

$$j_{ad} \approx j_0\exp(-E_r/4k_BT)\frac{\exp(e|V_{bias}|/4k_BT)}{\cosh\left(\frac{e(0.5-\gamma)V_{bias}-e\xi\eta}{2k_BT}\right)} \quad (70)$$

where, in the adiabatic case $j_0 = en\omega_{eff}/2\pi$.

With due account of the comment on n above, this expression is valid for both positive and negative values of the bias voltage. The current/overpotential dependence shows a maximum which is also described by eq 54 at $a = 0$. It can be shown with the use of eq 62 that the position of the maximum obeys eq 54 at arbitrary values of the bias voltage and Δ.[275] Equation 70 shows that the slope of the dependence of η_{max} on V in this approximation is also described by eq

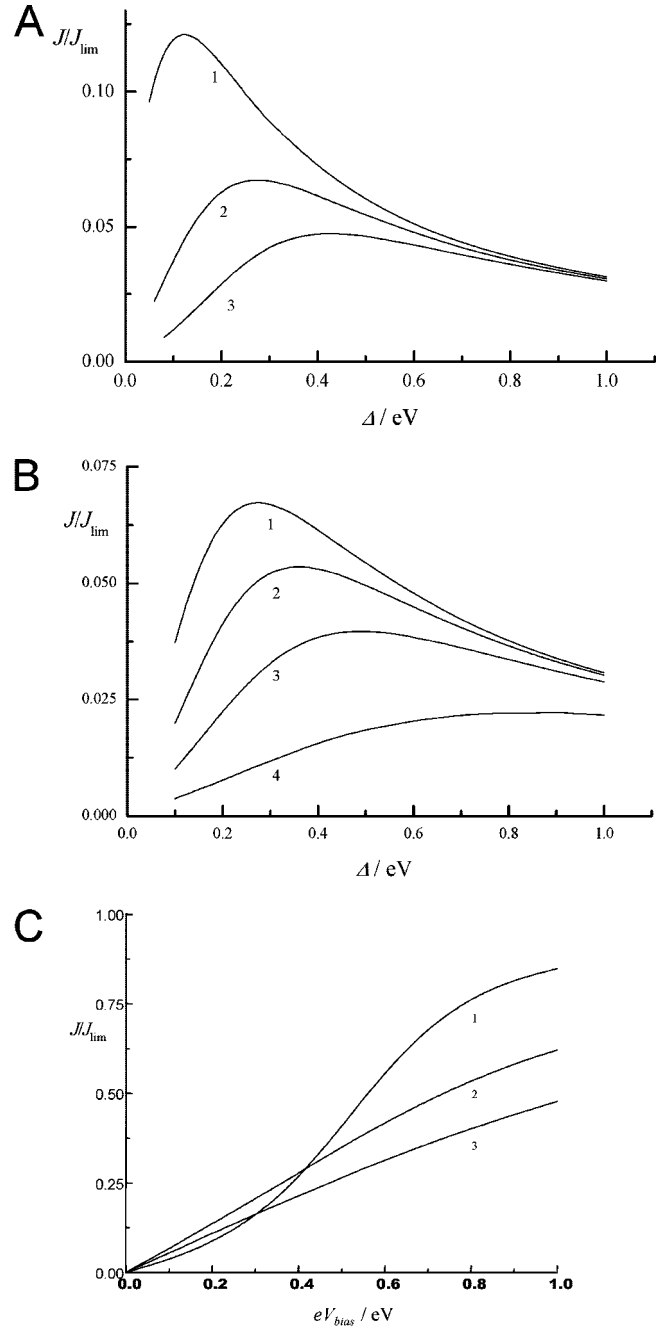

Figure 9. (A) The total tunneling current j in units of j_{lim} as a function of the total coupling strength Δ for $\Delta_{el} = \Delta_{tip} = \Delta/2$, $\eta_V = 0$, $eV_{bias} = 0.1$ eV, $k_BT = 0.025$ eV and different values of the reorganization Gibbs energy of the solvent. (1) $E_r = 0.25$ eV; (2) $E_r = 0.5$ eV; (3) $E_r = 0.75$ eV. (B) The total tunneling current j in units of j_{lim} as a function of the total coupling strength Δ for $\Delta_{el} = \Delta_{tip} = \Delta/2$, $E_r = 0.5$ eV, $V_{bias} = 0.1$ eV, $k_BT = 0.025$ eV and different values of the effective overvoltage. (1) $e\eta_V = 0.2$ eV; (2) $e\eta_V = 0.1$ eV; (3) $e\eta_V = 0.2$ eV; (4) $e\eta_V = 0.5$ eV. (C) The total tunneling current j in units of j_{lim} as a function of the bias voltage for $\Delta_{el} = \Delta_{tip} = \Delta/2$, $E_r = 0.5$ eV, $h_V = 0$, $k_BT = 0.025$ eV and different values of the total coupling strength Δ. (1) $\Delta = 0.1$ eV; (2) $\Delta = 0.3$ eV; (3) $\Delta = 0.5$ eV.

56. Analysis of eq 62 shows that the same equation is valid at $E_r < 0.5$ eV, $\Delta < eV_{bias}$, eV_{bias}, $e\eta < E_r$.

The effect of spin degeneracy is not in general reduced to a change of the number of electrons transferred, n. Equation 70 is valid for small values of the overpotential, bias voltage, and redox group energy level broadening, Δ_η (as compared with the reorganization energy). If these values are close to the reorganization energy, the activation free energy becomes different (explored in[271] for the spin-less model). Electron spin and the repulsion energy will cause additional effects.

Equation 70 corresponds to the thermally activated regime when the AGES have two potential wells and one transition point. With the increase of Δ or V_{bias}, AGES can have three potential wells or a single potential well.[271] We refer to the latter case as the adsorption regime of STM. At $eV_{bias} > E_r$ (the adsorption region) the first two terms on the rhs of eq 67 can be neglected. The total current is then given by eq 64 ε_B is independent of q and equal to $\varepsilon_B = -e\eta - \gamma V_{bias}$. It can be shown that, as in the nonadiabatic limit, $\Delta_\eta = V_{bias}$ in this case.

Using eq 62, the tunneling current for intermediate values of Δ and V_{bias} can be calculated.[271] Figure 9A shows the dependence of the tunneling current on Δ for the electronically symmetric case in the small bias limit for $\eta_V = 0$ and different values of E_r. The curves 1−3 indicate clearly the thermally activated region (the small Δ region), the crossover region and the adsorption region (the large Δ region). Figure 9A rather shows the strong dependence of the tunneling current on Δ in the thermally activated region. This dependence was not taken into account in eq 70. The tunneling current increases with increasing Δ in the region of small Δ due to the decrease of the activation free energy. Reaching a rather broad maximum, the current decreases in the adsorption region with the increase of Δ due to the increase of the total width of the redox level and, therefore, the decrease of the number of resonance states of the redox level in the energy window of STM

Figure 9A confirms the prediction of eq 70 concerning the dependence of the tunneling current on E_r in the small bias voltage limit: j decreases with the increase of E_r due to the increase of the activation barrier. However, the dependence of j on E_r is almost absent in the adsorption regime because, at $\eta_V = 0$, the redox level has a fixed position in the middle of the energy window.

Figure 9B shows the dependence of the tunneling current on Δ for different values of the effective overvoltage η_V in the electronically symmetric case and the small bias voltage limit. Since $\eta_V = \eta$ at $\gamma = 1/2$, Figure 9B shows the expected[35,216] dependence of the tunneling current on the overpotential in the small Δ and the small bias voltage limit: the smaller η, the higher the tunneling current. This is due to two reasons. First, eq 67 shows that with the increase of η_V, the redox level leaves the energy window of STM. Second, in the thermally activated regime, increase of η_V shifts the potential wells of the AGES with respect to each other so that the activation Gibbs free energy for transitions from the lower potential well to the potential barrier top increases. However, as shown, the partial current $j(q)$ takes its maximum value just at the point q_{max} near the position of the potential barrier.

Figure 9C shows the tunneling current as a function of the bias voltage for different values of the total coupling strengths Δ. Curves 1−3 show the crossover from the small bias voltage region (discussed in detail in connection with Figure 9A) to the large bias voltage region. As follows from Figures 1, 3, and 4 in ref 271, the large bias voltage region is identical to the adsorption region for $\eta_V = 0$ so that curves 1−3 are arranged according to values of Δ in this region.

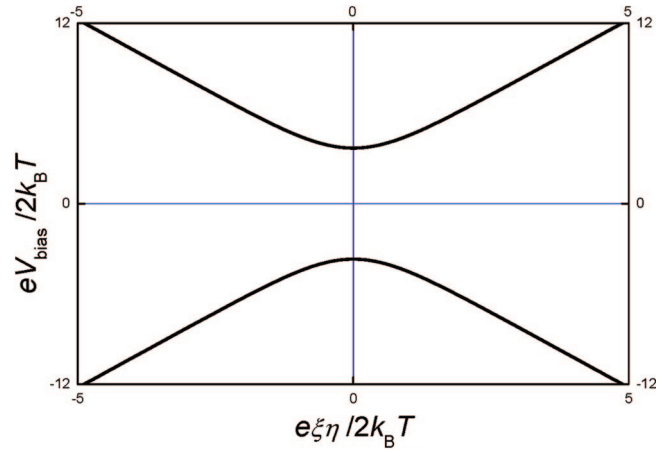

Figure 10. Constant-current plots ("diamond plots") for the symmetric contact according to eqs 71 and 72. $\gamma = 1/2$; $E_r/2k_BT = 10$; $A = 0.5$.

An approximate equation similar to eq 70 can be obtained also in the nonadiabatic limit with $j_0 = \sqrt{2e\pi\kappa\rho k_B T}(\omega_{eff}/2\pi)$ where it is implicitly assumed that the coupling with both electrodes is approximately the same. Equation 70 allows plotting the lines of constant current ("diamond plots"). A parametric form is useful

$$|eV_{bias}| = 4k_BT\left[\ln A + \frac{E_r}{4k_BT} + \ln\cosh\left(\frac{s}{2k_BT}\right)\right] \quad (71)$$

$$e\xi\eta = s \pm \left(\frac{1}{2} - \gamma\right)4k_BT\left[\ln A + \frac{E_r}{4k_BT} + \ln\cosh\left(\frac{s}{2k_BT}\right)\right] \quad (72)$$

where s is a running variable and $A = j/j_0 = \text{const}$. The signs plus and minus correspond to positive and negative values of the bias voltage respectively. When $\gamma = 1/2$ the plots are symmetric (Figure 10).

3.5. Two-Center Molecular Redox Targets

The first theoretical discussion of tunnel contacts with a two-center molecule confined in the tunneling gap in vacuum was given by Aviram and Ratner.[279] They showed qualitatively that the current/voltage characteristics in a vacuum system can be asymmetric with respect to the sign of the bias voltage thus demonstrating a sort of molecular scale rectification. The suggested mechanism rested on the assumption that the two centers of the bridge molecule are located in a sequence between the electrodes and each center possesses a vacant electronic energy level. The asymmetry of the current/voltage characteristics is based on the specially designed nonsymmetric location of the electronic energy levels with respect to the Fermi levels of the electrodes. Molecular rectification has recently been overviewed.[181]

A bridge molecule with two redox groups in the tunnel gap of an electrochemical contact has attracted attention due to advantages of this environment compared to vacuum. Most important is the possibility to control the position of the energy levels with the independent variation of two electrode potentials (overpotential and bias voltage) and the fact that this system can operate under ambient conditions (in condensed media at room temperature). This system offers a large variety of physical

situations related with the fact that each redox group may exist in two valence states (reduced and oxidized).

Theoretical and experimental studies of these systems have been reported[280–284] with focus on the nonadiabatic and partially adiabatic limits.[283–285] Tunneling through resonance states of mobile molecular groups at the electrodes were reported in ref 282. In both cases a maximum of the current as a function of the bias voltage was predicted. A main experimental result[282] is a sigmoidal curve for the current/bias voltage characteristics and a maximum of the current/overpotential relation in the neighborhood of the equilibrium electrode potential. Calculations of sequential stepwise electronic transitions between redox groups with full relaxation of the intermediate states result in both diode-like and transistor-like effect.[284]

3.6. Low-Temperature Behavior of a Multilevel Molecular-Scale Bridge

An interesting system representing a variety of physical situations is represented by a single center redox bridge molecule with two closely located electronic energy levels ε_1 and ε_2.[36] This is a particular case of multivalent molecules with several redox states. The limit of strong coupling of the redox group with both electrodes and with the bath phonons (q_k) was considered in[36] neglecting interaction between the electronic states. A simple adiabatic free energy profile form along a single reaction coordinate q is

$$U(q) = \frac{1}{2}\hbar\omega_{\mathrm{eff}}q^2 - \hbar\omega_{\mathrm{eff}}\int_0^q \mathrm{d}q\,[n_1(q)g_1 + n_2(q)g_2] \qquad (73)$$

where g_1 and g_2 are the electron−phonon coupling constants and ω_{eff} the effective phonon frequency. The occupation numbers of the electron energy levels $n_1(q)$ and $n_2(q)$ that depend explicitly on q and are calculated with the use of the Anderson-like model, eqs 65 and 66. The tunneling current at each given q value is given by

$$j(q) = e\sum_{b=1}^{2} T_b \left[\arctan\frac{\varepsilon_{\mathrm{b}}^0 - \varepsilon_{\mathrm{FL}} - \hbar\omega_{\mathrm{eff}}g_{\mathrm{b}}q - e\xi\eta(t) + e(1-\gamma)V_{\mathrm{bias}}(t)}{\Delta_{\mathrm{b}}} - \arctan\frac{\varepsilon_{\mathrm{b}}^0 - \varepsilon_{\mathrm{FL}} - \hbar\omega_{\mathrm{eff}}g_{\mathrm{b}}q - e\xi\eta(t) - e\gamma V_{\mathrm{bias}}(t)}{\Delta_{\mathrm{b}}}\right] \qquad (74)$$

where ξ and γ quantify the effect of the overpotential and bias voltage at the site of the redox group and

$$T_{\mathrm{b}} = \frac{2}{\pi\hbar}\frac{\Delta_{\mathrm{Lb}}\Delta_{\mathrm{bR}}}{\Delta_{\mathrm{b}}} \qquad (75)$$

where Δ_{lb} and Δ_{br} are the couplings of the electronic states of the redox group with the left and right electrodes, respectively.

The steady-state current at room temperature is obtained by averaging eq 74 over the equilibrium distribution for the q coordinate, cf. section 4.[271] Computer simulations with stochastic motion along the adiabatic free energy surface can also be undertaken.[215] An interesting behavior may be observed at low temperature where the activation processes are strongly suppressed and only relaxation along the q coordinate allowed.[36] Peaks and steps in the current/time dependences can appear depending on the relationships between the physical system parameters due to the sequential passage of the electronic energy levels through the energy window between the Fermi levels of the electrodes in the relaxation process along the q coordinate.[36] The peaks may be highly asymmetric if the variation of the overpotential or bias voltage is much slower than the characteristic relaxation time along the q coordinate.[36,285]

A sort of avalanche mechanism may operate when several closely located electronic levels interact with the same vibrational coordinate. The relaxation of the lowest energy level toward the reduced (occupied state) will then "draw" excited energy levels sequentially through the energy window with transition of a large number of electrons in a single relaxation step. This multilevel mechanism is different from the avalanche caused by vibrational excitation in the bridge group by sequential passage of several electrons through a single bridge group energy level.[266] The latter crucially depends on the vibrational relaxation time and appears as a random process. The multilevel avalanche is, however, independent of the vibrational relaxation time and appears at each reduction and oxidation step.

The relaxation along the q coordinate (if not observed directly in the current/time measurements) can be reflected in the steady state current as hysteresis in forward and reverse cyclic potential scans.[36] Some qualitatively similar observations were subsequently reported.[75]

3.7. Redox Switching of the Bridge Molecule

A different dependence of the tunneling current compared to that described in sections 3.4.1 and 3.4.2 is expected if dramatic changes in the electronic or conformational states of the bridge molecule accompany the reduction/oxidation process.[71–73,186] This may result in a change of the average conductivity due to the change of the redox state of the bridge molecule with the variation of the potentials[71–73]. Spontaneous transitions between two redox states of the bridge molecule may then take place, resulting in random spontaneous increase and decrease of the conductivity in time at fixed overpotential and bias voltage.[72,73]

A change of the conformation of the bridge molecule caused by reduction or oxidation is often considered as one of the reasons for the change of its conductivity. This may lead to a change of the electronic properties of the molecule itself or to a change of its contacts with the leads. In any case the change of the conformation (if any) is a considerable intramolecular reorganization which affects also the rate of the transition between the oxidized and reduced states. In the harmonic approximation this effect is reduced to a change of the reorganization energy. Methods of incorporating anharmonic modes have also been developed.[286] If the conductivity of the bridge molecule is different in two redox states the average steady-state current through such a molecule will be described by[36,287]

$$j_{\mathrm{t}} = j_{\mathrm{ox}}C_{\mathrm{ox}} + j_{\mathrm{red}}C_{\mathrm{red}} \qquad (76)$$

j_{ox} and C_{ox} and j_{red} and C_{red} are the currents and "concentrations" of oxidized and reduced forms.

Under steady-state conditions the concentrations are

$$C_{\mathrm{ox}} = \frac{k_{\mathrm{red\_ox}}}{k_{\mathrm{red\_ox}} + k_{\mathrm{ox\_red}}}; \quad C_{\mathrm{red}} = \frac{k_{\mathrm{ox\_red}}}{k_{\mathrm{red\_ox}} + k_{\mathrm{ox\_red}}} \qquad (77)$$

Using approximate expressions for the rate constants at small overpotential and bias voltage and neglecting a possible

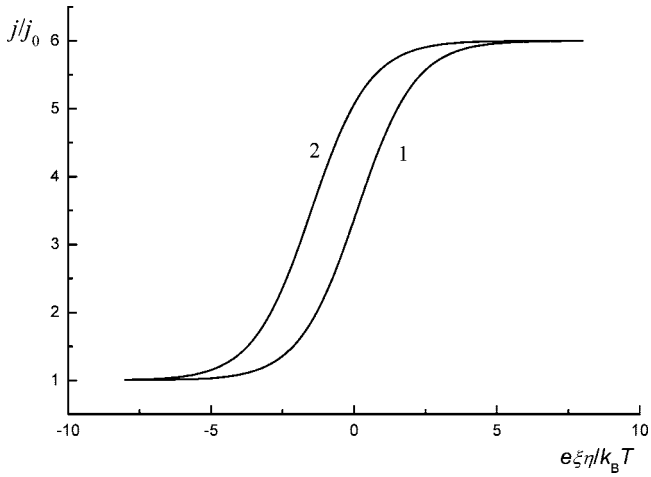

Figure 11. Dependence of the tunneling current on the overpotential according to eq 78. $eV_{bias} = 4k_BT = 0.1$ eV, $j_{red}(V_{bias})/j_{ox}(V) = 6$. 1: $\gamma = 0.3$; 2: $\gamma = 0.7$.

difference in the reorganization energies for the electron exhange at the left and right electrodes the following current form is obtained[285]

$$j_t = j_{ox}(V_{bias})\frac{1}{1+2\exp\left[\frac{e\xi\eta + e(\gamma-0.5)V_{bias}}{k_BT}\right]} + j_{red}(V_{bias})\frac{1}{1+0.5\exp\left[-\frac{e\xi\eta + e(\gamma-0.5)V_{bias}}{k_BT}\right]} \quad (78)$$

A possible dependence of the currents j_{ox} and j_{red} on the overpotential is neglected. Equation 78 describes a sigmoidal dependence of the current as a function of overpotential, Figure 11. The derivative of the current/overpotential correlation discloses a maximum in the vicinity of the equilibrium potential. Correlations of this type have been observed.[87,186] Figure 11 demonstrates switching between two conductivity levels in a narrow potential range.

3.8. Noise in Bridge Molecular Tunneling Contacts

The study of noise effects offers other information about molecular junctions.[74] The total number of theoretical reports on noise in tunnel junctions is large. The number of studies of bridged and quantum dot contacts with interaction of the bridge group or quantum dot electronic states with phonons is, however, much smaller[75] and with the low-temperature limit and inelastic effects related to the excitation of phonons usually in focus.

At the present level of experimental techniques the zero-frequency noise S is the most promising. The noise is usually proportional to the current I

$$S = 2eIF \quad (79)$$

where F is the so-called Fano factor. Theoretical calculations of the noise are usually based on numerical approaches.[75] The cases of weak and strong coupling with phonons have been analyzed. Opening of inelastic resonant tunneling channels for the weak-coupling limit were found either to increase or decrease the Fano factor depending on the symmetry properties of the contact.[75] As a rule results for strong electron−phonon coupling were obtained for weak interactions of the bridge molecule with the leads.[75] A main phonon peak and sidebands in the noise dependence on the bridge energy are predicted.

3.8.1. Shot Noise

Simple analytical expressions are available for the shot noise of quantum dot contacts.[287] The method in ref 287 was used in[285] to calculate the shot noise of the redox-mediated contact. Simple expressions were obtained for sequential ET[285]

$$S_{seq}(\omega = 0) = 2eI\frac{k_{SB}^2 + k_{BD}^2}{(k_{SB} + k_{BD})^2} \quad (80)$$

which operates both for weak electronic coupling with the source (S) and drain (D) electrodes, and for the coherent mechanism

$$S_{coh}(\omega = 0) = 4neI\frac{k_{SB}^2 + k_{BD}^2}{(k_{SB} + k_{BD})^2} \quad (81)$$

that operates when the coupling is strong. k_{SB} and k_{BD} are the rate constants for ET between the molecular bridge group and the source and drain electrode, respectively.

Equation 80 reduces to the Schottky formula if one of the rate constant is much larger than the other (then $F = 1$) while the same limit in eq 81 gives a twice as large result. This is related to the different physical mechanism of the transition in the two cases.[285] In the first case this limit corresponds to a Poisson process where the reduction and oxidation steps occur in pairs resulting in the transition of one electron from the source to the drain. In the second case the same process leads to the transition of a large number of electrons in each step (reduction and oxidation).

Figure 12A shows the dependence of the Fano factor on the overpotential caused by the corresponding dependences of the rate constants.

3.8.2. Telegraphic Noise

If two redox states are characterized by different values of the conductivity of the contact, the transitions between these states will produce so-called telegraphic noise.[74] The expression for the zero-frequency telegraphic noise of the redox-mediated contact is[285]

$$S(\omega = 0) = 4C_{Ox}C_{Red}(\delta j)^2/(k_{o/r} + k_{r/o}) = 4(\delta j)^2\frac{k_{o/r}k_{r/o}}{(k_{o/r} + k_{r/o})^3} \quad (82)$$

where $\delta j = j_{red}(V_{bias}) - j_{ox}(V_{bias}) = \delta\sigma V$. $k_{o/r}$ and $k_{r/o}$ are the rate constants for redox group reduction from the source electrode and for reoxidation of the reduced level by the drain electrode, respectively. It is assumed that the difference of the conductivities $\delta\sigma$ is independent of the overpotential and bias voltage. Equation 82 describes a curve with a maximum in the overpotential dependence, Figure 12B. It is seen that the effect of the bias voltage is nonmonotonous. Small bias voltage enhances the noise whereas large values suppress it. It follows from eq 82 that the noise increases with increasing reorganization energy, i.e., with increasing "phonon" coupling strength.

3.9. Double Tunneling Contact with a Redox Group (Redox Molecule/NP Hybrids)

Double tunneling contacts in vacuum are most frequently used for the study of the Coulomb blockade.[288] The first experimental study of in situ double tunneling contacts of a new type was reported in.[186] One of the contacts represented an ordinary tunneling contact between a nanoparticle and an STM-tip while the other one was a redox-mediated contact between the Au-nanoparticle and a substrate electrode. A theory of the operation of such a contact when the nanoparticle is large enough to avoid Coulomb blockade effects was offered in ref 289. The current/voltage characteristics is calculated according to

$$i(V_{bias}) = i_1(V_1) = i_2(V_2); \quad V_{bias} = V_1 + V_2 \qquad (83)$$

where i_1 and i_2 and V_1 and V_2 are the currents and potential drops across each contact.

The following features were disclosed: (1) a resonance in the differential conductance as a function of the bias voltage, (2) dependence of the resonance position on the overpotential (gate voltage), (3) a maximum in the current/overpotential relation, and (4) a bias voltage effect on logarithmic slopes of the current dependence on the tunneling distance.

Coulomb blockade effects appear when the nanoparticles are small. However, both the effect itself and the conditions for its observation are different from vacuum contacts.[290] The effect appears as steps in the logarithm of the current as a function of the voltage rather than directly in the current/voltage dependence.[290] An approximate current form is[290b]

$$i_{tunn}^{adiab} = en(eV_{ext})\frac{\omega_{eff}}{2\pi}\exp\left(-\frac{E_r - eV_1}{4k_BT}\right) \times \cosh^{-1}\left[\frac{\left(\frac{1}{2}-\gamma\right)eV_1 - e\xi\eta}{2k_BT}\right] \qquad (84)$$

where $V_{ext.}$ is the applied potential and $V_1 = V_{ext.}C_2/C_t$ the potential drop across the first, redox mediated contact

$$n(V_{ext.}) \approx \sum_n \theta[V_{ext}\frac{C_2}{e} - (n+\frac{1}{2})] \qquad (85)$$

C_2 is the capacitance of the second contact, $C_t = C_1 + C_2$ and $\theta(x)$ the step function. Another recent case of single-particle in situ Coulomb blockade[246] will be discussed in section 5.

3.10. Some Concluding Observations on Redox Mediated Single-molecule Contacts

The expressions for the current in the nonadiabatic limit take into account only sequential electronic transitions with the probabilities calculated in first order in the interactions with the metals. The adiabatic tunneling current involves both resonance and off-resonance electron tunneling, the latter commonly denoted as superexchange. This notion goes back to the early theory of bridge-assisted ET in bulk solution.[258] Similar processes in solid state contacts have been denoted "co-tunneling".[266]

As noted, section 3.1 reports of experimental work on in situ tunneling through a redox molecule have appeared recently,[83–92] in some cases showing a strong tunneling current maximum close to the equilibrium potential. The dependence of the position of the maximum on the bias voltage was studied in refs 124, 125, 269, and 280. The dependence of the maximum tunneling current position on the bias voltage was linear with a slope close to −0.5 for the osmium complexes.[269] Taking into account that the data were plotted with the use of the overpotential $\eta_a = \varphi_L - \varphi_L^0$, the sign of the slope must be changed when eq 54 is used. As noted, the slope 0.5 is typical for a symmetric contact where $\gamma(z; L_d) = \gamma(L - z; L_d) = \gamma(L/2; L_d)$. Unfortunately there were not enough data to determine the absolute value of $\gamma(L/2; L_d)$. The Os-based system also showed the "boost" of a large number of electrons expected when the electronic interaction between the redox molecule and the enclosing electrodes is strong.[268,269]

The tunneling current through a single azurin molecule attached to a gold electrode also showed an approximately linear dependence of the maximum position on the bias voltage with the slope approximately equal to −0.5.[124,125] This would correspond to a redox center located symmetrically within the tunneling gap ($S = 1/2$ in our present notation) or to another location in the case of strong screening ($S \approx 1/2$). In spite of the scatter of the data some observations concerning the width and the height of the maximum are appropriate. The width of the maximum increases with increasing bias voltage (from 50 to 300 mV). The height of the maximum also increases which is in keeping with general predictions of the theory. These results were fitted in[125] with the use of the approximate eq 52 (with $a = 0$) within the sequential stepwise mechanism. The electronic coupling

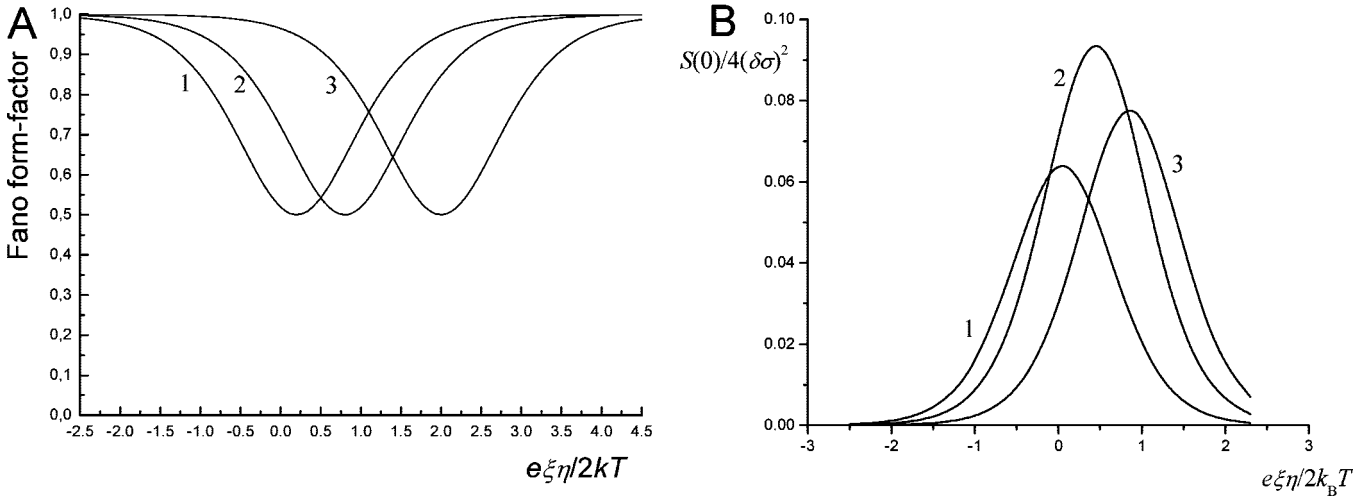

Figure 12. (A) Dependence of the Fano factor on the overpotential according to eqs 80 and 81. $\gamma = 0.3$, (1) $eV_{bias} = 2k_BT$, (2) $eV_{bias} = 8k_BT$, (3) $eV_{bias} = 20k_BT$. (B) Dependence of the telegraph noise on the overpotential according to eq 82.

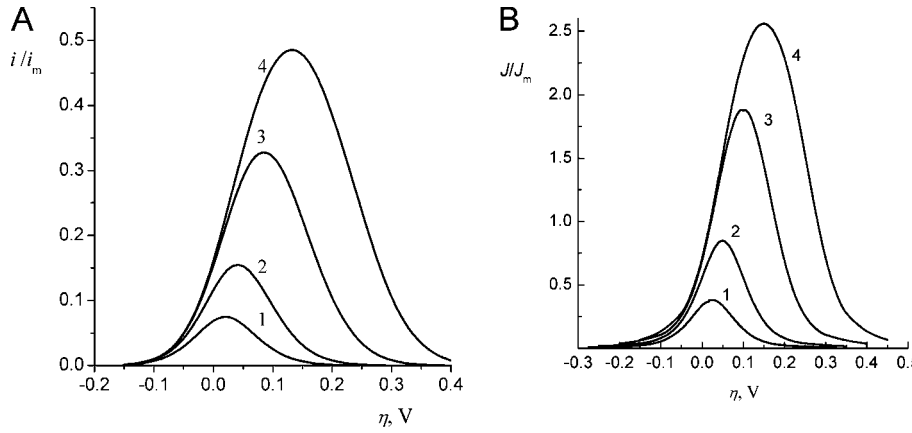

Figure 13. Left: Dependence of the tunneling current on overpotential in the totally nonadiabatic regime calculated according to eqs 1, 20, and 22 with $E_r = 0.1$ eV, $\gamma \approx 0$, $\xi \approx 1$ for different values of the bias voltage normalized to $j_m = k_L^0$, $k_L^0 = k_R^0$: (1) $V_{bias} = 50$ mV; (2) 100 mV; (3) 200 mV; (4) 300 mV. Right: Dependence of the tunneling current on overpotential in the totally adiabatic regime calculated according to eqs 62–68 with $E_r = 0.1$ eV, $\gamma \approx 0$, $\xi \approx 1$, $\Delta = 0.025$ eV for different values of the bias voltage normalized to $j_m = 2e\Delta_L\Delta_R/\pi\hbar\Delta$, $\Delta_L = \Delta_R$: $V_{bias} = 50$ mV; (2) 100 mV; (3) 200 mV; (4) 300 mV.

matrix element was also used as a fitting parameter. However, there are no reasons to assume that the matrix element depends significantly on the bias voltage.

The current/overpotential dependences were calculated in[38] at different values of the bias voltage with the use of exact equations for the strong and weak coupling limits (eqs 1, 5, 20, 21, 23, and 60–67) keeping the electronic matrix element (and therefore Δ) constant. Figure 13 shows that the experimental data in[125] are reproduced rather well with respect to the width of the current/overpotential maximum. It was assumed that the Debye screening is strong so that $\gamma \approx 0$ and $\xi \approx 1$. The reorganization energy was chosen to be 0.1 eV in both limits. However, the ratio of the current maximum values for the values of the bias voltage 300 and 50 mV are about twice as large as the experimental value in both cases. These calculations thus do not allow discriminating between the weak and strong coupling limits for the data in ref 125.

4. A Primary Target Class: Small Nonredox Molecules

4.1. Self-Assembled Molecular Monolayers: Nonredox Paradigms

In addition to surface structural mapping, surface functionalization by self-assembled molecular monolayers (SAMs) of molecules with systematically variable surface groups is extremely important. This perspective can be linked with comprehensive surface studies by UHV methods (ex situ methods). Electrochemical SAM formation is not restricted to surface structure characterization but extends to the electrochemically controlled dynamics of molecular SAMs where, e.g., two-dimensional phase transitions have been studied.[291,292] The evolution of SAM formation in real time with molecular-scale identification of several kinetic phases and intermediate states[33,293] is another aspect of electrochemical SAM dynamics.

The perspectives of UHV or electrochemically controlled SAMs are often related to surface technology in contexts of analytical chemical devices (chemical "sensing"), corrosion protection, nanoscale "electronic devices", etc.[167,168] We address here instead fundamental properties of electrochemical SAMs which are in some way "functionalized". Functional groups can be nonredox groups but electrochemically active surface group properties such as capacitive voltammetric properties[294] are indicative of subtle surface molecular dynamics. Functionalized SAMs are also important as supports for other immobilized active molecules such as redox metalloproteins and metalloenzymes with highly surface sensitive ET and enzyme function. In a second major SAM class the SAM molecules themselves contain an electrochemically active redox center that arouses other electronic properties addressed in Section 5. In view of the voluminous literature on nonredox molecular SAMs in UHV (e.g., see refs 167 and 168) our focus is on electrochemical SAMs where the well-defined SAM-structure can be correlated with dynamic electrochemical features such as potential induced molecular configuration changes or the SAM formation process itself.

In the still few cases where given molecular adsorbate molecules under both UHV and electrochemically in situ conditions can be directly compared, strong environmental effects have been observed. Solvation effects on electrostatically charged adsorbates can be as strong as the chemisorption forces such as the Au−S bond in functionalized alkanethiol surfaces.[33] Further, even the identity of given target molecules, say amino acids cf. section 4.3.1 is quite different in the two environments.[165,295,296] Different electrolyte media also induce different molecular SAM packings.[165,297,298] The overall structural packing in molecular SAMs and the accompanying, dynamics therefore rests on a composite interplay between molecular adsorbate binding, lateral intermolecular interactions, and interactions between the molecular adsorbates and the solvent or electrolyte ions.

4.2. Electrochemistry and In Situ STM Imaging and Image Interpretation

High-resolution imaging of intermediate-size molecular adsorbates in well-defined ordered SAM environments under electrochemical potential control was introduced particularly by Kolb,[4] Nichols,[299,300] Wandlowski,[292,301] Tao,[302] Itaya,[303–305] and their associates. Target molecules include halide ions, organic molecules, aromatic heterocycles such as pyridine and bipyridine, nucleobases such as adenine and uracil, and macrocyclic transition metal complexes[299–305] In addition to

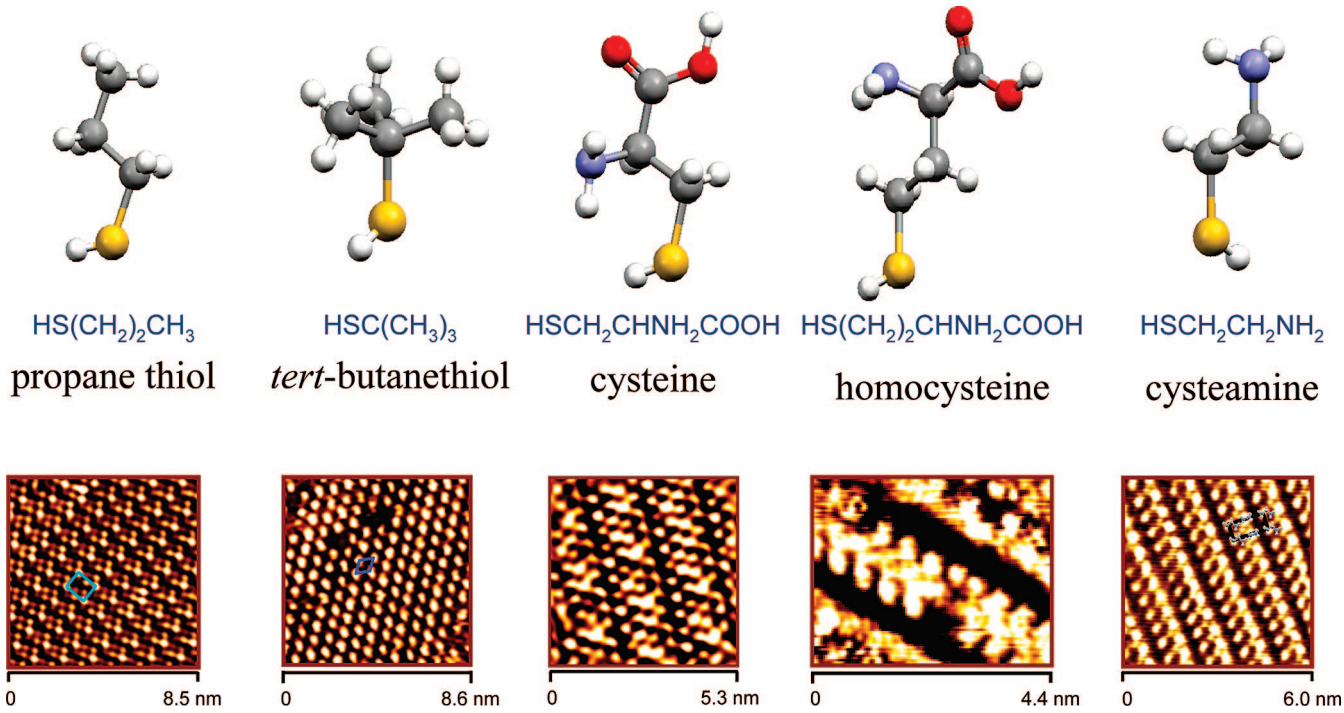

Figure 14. Overview of molecular structures and in situ STM images on Au(111)-electrode surfaces in aqueous buffer solution discussed in the text. The images show: cysteamine,[33] cysteine,[165,295] 1-propanethiol[293] and tert-butanethiol,[310] and homocysteine.[294] Details in these references.

image resolution at an amazing submolecular level, details of lateral bonding, say hydrogen bonding networks, and surface dynamics focused on two-dimensional phase transitions could be mapped. Other electrochemical molecular interfacial ET phenomena were also observed. Depending on the electrochemical potential, in situ STM of porphyrin-based molecules adsorbed on Au(111)-electrode surfaces pretreated by iodide adsorption could, for example be brought to show either the porphyrin molecules or the (iodide-modified) Au(111)-electrode surface.[303]

As (electrochemical) in situ STM rests on the electronic conductivity of the molecules and not directly on surface topography ("shape"), image interpretation must involve electronic structure notions. Such understanding is quite advanced for pure surfaces[306,307] and for small molecular adsorbates.[296,306–308] However, extension of such computations to whole unit cells in ordered molecular SAMs, not to say electrochemically controlled aqueous electrolyte poses prodigious challenges.[33] The case studies addressed below illuminate openings and limitations along these lines. These studies are based on variably functionalized alkanethiol SAMs directed by the strong chemisorptive Au−S bond, functional variability, and relative ease of preparation. Alkanethiol-based SAM surface chemistry and physics under UHV conditions has been reviewed.[167,168,306,307] The cases below focus on functionalized alkanethiol SAMs in aqueous electrolyte solution and under electrochemical potential control.

4.3. Electrochemistry and In Situ STM of Nonredox Alkanethiol-Based Molecules

The following alkanethiol derived adsorbates on well-defined electrochemical Au(111)-electrode surfaces illustrate aspects of surface structure reflected in molecular packing, potential-induced configurational changes, and correlations between molecular adsorbate structures and molecular conductivity, Figure 14.

4.3.1. Packing Modes and Image Interpretation of Straight and Branched Alkanethiols

Straight alkanethiols with no other functional end group than the terminal methyl group constitute a prototype SAM-forming molecular class. Comprehensive studies, mostly relating to UHV have addressed the Au-binding sites primarily on Au(111) and other low-index Au surfaces (3-fold hollow, bridge, and atop as well as deviations from these sites), tilt angle, and variable-length alkyl group packing features.[167,168,306,307] In view of the weakly solvated terminal alkyl group facing the solution at aqueous electrochemical electrolyte interfaces, much of this may carry over to electrochemical aqueous electrolyte environment. Recent studies of more composite alkanethiols with branched or adamantane-based thiols illustrate, however, other aspects of straight- and branched-chain molecular packing.[309,310] Two recent reports illuminate aspects of the subtle packing features at the single-molecule level, Figure 15.[310,311] *tert*-Butanethiol immobilized on electrochemical Au(111)-surfaces, with 1-propanethiol and 1-decanethiol monolayers as straight-chain references were studied by a combination of electrochemistry, in situ STM, and theoretical and computational methods.

Electrochemical reductive desorption of pure and functionalized alkanethiols, i.e., the process

$$\text{Au-SR} + e^- \rightarrow \text{Au} + \text{RS}^- \qquad (86)$$

is a basic feature of alkanethiol-based voltammetry,[212,312] Figure 15 and below. The reductive desorption potential reflects features of the Au−S bond strength. The peak shape is at the same time a fingerprint of the SAM structural homogeneity. The corresponding charge is a direct measure of the surface coverage and a crucial factor in the in situ

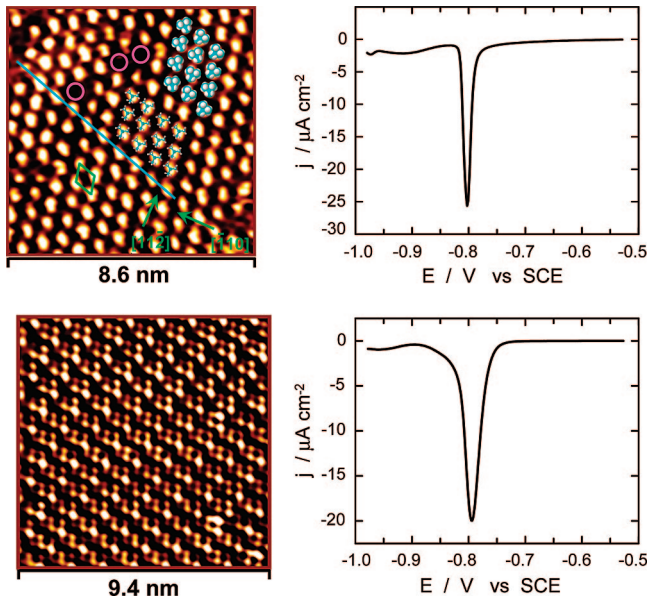

Figure 15. Top: In situ STM image, left, and reductive desorption voltammogram, right of *tert*-butanethiol. Bottom: Similar in situ STM image and reductive desorption voltammogram for 1-propanethiol. Imaging in 5 mM ammonium acetate buffer, voltammograms in 0.1 M NaOH. Reprinted with permission from ref 310. Copyright 2006 American Chemical Society.

STM image interpretation.

Although fixed by the same fundamental Au−S chemisorption base, branching of the alkanethiol leads to drastic changes in the surface packing on electrochemical Au(111)-electrode surfaces. Straight-chain alkanethiols adsorb in a relatively simple ($\sqrt{3} \times \sqrt{3}$)R30° lattice, or as for the reference molecule, 1-propanethiol, in a ($2\sqrt{3} \times \sqrt{3}$)R30°-4 lattice.[310] Each unit cell holds one strong and three weaker in situ STM contrasts, Figure 15. Such a pattern is indicative of target molecules in different surface orientations. In comparison the branched *tert*-butanethiol of roughly the same structural length shows a ($2\sqrt{7} \times \sqrt{7}$)R19° unit cell with just a single molecule per unit cell, Figure 15. The purple circles show missing single molecules. Interestingly, the individual molecular rows are not strictly aligned but display a slight zigzag packing feature indicative of two molecules per unit cell. Another difference is that no pitting of the Au-surface was observed, whereas extensive pitting is common for linear alkanethiols.

The expectedly weak solvent interaction for these hydrophobic molecules has warranted electronic structural computational analyses that disregard solvation effects.[311] This has provided detailed understanding of the packing of the branched alkanethiol and illuminated the difference from linear analogues. The adsorption sites are different and the Au−S bond on flat surfaces stronger than for linear alkanethiols, according with the more negative reductive desorption potential. The stronger bond also bypasses alkanethiol adsorption to "mined" Au-atoms according with the much less pronounced pitting. The more sparsely populated ($\sqrt{7} \times \sqrt{7}$)R19° lattice compared with ($\sqrt{3} \times \sqrt{3}$)R30° for linear alkanethiol adsorption is understandable from the steric repulsion among the terminal methyl groups. The prevalence of a ($2\sqrt{7} \times \sqrt{7}$)R19° lattice with two molecules in the unit cell over a ($\sqrt{7} \times \sqrt{7}$)R19° lattice with a single molecule as the origin of the observed zigzag superstructure could finally be assigned to two almost isoenergetic surface orientations with all the methyl groups in staggered conformations but surface site and the S−C bond orientations slightly different. This supports at the same time the slightly different STM contrasts and the observation of only a single sharp electrochemical reductive desorption peak.

Comparative studies such as these based on both experimental and theoretical single-molecule approaches have thus disclosed a wealth of molecular-scale information. As a final note of difference between similar-sized molecular monolayers of straight (1-propanethiol) and branched (*tert*-butanethiol) alkanethiols, simple electrochemical ET reactions ($[Fe(CN)_6]^{3-/4-}$, $[Co(phen)_3]^{3+/2+}$, phen = 1,10-phenanthroline) at Au(111)-electrodes modified by short straight alkanethiol (1-propanethiol) SAM's display almost ideal diffusion controlled voltammetry.[310] The same processes at Au(111)-electrode surfaces modified by *tert*-butanethiol display an intriguing asymmetry with the anodic process notably favored. Electronic Au−S-based surface states were invoked as a clue but the nature of these states and their different appearance in straight and branched alkanethiol-modified Au(111)-electrode environments remain elusive.

4.3.2. Structural and Electronic In Situ STM Interpretation: Cysteine, Cystine, and Homocysteine

Sulfur in the form of a thiol or a disulfide group is the common feature of this amino acid family and leads these molecules to bind strongly to Au- and other electronically "soft" metal surfaces (such as mercury).[313,315] At the same time the other two functional groups, the ammonium and the carboxylate groups lead to specific binding or surface organization that depends sensitively on the environment (UHV vs electrolyte medium, different electrolyte media, pH) and on the structural homology of the molecules (cysteine vs homocysteine).

Cysteine monolayers on metal/UHV and metal/liquid surfaces have long been studied using a variety of surface techniques.[295] By its composite surface (with both positive and negative charges), cysteine (and its dimer cystine) has also emerged as supporting linkers to immobilize redox metalloproteins that retain their subtle functional activity in the immobilized state.[39–42,133] Recent studies have focused on cysteine adsorption on single-crystal Au(111) surfaces in different aqueous electrolyte media.[295,297,298] An interesting observation is that voltammetry and in situ STM images of cysteine and its dimer homologue, cystine appear indistinguishable.[295] This suggests that cystine is dissociatively adsorbed with the disulfide bond broken but conclusive proof that this is in general the case has not been offered. The attractive properties of the cysteine/cystine couple as core targets in single-crystal adsorption and imaging to molecular resolution have also warranted theoretical and computational efforts that have helped to understand binding modes, molecular surface orientation and other adsorption and conductivity patterns of the molecules.[166,296,316,317]

While cysteine and cystine show largely similar voltammetry and *in situ* STM images on Au(111)-electrode surfaces, the higher cysteine homologue, homocysteine, with one additional $-CH_2$ group in the molecular backbone, Figure 14 behaves quite differently.[294] Homocysteine has other important roles in biology and clinical medicine associated with its appearance in metabolic branching points. In comparison with the many reported studies of cysteine surface chemistry and physics, and corresponding reports

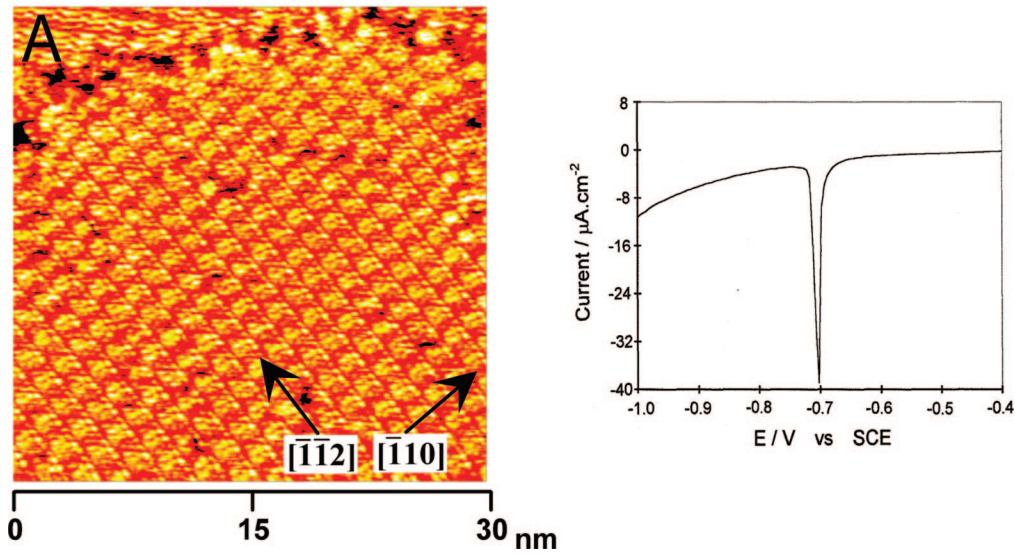

Figure 16. Left: In situ STM image of cysteine on a Au(111)-electrode surface. Five mM ammonium acetate, pH 4.6. Right; Linear voltammetric reductive scan of cysteine monolayer on Au(111)-electrode surface. 0.1 M NaOH. Reprinted with permission from refs 165 and 295. Copyright 2000 and 2006 American Chemical Society.

relating to homocysteine are few.[294] At the same time, the structural flexibility caused by the additional $-CH_2$ group evokes a completely different dynamic adsorption pattern in which either the negatively charged carboxylate group or the positively charged ammonium group can be brought to approach the Au(111)-electrode surface.

4.3.2.1. Cysteine/Cystine Adsorption on Electrochemical Au(111) Surfaces. In situ STM of cysteine adsorbed on Au(111)-electrode surfaces was introduced by Dakkouri et al.[297] who observed $(\sqrt{3} \times \sqrt{3})R30°$ adlayer structures and surface reconstruction lifting in perchloric acid solution. Xu et al. observed $(4 \times \sqrt{7})R19°$ packing in the same perchloric acid medium.[298] However, as cysteine in aqueous media is a zwitterionic molecule, both the amine and carboxylic acid groups can assume different charge states, sensitive also to the composition of the ionic medium. A rather different packing mode, i.e., a $(3\sqrt{3} \times \sqrt{6})R30°$ surface structure with six cysteine or three cystine molecules packed by hydrogen bonds and electrostatic forces was observed by in situ STM in aqueous acetate buffer, pH 4.6.[165,295] Later UHV studies of cysteine on Au(110) at cryogenic temperatures showed individual clusters at the reconstructed (2×1) Au(110) surface.[296] The reports in[165,295] illuminate multifarious surface binding interactions of a multiply charged adsorbate molecule and emphasize the importance of combining in situ STM with voltammetry to obtain the overall surface coverage as an important tool in the in situ STM interpretation.

Cysteine and cystine on Au(111)-electrode surfaces give a sharp reductive desorption voltammogram that testifies to highly ordered SAMs, Figure 16. In situ STM shows a highly organized pattern, very different from those of nonfunctionalized alkanethiols. By comparison with the voltammetrically determined surface coverage, each superstructural element is found to contain six cysteine molecules. The dark spots in Figure 16 show single missing cysteine molecules.

Computational DFT-based analysis has illuminated the cysteine binding modes and supported that the surface order is controlled by electrostatic and hydrogen bonding interactions.[166,316,317] A-top adsorption of the approximately electrostatically neutral Au−S cysteine radical state with the carboxyl group facing the Au(111) surface both gives the most stable configuration and accords best with the observed images. Most configurations give a single, sulfur-dominated STM image with significant contributions from nitrogen. Detailed representations of the (strong) solvation effects were not achieved but analysis showed that the attractive lateral dipolar interactions screened by a continuous dielectric medium stabilizes around a cluster size of six cysteine molecules according with the images. This combined approach has therefore offered new insight into the composite adsorption patterns of an intermediate-sized molecule in real chemical or biological environments.

4.3.2.2. Potential Controlled Dynamics of Homocysteine on Au(111) Surfaces. The cysteine homologue, homocysteine, shows intriguing differences from cysteine. The additional $-CH_2$ group makes the molecule long enough that it can "bend over" and either the carboxylate or the ammonium group of the Au−S fixed molecule contact the Au(111)-electrode surface. At the same time, a pair of reversible very sharp voltammetric peaks strongly suggests that interconversion among such configurations close to the potential of zero charge occurs.[294] The peaks are capacitive and sharp enough to resemble those of a phase transition. In situ STM has mapped the conversion in real time. Ordered domains appear close to the peak potential while complete disorder prevails on either side of this potential, Figure 17. Modeling based on these structural views indeed gives a capacitive peak at the potential of zero charge but the very narrow peak width can only be reconciled with the data if phenomenological "cooperative" parameters are also included.[294] Electrochemically controlled homocysteine surface dynamics therefore offer this molecule as a novel target for molecular surface "switching" which may, for example be combined with protein immobilization and configurational control of metalloprotein surface function.

4.3.3. The SAM-Formation Process in Real Time: Cysteamine and 1-Propanethiol

Other recent combined voltammetric, spectroscopic and in situ STM studies have mapped, namely the whole SAM formation process in real time to single-molecule resolution. Several kinetic phases in the two-dimensional surface layers of cysteamine could be followed directly in great detail from

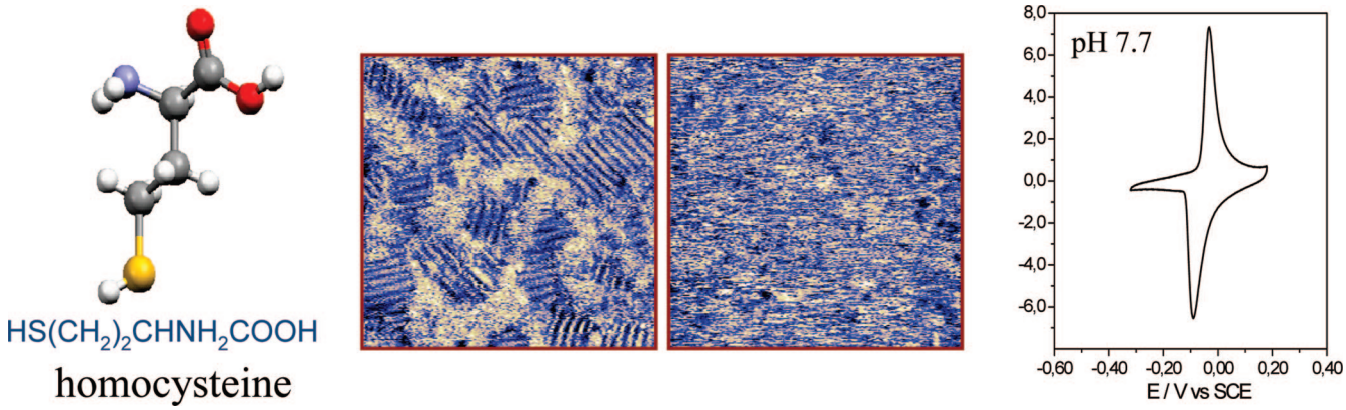

Figure 17. Left: Homocysteine molecular structure. Middle: Ordered homocysteine domains close to the potential of zero charge (pzc) and disordered layers on either side of the pzc. Right: Cyclic voltammetry peaks of homocysteine SAM. Five mM ammonium acetate, pH 4.6. Details in ref 294.

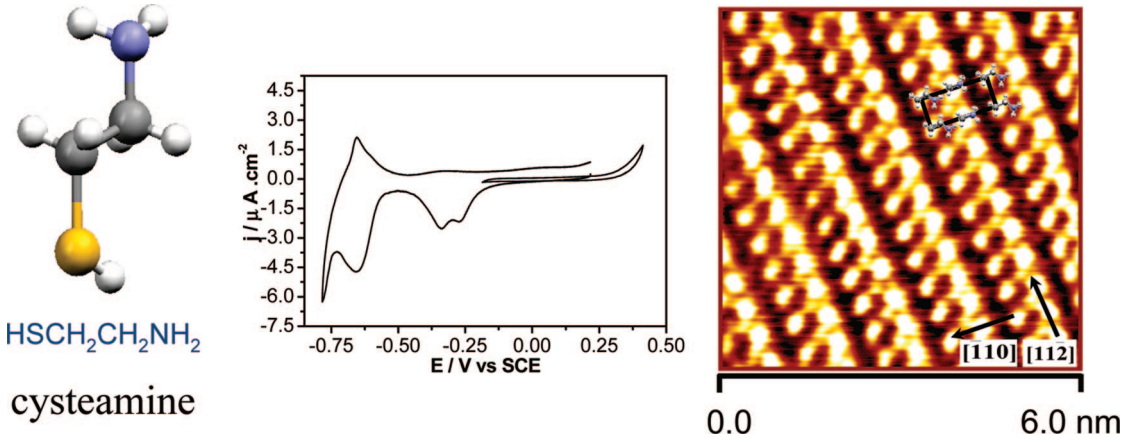

Figure 18. Left: Molecular structure of cysteamine. Middle: Cyclic voltammogram of cysteamine on Au(111)-electrode surface. The cathodic peak at −0.70 V (vs SCE) is caused by reductive desorption. The doublet around −0.40 V was assigned to catalytic proton reduction.[33] Right: In situ STM image of full cysteamine monolayer on Au(111). Five mM ammonium acetate, pH 4.6. Ar-atmosphere. Reprinted with permission from ref 33. Copyright 2005 American Chemical Society.

the pure reconstructed ($\sqrt{3} \times 22$)R30° Au(111)-surface right up to the fully formed ordered ($\sqrt{3} \times 4$)R30° cysteamine adlayer in an overall approximately 30 min' process. Reconstruction lifting, random cellular networks, disordered monolayers, pit formation and erosion, step edge dynamics and island formation are all intermediate states that could be imaged along the way to full monolayer formation.

Cysteamine, Figure 18, is a simpler functionalized alkanethiol than cysteine, with the ammonium group as a single terminal functional group opposite the linking thiol group. Like cysteine, cysteamine is an efficient linker for metalloprotein and metalloenzyme voltammetry and has been a target molecule in biofuel cell and biosensor contexts.[318] Cysteamine on polycrystalline and single-crystal Au-electrode surfaces has been addressed by a variety of surface spectroscopy.[319,320] Cysteamine is also an example that nonredox molecules display strong voltammetric signals other than reductive desorption, cf. homocysteine. It is probably the first case where the in situ STM images have been supported by state-of-the-art theoretical computations that include both DFT and molecular dynamics computations with an adequate number of solvent water molecules included.[33] These efforts have pointed to the importance of solvation forces comparable in strength to the central Au−S bond immobilizing the solvated electrostatically charged alkanethiol-based molecule.

Figure 18 shows a voltammogram of cysteamine on a Au(111)-electrode surface. The cathodic peak at −0.70 V (vs SCE) is the reductive desorption. The peak around −0.40 V was assigned to catalytic proton reduction. The doublet nature of the peak is indicative of the coexistence of two cysteamine conformations, Figure 19 supported by both in situ STM and the theoretical computations.[33]

The equilibrated monolayer, Figure 18 shows a strong and a weak in situ STM spot in the unit cell. Each represents a single cysteamine molecule, indicative of two differently conducting molecular surface conformations. The stronger contrast accords with through-bond conductivity of a molecule in an upright orientation. The weaker contrast may involve partial through-space or through-solvent conductivity. This expectation was notably borne out by the combined molecular dynamics and structure optimized DFT computations,[33] Figure 19. Out of a large number of molecular conformations, a single one accorded with the in situ STM images. Most others showed no resemblance at all. Two different contrasts were computed. The large assembly of water molecules were moreover found to determine crucially the packing. The two contrasts indeed reflect cysteamine in upright and slightly more tilted orientations. The contrasts are at the site of the ammonium group which is the molecular fragment closest to the STM tip but with significant electronic density contributions from the bound sulfur atom laterally displaced from the ammonium group. The apparent height difference of the protonated nitrogen atoms above the surface was found as 0.6 Å which could be reconciled with the

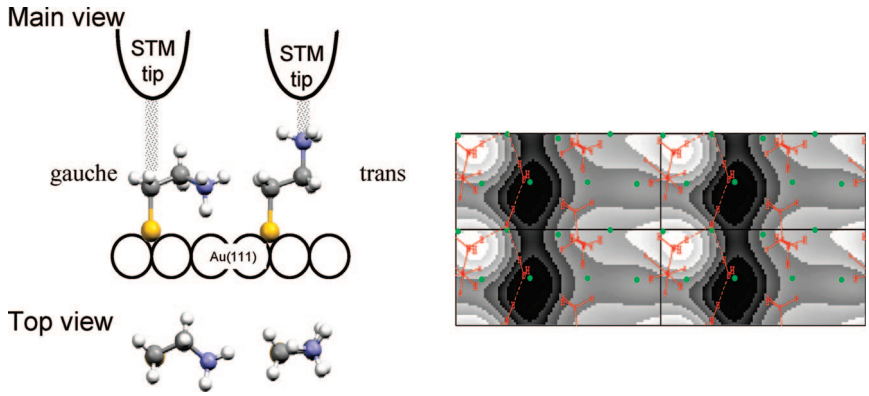

Figure 19. Left: Cysteamine in two surface orientations. Right: Combined molecular dynamics and structure optimized DFT computation of a full cysteamine unit cell and a large number of water molecules. A single one of the unit cell structures addressed accords with the in situ STM images. Reprinted with permission from ref 33. Copyright 2005 American Chemical Society.

voltammetric splitting of the −0.40 V peak from corresponding electrostatic image forces.

Comparable detail in real time molecular-scale SAM formation mapping by in situ STM was observed for 1-propanethiol[293] Physi- and chemisorption, pit formation and evolution, and domain growth were identified intermediate steps and represented as real time movies toward full SAM formation. Four 1-propanethiol molecules per $(2\sqrt{3} \times 3)$R30° unit cell could be identified, each giving a different in situ STM contrast. Cysteamine and 1-propanethiol have thus pointed to the feasibility of mapping structural and dynamic detail of intermediate-size molecular SAM's to atomic or molecular resolution directly in aqueous solution under electrochemical potential control. Cysteamine is probably so far the only case for which the whole variability of voltammetry, in situ STM, and other spectroscopic techniques have been combined with large computations to disclose all the structural details of the electrochemical in situ adlayer as well as mapping the adlayer formation process.

4.3.4. Thermally Gated Single-molecule Conductivity of Nonredox Molecules

Electronic conductivity and STM of nonredox molecules involves still another aspect, i.e. the role of the conformational and other intramolecular dynamics in the conduction process. The molecular conductivity is determined not only by the equilibrium molecular structures but also by the instantaneous, nonequilibrium conformation caused by thermal fluctutations induced by interactions with the solvent, gas ambient or even phonons of the enclosing electrodes. "Gating" is a common notion assigned to these phenomena, long known in molecular charge transfer (ET and proton transfer) science.[202,203] "Gating" implies that a structural nuclear equilibrium configuration exists along with a distribution of other configurations of higher but thermally accessible energies. Tunneling through the minimum energy configuration is unfavorable compared to the higher energy conformations which offer more facile tunnelling in return for thermal activation due to better electronic overlap or smaller energy gaps between the Fermi levels of the electrodes and appropriate molecular HOMOs and LUMOs, section 3.[161–167] Apparent thermal activation energy of the conduction process is a crucial reflection of gated molecular conductivity of nonredox molecules. "Apparent" means that the conducting structural molecular entity itself, i.e. the molecular conformer(s) change with temperature. These features resemble a separate "chemical reaction step" prior to the tunneling conductivity step.

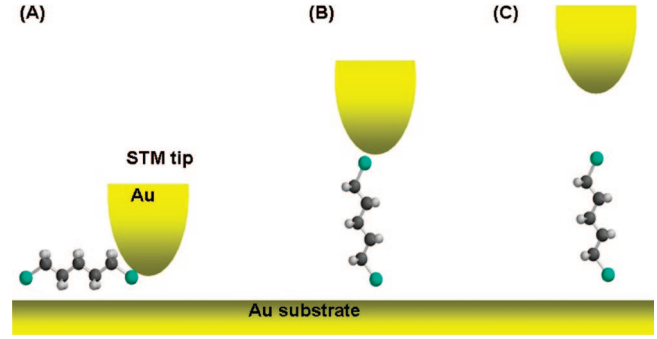

Figure 20. The $I_{tunn}(t)$ and $I_{tunn}(z)$ principle, schematically. Reprinted with permission from ref 163. Copyright 2007 American Chemical Society.

Thermally controlled gating of single-molecule conductance has been explored by Haiss, Nichols, and their associates[161,163] Accompanying theoretical frames have been offered in refs 272 and 277. Haiss, Nichols, and associates developed single-molecule techniques where the tunneling current through a single molecule (or a few molecules) are followed in time or by vertical retraction of the tip from the surface.[161,162] An STM Au tip was brought to approach a (well-defined) Au surface onto which sulfur-linked molecular targets are immobilized. An exposed sulfur-based second molecular linker unit would then catch the approaching tip. This process could be followed either in real time, *t*, or once (a) molecule(s) caught, other features such as tunnelling current/distance (*z*) or current/voltage spectroscopy could be recorded, Figure 20. An important point is that a single or a few molecules at a time are caught. Stochastic features of a single- or few-molecule system are therefore recorded. This issue is important in comparison with single-molecule patterns of molecules in ordered monolayers where conductivity and thermally induced gating features are different.

As an illustration, Figure 21 shows apparent Arrhenius plots of variable-length single-molecule conductivity. The apparent activation energy increases conspicuously with increasing chain length, all merging into a single point close to zero at the *y*-axis of a chain length correlation. This pattern is closely in keeping with thermal gating notions. Other recent data by Haiss, Nichols, and associates have supported these views by studies of structurally more rigid dithiol-based molecules which show much weaker temperature effects.[321]

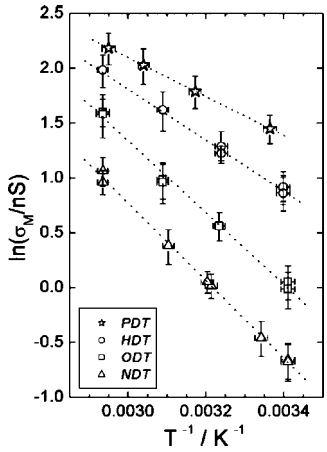

Figure 21. Logarithmic plot of the single-molecule conductance of several alkane dithiols against the inverse temperature. PDT = 1,5-pentanedithiol, HDT = 1,6-hexanedithiol, ODT = octanedithiol, NDT = nonanedithiol. Reprinted with permission from ref 248. Copyright 2006 The Royal Society of Chemistry.

5. Redox Molecules and New Electrochemical Molecular Tunneling Paradigms

5.1. Single-Molecule Electrochemical Tunneling Spectroscopy of Redox Molecules

The importance of accessible redox levels in the tunneling current/voltage patterns of molecular-scale contacts is recognized in solid state molecular electronics, section 2. The charge state of the redox molecules is, however, hard to assess when charge transport through the molecule is controlled solely by two enclosing electrodes. Such configurations have mostly been in the focus of solid state molecular contacts but solid state three-electrode field effect (FET) devices with a controlling gate electrode have also been constructed.

As noted, three-electrode electrochemical configurations with a reference electrode hold close analogies to the FET. Miniaturization to the molecular scale is offered by electrochemical in situ STM and by nanogap electrode configurations, Figure 1. Electrochemically controlled molecular conductivity implies that a conducting, usually strongly polar medium is the environment. This would be a challenge but is not prohibitive in perspectives for electronic devices. With this analogy, the two key correlations in single-molecule electrochemically controlled molecular conductivity, are then, cf. section 3: (a) The tunneling current/overpotential correlation at fixed bias voltage; this is the correlation closest to interfacial electrochemical ET and equivalent to the FET current/gate potential correlation. (b) The tunneling current/bias voltage relation at fixed electrochemical overpotential, equivalent to the current/bias voltage relation at fixed gate potential in the FET.

In the present Section we overview some molecular-scale systems that accord broadly with the notions of two-step single-molecule interfacial electrochemical ET. The systems display, however, "non-traditional" features associated explicitly with the single-molecule nature and electrochemical nanogap configurations with no immediate analogues in macroscopic interfacial electrochemistry. Electrochemical tunneling spectroscopy in the sense of single-molecule tunneling current/overpotential correlations was pioneered by Tao's report on Fe-protoporpyrin IX,[83] followed by other studies addressing a variety of molecular organic and inorganic systems and accompanied by increasingly precise theoretical frames. Reported systems that follow the basic views of single-molecule interfacial electrochemical ET include (1) metalloporphyrins,[83,303–305] (2) organic aniline- and polyaniline-based molecules,[89–92,322] (3) other organic molecules, the viologens in particular,[87,88,163] and (4) transition metal complexes in different binding modes and microenvironments.[83–85,112,113,179–181,219] We address these system classes below. The evolving area of single-molecule metalloprotein electrochemistry is addressed in section 6.

5.2. Metalloporphyrins and Metallophthalocyanines

Tao's study of Fe-protoporphyrin IX on HOPG electrodes under electrochemical potential control[83] showed, first in situ STM images with single-molecule resolution. In situ STM contrasts of the Fe-free ligand molecule far from the equilibrium redox potential were indistinguishable from those of the Fe-complex. As the electrochemical overpotential was scanned across the equilibrium potential, at fixed bias voltage, a clear spectroscopic feature in the form of a five times current rise followed by a corresponding current decrease was observed. The current was recorded as the apparent molecular "height" of the in situ STM contrasts. The data have been framed by a view of the process as coherent resonant tunneling via the molecular redox center.[217] However, the whole pattern, particularly the maximum at the equilibrium potential is in fact in keeping with the sequential two-step ET view with no need for additional assumptions,[35] cf. section 3.

Lindsay and associates,[183] and Itaya and associates[303–305] have reported in situ STM imaging of metalloporphyrins and - phthalocyanines with different metal centers, sometimes to amazing submolecular resolution. Similar resolution for metallophthalocyanin complexes by ex situ STM were reported by Hipps and associates.[180,181] Metalloporphyrins are robust metal complexes stable in a variety of environments and offer a multitude of metal- and ligand-based redox processes. The metalloporpyrins may be expected to come forward as a prototype molecular-scale "switching elements" in electrochemically controlled molecular electronics. In situ STM image interpretation, conductivity, and general electronic functionality of the metalloporphyrins are, however, complicated by electronic spin changes and molecular structural changes, say from four- to five-coordinate structures of the macrocycle that accompany the redox process. While such features may complicate molecular electronics considerations, they hold perspectives for understanding other single-molecule electronic properties under well-defined conditions.

5.3. Organic Redox Molecules in Electrochemical Break-junctions

Tao, Lindsay, and associates,[89–92,101,103,141,322,323] Haiss, Nichols, and associates,[88,161–163] and Wandlowski and associates[87] have developed "break-junction" technology where nonredox and redox molecular conductivity at the level of the single molecule can be obtained, Figure 20. The break-junction appellation implies that a direct contact between a STM substrate and tip or between nanoelectrodes via the target molecules is established in a liquid environment by mechanical interaction or by electrochemical metal deposition. The metallic or molecular contact is gradually weakened

by tip retraction or electrochemical metal dissolution. In the former case, just as the metallic contact is broken, target molecules fill the molecular-scale opened gap. Tip retraction when the molecular contact has been established can then control sequential decreasing conductivity steps from multiple molecular contacts right down to a single-molecule contact. Once this level is reached, tunneling conductivity in two- or three-terminal STM or nanogap electrode modes can be recorded.

Organic nonredox and redox molecules have been characterized. Benzene dithiols and 4,4′-bipyridine have been among the former.[88,90] Perylene tetracarboxylic diimide (PTCDT) and oligoanilines have been specific organic redox target molecules.[91,92,322] There are some common features that testify both to true single-molecule conductivity and that the redox molecules follow the notions of sequential two-step ET, but the precise understanding of other features relating particularly to the notion of negative differential resistance are more elusive:

(a) Tip retraction in liquid state STM showed a stepwise conductivity decrease reflecting successive single-molecule release from the tunnelling gap. The emerging single-molecule conductance assumed much smaller values, say a fraction of a nS than the fundamental quantum conductivity, $2e^2/h$ (=77 μS) where e is the electronic charge and h is Planck's constant. These features were also observed by Haiss, Nichols, and associates.[88,161–163]

(b) Single-molecule tunneling current/overpotential correlations of redox molecules showed a maximum (oligoanilines) or strong rise (PTCDT) around the equilibrium redox potential.[89–92,322,323] This is understandable from the electrochemical two-step ET notion but no detailed analysis is available. Conspicuous noise reflecting the stochastic nature of the single-molecule process was also observed.

(c) A negative differential resistance feature in the conductivity/bias voltage around the equilibrium redox potential is expected for electrochemical two-step ET. The corresponding feature in the current/bias voltage correlation is an inflection point, section 3. The different redox molecules probed show, however, different patterns that can only claim to be partly understood. The current/bias voltage relations under electrochemical potential control are smooth and nonlinear but with asymmetric rectification around zero bias voltage.[323] Such effects are expected when a low-lying redox state controls the molecular conductivity process whether in the sequential ET mode or by superexchange. A peak in the current/bias voltage relation was, however, also reported for the oligoanilines.[323] This effect cannot be directly reconciled with the electrochemically controlled two-step ET. This discrepancy was noted.[323] Together with other reports, section 5.5, these studies have opened a new area of single-molecule interfacial electrochemistry. In some way these observations have been preceded by theoretical recognition and followed by other evolution of theoretical frames.

Single-molecule redox systems have opened another perspective, i.e., the importance of fluctuations of observable molecular properties, reflected in distributions of current/overpotential and current/bias voltage correlations.[87,183,273] A different kind of fluctuations is associated with random electronic level population and depopulation sometimes denoted as "telegraphic noise", cf. section 3.8, known in nanoscale metal-oxide-metal and semiconductor junctions[71,72] and in a polyaniline junction between a pair of nanoscale Au-electrodes.[73] This feature is directly associated with stochastic forward and reverse interfacial ET between the electrodes and the molecular redox states.

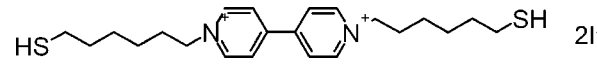

Figure 22. The core viologen redox unit $MV^{2+/+}$.

The following data are illustrative.[73] Two-level electronic switching between polyaniliine conducting (oxidizing "on") and nonconducting (reduced "off") states was controlled by the electrochemical potential. The system displays random transitions between "on" and "off" states with millisecond lifetimes at the small bias voltage of 20 mV. The amplitudes depend on the electrode potential, ranging from a fraction of a nA at low potentials to several tens of nA at high potentials. This accords with sequential two-step ET when the redox levels are close to the Fermi levels and the nuclear reorganization free energy does not exceed a few multiples of k_BT. The average lifetimes of the "on" state and the "off" states are

$$\tau_{on} \approx (k_{o/r})^{-1};\ \tau_{off} \approx (k_{r/o})^{-1} \tag{87}$$

The current amplitudes at the single-molecule level is, however, different from the steady state current given in section 3.4 and given instead by

$$i_{ampl} \approx \frac{e}{\tau}\tau \approx \frac{\hbar}{\Delta_L} + \frac{\hbar}{\Delta_R} \approx \frac{\hbar}{\Delta} \tag{88}$$

with the broadening following roughly the superexchange energy dependence

$$\Delta \approx \frac{|T_{\varepsilon_L}||T_{A\varepsilon_R}|}{(\varepsilon_F - \varepsilon_{ox})} \tag{89}$$

An inverse relation between lifetime and amplitude is thus expected.

Observation of the vacant "on" state entails that ε_{ox} is close to the Fermi levels, at a given negative overpotential. If the levels are too close the lifetime is too short to observe fluctuations. Asymmetry arises as the occupied level is trapped further below the Fermi levels than the vacant level above the Fermi levels. The lifetime is therefore shortest for the "on" state. The amplitude increases with increasing negative overpotential due to the decreasing energy denominator in eq 89. These expectations are broadly as observed.

5.4. The Viologens

Viologens, Figure 22, are a class of quaternary aromatic redox active pyridine molecules which have acquired a status as targets in the electrochemical mapping of single-molecule redox molecular conductivity.[87,161–163] The viologen unit can be reduced electrochemically in two steps of which the $V^{2+} \leftrightarrows V^{+\bullet}$ transition is the important one. Two variable-length straight-chain pure or thiol terminated alkyl radicals conclude the N coordination.

The viologens can be linked to a Au-electrode surface via one of the thiol linkers. Several surface phases can form including a low-coverage disordered phase and a high-coverage, ordered but fragile monolayer phase. The adlayers have been characterized by voltammetry, surface enhanced infrared spectroscopy (SEIRAS) and in situ STM.[87,161–163] The latter has been applied to single-molecule resolution for both the isolated or highly dilute monolayer and of an ordered adlayer at high coverage.

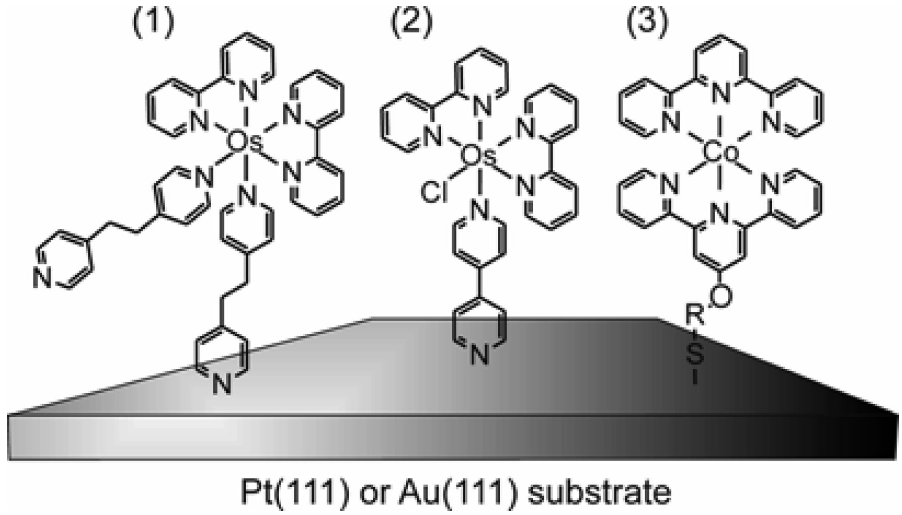

Figure 23. Os and Co complexes on single-crystal Au(111)- and Pt(111)-electrode surfaces (schematic) as transition metal complex based target molecules in single-molecule in situ STM and STS.

Single-molecule viologen conductivity was studied by Haiss, Nichols, Van Zalinge, and associates[161–163] and by Wandlowski and associates[87] using closely related $I_{tunn}(t)$ and $I_{tunn}(z)$ modes of in situ STM, Figure 20. The viologen molecule was linked to the Au-substrate via one of the alkylthiol linkers. The second linker could either be an identical alkylthiol group chemisorbed to the Au-tip giving a symmetric molecule or a nonfunctionalized alkyl residue with different conductivity patterns emerged.

Haiss, Nichols and associates further incorporated Au-nanoparticles as a conducting intermediate between the viologen probe molecule and the STM tip,[186] as also exploited by Lindsay and associates.[324] The different in situ and ex situ STM current/voltage patterns disclosed conspicuously different features depending on the microenvironment (ambient gas, nonconducting solvent, or aqueous electrolyte) and electrical circuitry (in situ three-electrode or two-electrode Au-nanoparticle configurations).

Electrochemical in situ STM addressing isolated single, doubly thiol-bound viologen molecules disclosed a pronounced tunneling current rise as the equilibrium redox potential was approached. However, both substantial inhomogeneous broadening and no direct resonance in the tunnelling spectroscopic features were observed.[163] At the same time, in an earlier study of the same molecule using two-electrode STM technology and an inert solvent, and via the Au-nanoparticle contact a pronounced resonance in the tunneling conductivity/bias voltage relation was found,[186] almost certain to reflect a transition between the oxidized and reduced viologen forms. Mechanistic details were suggested but the two-electrode nature of the experiment precluded a closer analysis. The data point to the hypersensitivity of the conductivity of large and conformationally flexible single molecules to the local environments, even when the molecule is hooked on to the enclosing electrodes by strong chemisorption.

Wandlowski and associates addressed several viologen-based molecules[87] that included both the symmetric doubly thiol-linked viologen molecule and the asymmetric analogue chemisorbed only to the Au-electrode. Their observations on the doubly linked molecule followed broadly those of Haiss, Nichols and associates but also with some differences. They observed for example a plateau in the current/overpotential relation whereas no such plateau was reached in the studies of Haiss, Nichols and associates. More importantly, the asymmetric singly thiol-bound viologen showed a quite different pattern with a pronounced maximum near the equilibrium redox potential in the current/overpotential correlation, following closely expectations for sequential two-step ET, section 3. Reasons for the difference between the closely similar symmetric and asymmetric molecules, and between the different environments (aqueous electrolyte, organic solvent/nanoparticle) are presently unsettled.

5.5. Transition Metal Complexes

Other transition metal complexes than metalloporphyrins have emerged as tunneling spectroscopic targets. A class of Os- and Cocomplexes, Figure 23 illustrates systematically electrochemical single-molecule ET and in situ STM spectroscopy.[84,85,113,219,269] Complexes such as these are attractive single-molecule ET probes. They are robust in at least two electrochemically accessible oxidation states and the ligand spheres offer a broad versatility for tuning redox potentials over wide ranges. Chemical synthesis as well as comprehensive other coordination chemistry support further the availability of these molecular target systems. They have, finally been addressed to the level of the single molecule in different environments including UHV,[111] aqueous electrolyte[84,85,219,269] and ionic liquid media.[113]

The complexes adsorb in monolayers on Au(111)- and Pt(111)-electrode surface via N- or S-linker units. Ordered domains among largely disordered areas are formed under the conditions used but long-range order is not a prerequisite for addressing these rigid molecules. The complexes show monolayer voltammetry with features suggestive of counterion and other specific effects. As a key issue, the electrochemical kinetics of the Os-complexes is much faster than for the Co complex with standard interfacial electrochemical ET rate constants $>10^6$ s^{-1} vs $\approx 10^3$ s^{-1}. This follows patterns for electron exchange in homogeneous solution and can be ascribed to significant intramolecular nuclear reorganization and less favorable electronic coupling of the Co complex to the enclosing electrodes. No significant structural changes thus accompany the ET processes of the Os-complexes, although intriguing metal-to-ligand charge relocation does appear to do so[325]

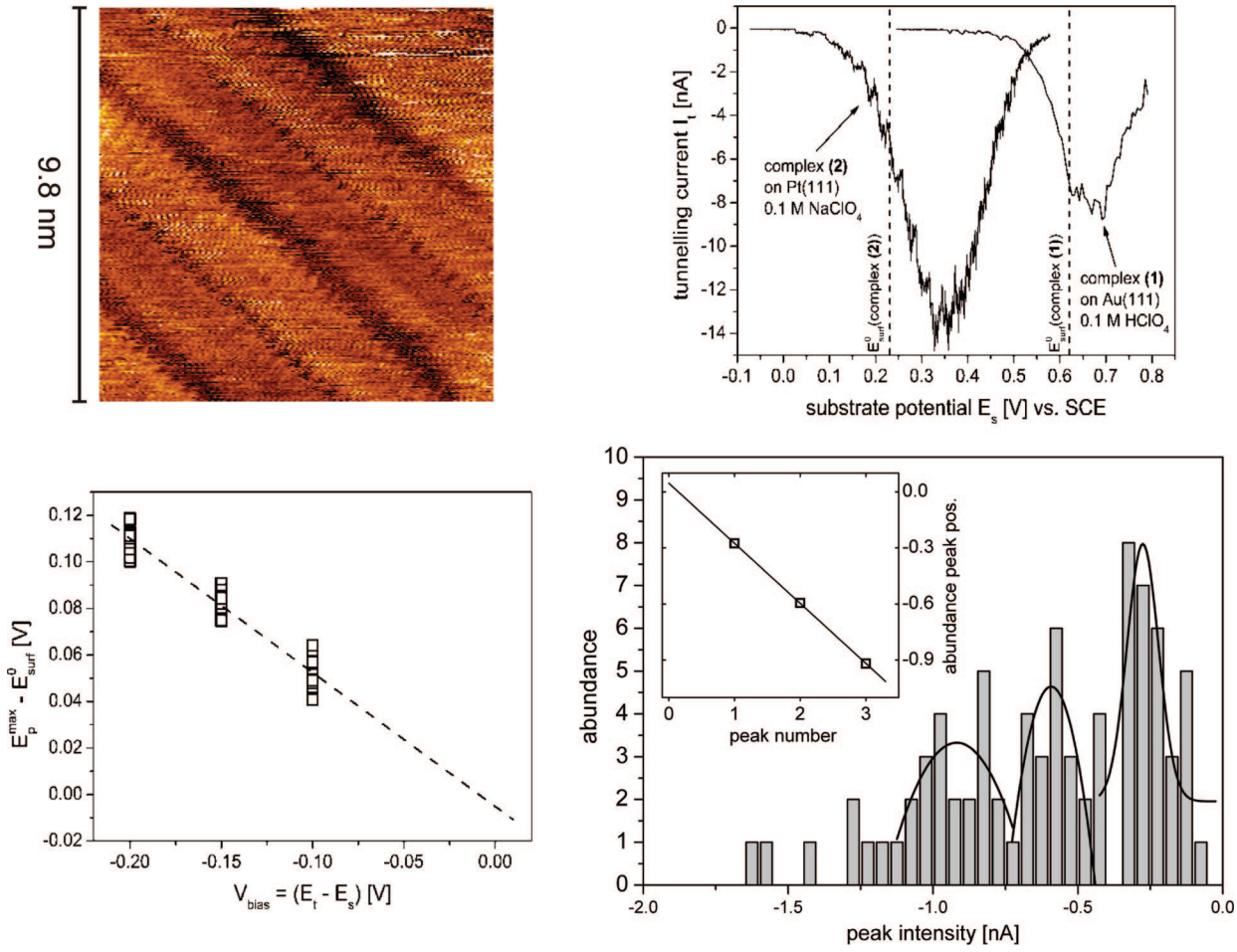

Figure 24. Top left: In situ STM image of Os-complex (1) on Pt(111)-electrode surface. 0.1 M $HClO_4$. Top right: Tunneling current/overpotential correlations, $I_t(\eta)$, $V_{bias} = -0.15$ V; 0.1 M $NaClO_4$ and 0.1 M $HClO_4$. Bottom left: Effect of bias voltage on the peak maximum of the $I_t(\eta)$ correlation of complex (1). Bottom, right: Abundance of tunneling current peak intensities of $I_t(\eta)$ correlation of complex (1). Inset. Peak position vs peak number. 0.32 nA/peak. Data from refs 219 and 269. Reprinted with permission from ref 269. Copyright 2006 American Chemical Society.

Voltammetric patterns[84,85,113,219,269] and kinetic analysis[269] are offered elsewhere. Figure 24, left shows an in situ STM image of an ordered domain of the complex of the $[Os(bpy)_2(p2p)_2]^{3+/2+}$ complex (bpy = 2,2′-bipyridine, p2p = 1,2-bis(4-pyridyl)ethane). The molecules seem, interestingly to "stand on one leg" (linked via one of the two equivalent monodentate ligands). Figure 24, right shows an in situ STM tunnelling current/overpotential correlation under conditions where the notion of small bias voltage applies, section 3. This correlation shows the features expected for two-step sequential electrochemical ET, particularly (a) there is a strong maximum with close to 2 orders of magnitude tunneling current on−off ratio, close to the equilibrium potential; the width of the feature (200−300 mV) accords with a value in the range expected in the confined space between the substrate and tip. (b) There is a systematic, close to linear variation between the peak maximum in the tunneling current/overpotential relation and the bias voltage. A systematic variation is expected as the molecular redox center is exposed to part of the bias voltage drop. (c) Similar spectroscopic tunneling current/overpotential relations are obtained for two different Os-complexes, i.e., $[Os(bpy)_2(p2p)_2]^{3+/2+}$ and $[Os(bpy)_2(p0p)Cl]^{2+/+}$ (p0p = 4,4′-bipyridine) with widely different equilibrium redox potentials, +0.62 and +0.23 V (SCE). The peaks are displaced exactly by this amount along the overpotential axis, Figure 24. (d) A Co complex that closely resembles the Os complexes displays a STS feature of similar origin as for the Os complexes but much weaker.[219] This can be assigned to much slower interfacial electrochemical ET of the Co complex compared with the Os complexes, cf. above. (e) The latter correspondence has, finally a bearing on still another issue of interfacial electrochemical ET in electrochemical in situ STM. The strong electronic coupling between the Os complexes and the enclosing substrate and tip electrode offers a case for coherent multi-ET in the vibrational relaxation process of the intermediate molecular electronic state, section 3.

A recent analysis could isolate the tunneling peak conductivity of a single Os-complex molecule as for the viologens, Figure 24.[269] At the same time, subject to objective assumptions, the number of electrons transferred in a single two-step in situ STM tunneling event was estimated to several hundred electrons. The Os-complexes therefore offer a case where a "boost" of electrons amplifies the tunneling current switch effects by orders of magnitude.

The Os-complexes offer a probe system for highly efficient tunneling current amplification based on single-molecule interfacial electrochemical ET, operating at room temperature in condensed matter environment. The latter has been extended to ionic liquids closer to putative or real forthcoming molecular-scale electronic components, Figure 25. Both

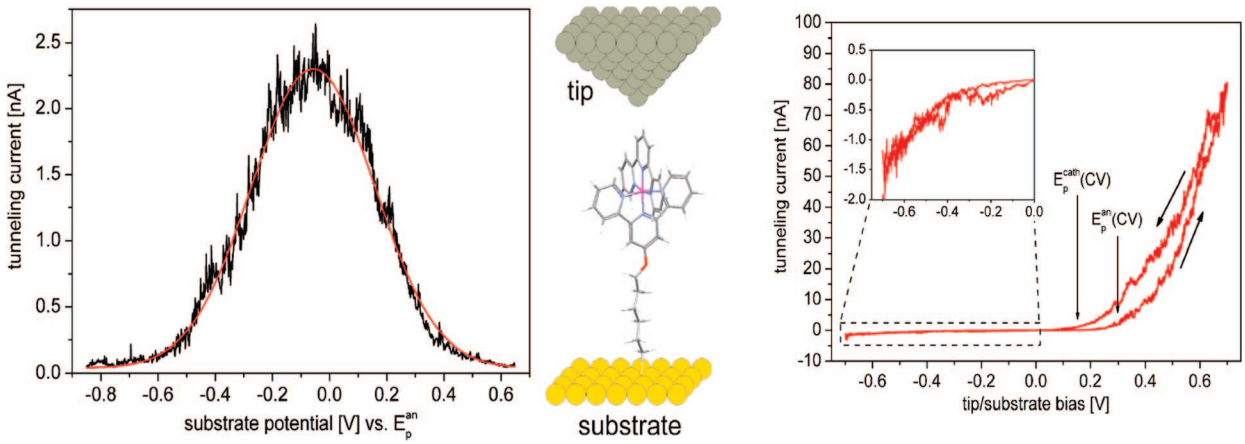

Figure 25. Correlations between the tunneling current and either the electrode potential (left) or the bias voltage (right) of a bis-terpyridine-based Os-complex in an ionic liquid medium (1-butyl-3-methylimidazoliumhexafluorophosphate). Left: Tunneling current/overpotential correlation at fixed bias voltage $V_{bias} = +0.7$ V, with a strong maximum around the equilibrium potential. Middle: Schematic view of the Os-complex in the tunneling gap between the Au(111)-surface and the Pt/Ir (80/20) tip. Right: Tunneling current/bias voltage at fixed electrode potential −0.3 V (forward and reverse scan shown) to show a strong rectification effect. Reprinted with permission from ref 113. Copyright 2006 American Chemical Society.

amplification and strong overpotential dependent molecular rectification, with up to 2 orders of magnitude rectification ratios were observed.[113] Current amplification induced by electrochemical current/overpotential switching was also studied for a ferrocene derivative,[183] and for electrochemical current/overpotential relations of two closely spaced mercury electrodes at which $([Ru(NH_3)_6]^{3+/2+}$ is successively oxidized.[326] The latter effects do not refer to the single-molecule level but do relate to nanoscopic and single-molecule redox cycling as pioneered by Bard[327] and with recent contributions by other groups.[328,329]

6. Bioelectrochemistry at Molecular Levels of Structural and Functional Resolution

Imaging of single biological macromolecules such as DNA and proteins by STM was an early vision of the scanning probe microscopies.[143] Phosphorylase kinase and phosphorylase b,[330] serum albumin,[331] immunoglobin G,[332] vicilin,[333] cytochromes,[334] hemoglobin,[335] catalase,[336] glucose oxidase,[337] lysozyme,[338] and the multicenter metalloproteins nitrogenase[339] and photosynthetic reaction centers[340] were early cases for molecular resolution. This was, however, for air ambient and often large bias voltages or, if in aqueous solution then without electrochemical potential control. Imaging of metalloproteins by electrochemical in situ STM in aqueous buffer dates from the mid-1990s. Immobilization of proteins in a functional state on the electrode/electrolyte interface poses recognized challenges. The "soft" nature of the biological macromolecules for which image resolution cannot be expected to compare with that of small rigid molecules is another important issue. As the molecules are "large", electric fields and pressure from the probing tip can be detrimental to the protein. Large bias voltages as often applied in early reports also means that multiple, little selective tunneling routes through the protein molecules compete with resulting congestion of the electronic conductivity-based STM contrasts.

Horse heart cyt *c* on glassy carbon[129] and horseradish peroxidase on electrochemically activated HOPG electrode surfaces[130] were the first cases for in situ STM of a metalloprotein with molecular resolution. Target molecules in other early reports of in situ STM of (metallo)proteins were covalently immobilized horse heart cyt *c* on Au- and Pt-electrode surfaces[341] and *P. aeruginosa* azurin chemisorbed on Au(111)-electrode surfaces.[116] Other early reports on metallothionin (rabbit liver),[342] rubredoxin (*Clostridium pasteurianum*),[343] and a thiolated cyt P-450 mutant on Au surfaces[344] although with molecular resolution, did not address electrochemically controlled systems and do not qualify for the notions of electrochemical in situ STM.

Proteins with given surface groups suitable for direct chemisorption such as the thiolate and disulfide group naturally present or introduced offer an attractive approach to protein immobilization in well-defined orientations. Compromises may, however, be needed. The covalent, electrostatic, or hydrophobic surface linking group may be close to the electrochemical redox center and this would support facile electrochemical ET but is not necessarily favorable in situ STM contrast. The latter may instead be achieved if the linker group is more remote from the redox center which is in return closer to the in situ STM tip.

6.1. Protein Film Voltammetry and Ordered Surface Structures of Linker Molecules

Dynamic electrochemistry as a strong notion in adsorption and interfacial ET of redox metalloproteins and metalloenzymes was introduced by Kuwana,[345] Niki[346] and Hill[347] about 30 years ago. Focus at first was on the three major classes of the smaller ET proteins, the heme, blue copper, and iron−sulfur proteins.[39–42] Focus lately has been on interfacial electrochemistry and electrocatalysis of more composite redox metallo- and nonmetalloenzymes immobilized in monolayers on pure and functionalized graphite, gold, and other electrodes. Development of enzyme monolayer film voltammetry has followed several lines. Armstrong, Butt, Hirst and their associates[40,41,348–357] have addressed comprehensibly the electrocatalysis of a number of enzymes based on fast scan voltammetry and spectroscopic methods. Target enzymes have been peroxidases,[351] and the multicenter redox enzymes hydrogenases,[40,41] multiheme nitrite reductase,[137,352] and large membrane-bound enzymes including fumarate reductase[353] and succinate dehydrogenase,[354] Mo-containing nitrate reductases[355] and sulfite oxidase,[356] and beef heart complex I.[357] Sequential ET steps,

accompanying proton transfer, intermediates such as Mo(V), and branched or bidirectional catalysis are features identified. Other reports along these lines relate to mechanistic studies of successive ET in laccase on gold electrodes,[358] carbon nanoparticle structures in the electrochemical contact between laccase and pyrolytic graphite electrodes[359] and mechanisms of the Mo-enzyme xanthine oxidase[360] Many studies on redox metalloenzyme film voltammetry have been reported by Gorton and associates[361,362] and by Scheller, Wollenberger, and associates.[363,364]

In another direction Gilardi and associates have combined metalloprotein and metalloenzyme voltammetry with biotechnological approaches to electrochemically supported biological ET chains.[365,366] Willner, Katz, and their associates have developed protein and large enzyme immobilization by other linking units that vary in size from the molecular to mesoscopic levels such as metallic or semiconductor nanoparticles, and nanotubes.[55,367,368] The molecular linker function can be tuned to on−off function by optical interception or by redox controlled charge states, and brought to control electrochemical charge relay through biological electron transport chain fragments such as a cytochrome *c*/cytochrome *c* oxidase complex. Conjugation of ET signals in "hybrids" between nanoparticles and the biomolecules holds other perspectives for controlling the contacts between the external circuit and broader biomolecular function including both electron transport chains[55,368] and biomolecular "recognition", protein based "nanocircuitry" and immunosensing.[369] Gooding and associates have addressed aspects of this comprehensive area focusing on electrode-protein contacts via carbon nanotubes.[370] Still another novel aspect of bioelectrochemistry and protein film voltammetry is related to interfacial electrochemistry of totally synthetic proteins, as developed by Dutton,[48] Willner,[49] Haehnel,[50] Degrado,[371] Jensen,[372] and their associates. This area of design and synthesis of functional ET and catalytic proteins parallels the introduction of novel physical electrochemistry particularly in situ STM in bioelectrochemistry.

With a few exceptions, redox metalloprotein voltammetry on gold surfaces is unstable or absent unless the electrode is modified by chemisorbed monolayers of linker or promoter molecules. The linker molecules are usually thiol-containing molecules which adsorb strongly on the Au surface, Figure 14. The opposite end holds a functional group that interacts "gently" with the protein, ascertaining that the protein is immobilized in a well-defined orientation retaining full ET or enzyme functional integrity. Strategies for specific linker/protein interactions are broadly available but the interactions are often subtle. Closely related linker molecules can induce widely different protein voltammetric responses, and linker groups with no immediate expectable protein compatibility can arouse strong voltammetric signals (e.g., ref 136). Surfaces of commonly used polycrystalline pure or functionalized gold or edge plane pyrolytic graphite electrodes obviously enable extracting molecular mechanistic information far beyond redox potentials. The surfaces are, however, inherently structurally ill-defined and restrict the use of other surface techniques, particularly the scanning probe microscopies. Single-crystal electrode surfaces offer at the same time improved voltammetric resolution and enable surface structural characterization at the atomic or molecular level directly in aqueous buffer solution.

Figure 14 showed in situ STM images of Au(111) surfaces modified by a variety of thiol-based linker molecules, all

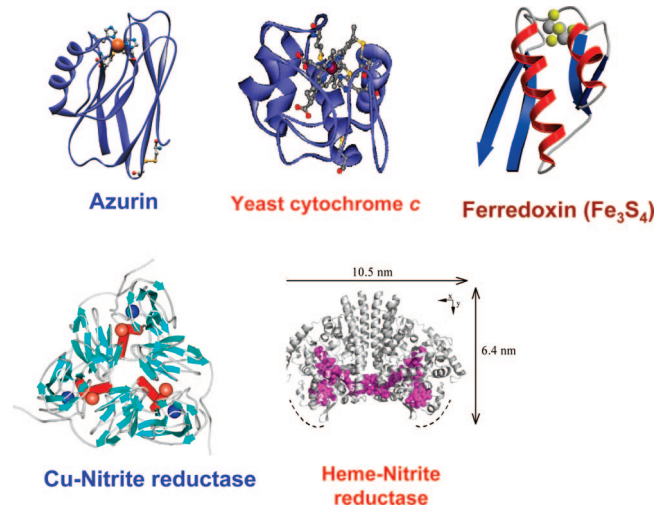

Figure 26. Redox metalloproteins characterized by protein voltammetry at single-crystal Au(111)-electrode surfaces and by electrochemical in situ STM. Origin of three-dimensional structures given as PDB file numbers. Reference numbers refer to the single-molecule studies. Top row: The blue copper protein *P. aeruginosa* azurin (PDB 4AZU, left),[118–126] yeast (*Saccharomyces cerevisiae*) cytochrome *c* (PDB 1YCC, middle),[131,132] and *Pyrococcus furiosus* ferredoxin (PDB 1SJ1, right).[133] Bottom row: *A. xylosoxidans* Cu-nitrite reductase (PDB 1UAU, left)[135] and *Escherischia coli* deca-heme nitrite reductase (PDB1GU6 right).[137]

forming highly ordered monolayers analyzed in structural detail. By their different positively and negatively charged, or hydrophobic and hydrophilic terminal functional groups the molecules have been efficient promoters in protein and enzyme voltammetry. Most of the linker molecules are stable over broad potential ranges limited by reductive and oxidative cleavage of the Au−S bond. High sensitivity to even traces of molecular dioxygen is, however, frequently encountered.[373] In situ STM images such as these offer an impression of the microenvironment in which immobilized redox metalloproteins and metalloenzymes "in action" operate.

6.2. Redox Metalloproteins at Bare and Modified Au(111) Electrodes

Interfacial electrochemical ET of metalloproteins has been reviewed extensively.[39–42,349,351] Figure 26 shows an overview of redox metalloproteins and metalloenzymes that have been characterized by protein film voltammetry at pure and modified single-crystal Au(111)-electrode surfaces, and further addressed by spectroscopic and other surface technique including particularly in situ STM under electrochemical potential control. Single-molecule focus has mostly been on imaging but tunneling spectroscopy in both ex situ and in situ STM or conducting AFM have also been reported, cf. below. We attend to these systems in turn.

6.2.1. Pyrococcus furiosus Ferredoxin

Pyrococcus furiosus ferredoxin (*Pf*Fd) is a representative of the iron−sulfur proteins as one of the three major classes of ET metalloproteins, with the molecular mass 7.5 kDa and a single $[3Fe\text{-}4S]^{+/0}$ redox center, Figure 26. The thermophilic bacterial protein is stable in anaerobic environments and retains biological activity even at 80 °C. The X-ray crystal structure at 1.5 Å resolution has become available.[374] The protein is strongly negatively charged except for a

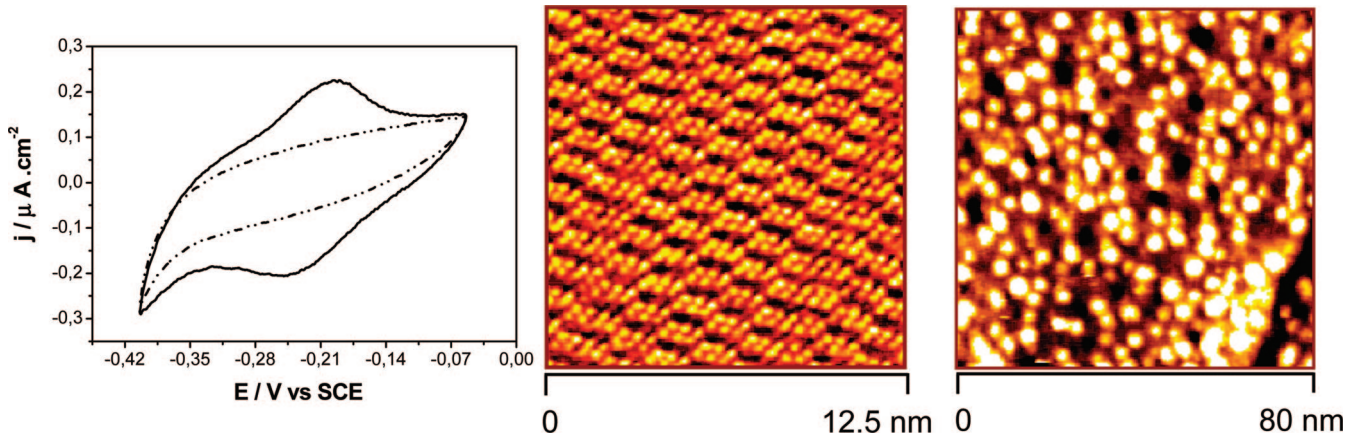

Figure 27. *Pf*Fd on single-crystal Au(111)-electrode surface modified by a highly ordered mercaptopropionic acid monolayer. 5 mM phosphate buffer, pH 7.0.[133]Left: Cyclic voltammogram corresponding to the $[3Fe4S]^{0/+}$ couple. Middle: In situ STM image of ordered MPA monolayer. Right: In situ STM image of *Pf*Fd molecules on the MPA/Au(111)-electrode surface. Reprinted with permission from ref 133. Copyright 2004 American Chemical Society.

positively charged "spot" around the surface-located [3Fe-4S] center. Direct electrochemistry of *Pf*Fd and other iron−sulfur proteins both in homogeneous solution and in the adsorbed state (at polycrystalline electrode surfaces) has been extensively studied (references in ref 133). Here we focus on monolayer voltammetry, surface organization, and in situ STM of *Pf*Fd at modified Au(111)-electrode surfaces.

Surface linking of fully active *Pf*Fd on a highly ordered monolayer of mercaptopropionic acid, MPA is achieved, Figure 27.[133] The *Pf*Fd/MPA/Au(111) electrode gives a single pair of redox peaks corresponding to the $[3Fe\text{-}4S]^{0/+}$ couple, Figure 27. Modification by binding to neomycin in solution induces a second pair of one-electron peaks probably corresponding to the $[3Fe\text{-}4S]^{0/-1}$ transition. Linking of the negatively charged protein to the negatively charged MPA/Au(111)-surface points to local positive charges around the surface [3Fe-4S] cluster and perhaps MPA-protonation as determining factors.

Figure 27 also shows an in situ STM image of the *Pf*Fd adlayer. As for *Pf*Fd voltammetry, in situ STM of this protein requires strict anaerobic conditions. Electron transferring protein molecules cover the whole surface, as seen by the high density of bright spots. The 3.0−3.5 nm diameter corresponds to the crystallographic dimensions of the *Pf*Fd molecule and the structural surface density accords with the coverage determined by voltammetry. The combination of high-resolution voltammetry and in situ STM thus points to a standing issue in protein film voltammetry, namely the fraction of adsorbed protein molecules that retains voltammetric activity in the adsorbed state. This fraction is about 60% for *Pf*Fd/MPA/Au(111). A small part of the surface-confined *Pf*Fd molecules appears as dimers, according with the existence of similar dimer structures in the crystal lattice of *Pf*Fd.[374]

The single-crystal voltammetry, surface promoter sensitivity, and in situ STM of *Pf*Fd illuminate the highly increased resolution in bioelectrochemical mapping of redox metalloproteins now available. In another recent study of the [4Fe-4S] form of *Pf*Fd, Heering and associates extended the single-molecule aspect of this protein toward a biosensor perspective.[375] The native and several mutant proteins were immobilized in electrochemically functional states via surface-exposed thiols on evaporated gold surfaces and were characterized by voltammetry, XPS and AFM. While complicated by nonelectrochemical gating and inhomogeneous broadening features addressed in the report, the protein largely retained functional integrity in the immobilized state as reflected in observed equilibrium potentials close to those of the protein in bulk solution. The AFM mode used was air ambient that raises issues as to the redox state and the compatibility with the anaerobic working aqueous environment of the protein. The monolayer stability was, however, checked by voltammetric sampling before and after drying. The AFM protocol is therefore perhaps at most "reversibly compromised" and the images representative of the protein in solution.

6.2.2. The Heme Proteins: Horse Heart and Yeast Cytochrome c, De Novo Designed Synthetic 4-Alpha Helix Bundle Heme Protein and Two-Center Cytochrome c_4

The group of small (MW ≈ 12 kDa) heme proteins, the cytochromes *c* have emerged as prime target metalloproteins both in the early pioneering studies of protein electrochemistry[345–347] and in many later studies of interfacial bioelectrochemistry at multifariously modified metal electrodes.[376–380] To this adds a wealth of studies of protein folding and other biophysical properties of cyt *c*-based molecules.[381,382]

Surface residues suitable for linking the protein to the electrode surface in orientations favorable for interfacial ET are noted as crucial. The molecular structures of mammalian, here horse heart, HHC and yeast cyt *c*, YCC, both important bioelectrochemical target metalloproteins, illustrate this, Figure 28. The redox active heme group is located asymmetrically in the protein structure as common for ET metalloproteins. The protein surface structure around this site is therefore crucial. A group of positively charged lysines around the heme group is a common characteristic of the cyt *c*'s and has been noted as crucial in the achievement of facile reversible cyt c voltammetry. The lysines interact with linker groups on the electrode surface by electrostatic forces or hydrogen bonding to keep the protein on the surface in an orientation favorable for electrochemical ET, gently enough that the protein retains structural and functional integrity.

The cyt c probe versatility offers another route to productive surface immobilization. As a difference from HHC, YCC has a Cysteine-based (Cys102) thiol group close to but not

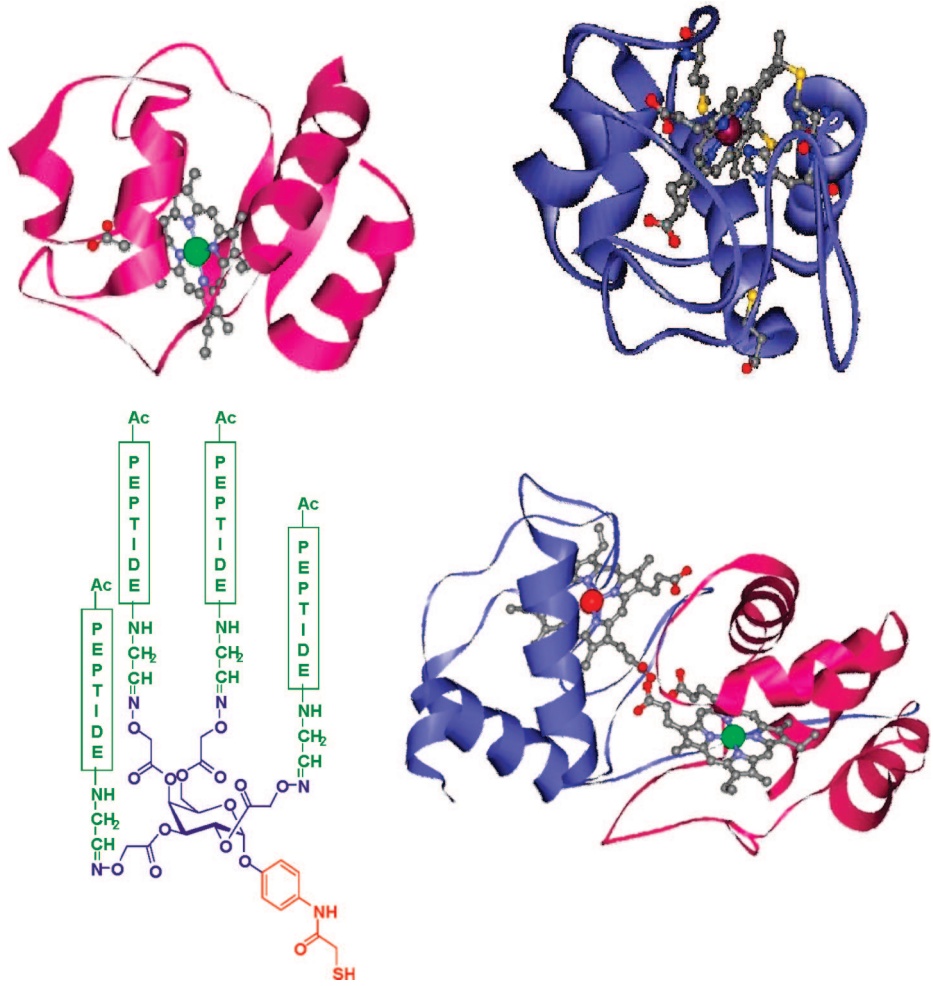

Figure 28. Three-dimensional structures of cyt *c*-based molecules addressed. Top left: horse heart cyt *c* (PDB 1HRC)[381,382] (regarded here as a "reference" molecule). Top right: yeast (*Saccharomyces cerevisiae*) cyt *c* (PDB 1YCC).[131,132] Bottom left: De novo totally synthetic *b*-type cyt *c*.[50] Bottom right: Two-center cyt c_4 (*Pseudomonas stutzeri*) (PDB 1EPT).[391]

directly at the protein surface, Figure 28. The Cys102 surface group is potentially a suitable linker for binding to electrochemical Au-surfaces. In spite of the Cys102 remote from the heme group, YCC binding via this group appears to retain protein ET function, although with different reported stability.[131,132] The Cys102 linking mode has also offered a route to AFM[132] and in situ STM imaging[131] at the level of the single molecule (see also ref 383).

6.2.2.1. Horse Heart Cytochrome *c*. As a key target, HHC is probably electrochemically the most comprehensively addressed metalloprotein. Focus in recent cyt *c* monolayer voltammetry as studied by Bowden,[376] Niki,[380] Hildebrandt and Murgida,[378,379] Waldeck and Khoshtariya,[377,379] and their associates has mapped in great detail structural and dynamic issues such as spectroscopic interconversions among different spin and axial ligand states by surface enhanced resonance Raman (SERS) and infrared spectroscopy (SEIRAS). These studies have disclosed the potential dependent structural and spin variability of surface-confined HHC of importance for the understanding of the behavior of HHC in the microenvironments of the bioelectrochemical electrode/electrolyte interface. Electrostatic and hydrogen bond-controlled binding of HHC and other mammalian cyt *c*'s to terminally functionalized thiol-based linker molecules of variable length and composition on Au-electrode surfaces has been in other focus. Cyt *c* is immobilized by electrostatic forces or axial ligand binding by terminal carboxylate and pyridine groups. Issues disclosed include electron tunneling across the variable-length linker molecules, viscosity effects and kinetic deuterium isotope effects.[378,379]

A common observation is a bimodal dependence of the standard electrochemical rate constant on the length (electrochemical ET distance) of the molecular linkers,[377–379] reencountered in the binding mode of the blue copper azurin, cf. below.[120,121,384] Exponential distance decay with decay factors that clearly reflect electron tunneling, say $\approx$ 1/linker molecular unit (-CH_2-group) is observed above a certain chain length (4−10 linker units). Distance independence is consistently observed at shorter chain lengths. Surface preorganization, or transition from diabatic to relaxational adiabatic control are rationales offered for this pattern.[377–380,384]

In spite of the comprehensive studies of interfacial electrochemical ET dynamics of HHC and related mammalian cyt *c*'s, single-molecule in situ STM structural and functional mapping has been frugal.[187,377,386] Reported studies are fraught with reservations regarding the use of high bias voltage, lack of control of the redox state of the protein, and pretreatment (Piranha solution) known to leave the Au-surface in very rough structural surface states.[387]

6.2.2.2. Yeast (*Saccharomyces cerevisiae*) Cytochrome *c*. Yeast cyt *c* (*Saccharomyces cerevisiae*), YCC, Figure 28 has been a target protein in recent reports that have addressed electrochemical ET at the monolayer and single-molecule

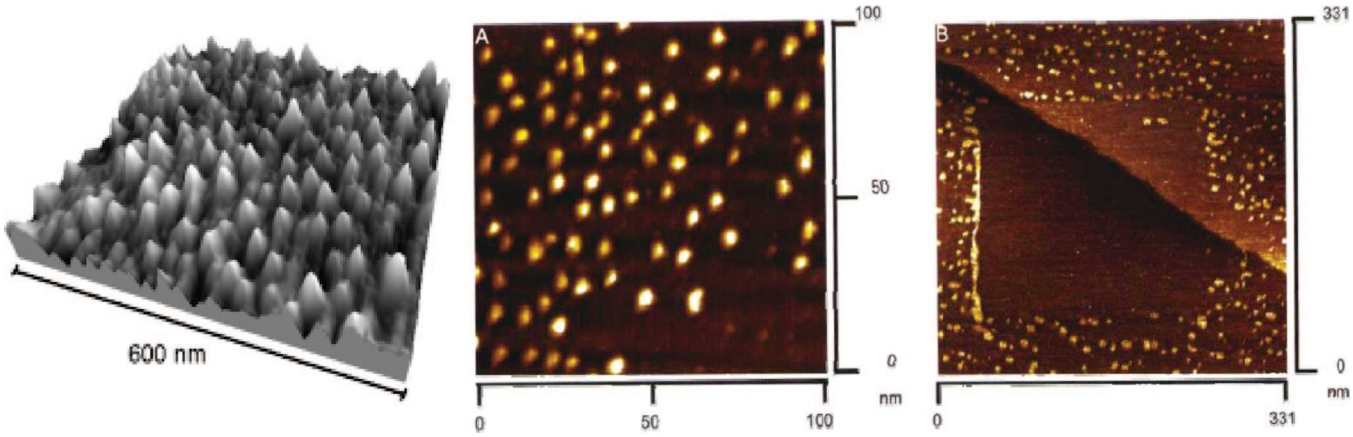

Figure 29. Left: AFM image of YCC on flame annealed Au-on-mica surface. Middle: In situ STM image of YCC on single-crystal Au(111)-electrode surface. Ten mM phosphate buffer, pH 7.5. Right: Controlled tip-induced YCC desorption in a rectangular surface area. Details in refs 131 and 132.

levels.[131,132] The protein surface charge distribution resembles that of HHC and similar patterns of diffusion controlled cyclic voltammetry have been obtained. As noted, YCC offers a second surface linking residue, Cys102 structurally almost opposite the heme group. YCC immobilization by Cys102 thiol linking to Au surfaces may involve conformational adjustment to local electrode surface structures with variability in voltammetric patterns. These expectations are strikingly borne out.

As a nanoscale target ET metalloprotein, YCC has been addressed by protein film voltammetry and other electrochemical methods, AFM, in situ STM, XPS and microcantilever technology.[131,132,383] Voltammetric behavior of Cys102-linked YCC in three reports[131,132,383] ranges from transient via signals of partially denatured protein and strongly inhomogeneous to robust signals of the native protein. The latter extend to catalytic efficiency toward cyt c peroxidase and hydrogen peroxide reduction.[383] The conjecture arises that the Cys102 location slightly below the protein surface may in fact favor slightly roughened electrode surfaces, while single-crystal, atomically planar surface microenvironments may be "too planar" that full structural protein integrity is retained.

XPS and microcantilever technology testify in other ways that YCC binds to Au surfaces via a Au−S link.[131] The similar YCC and HHC XPS sulfur signals are, however, notable. The UHV conditions of XPS are probably detrimental to these heme proteins with their α helix based secondary structures, in contrast to the beta-stranded blue copper proteins, cf. below. Both YCC and HHC are likely to unfold completely, exposing all sulfur to the Au surface. Gold-plated microcantilevers of the same kind as used in AFM can be brought to register deflections on adsorption of thiol-linking molecules including Cysteine and YCC.[131] A merit of this technology is that it can register the adsorption process in real time at the monolayer level. Limitations are the polycrystalline nature of the gold layers, the absence so far of electrochemical potential control, and notable difficulties in the reproduction of the signals which are hypersensitive to the structural state of the individual cantilevers.

Two representative scanning probe images of YCC in aqueous buffer are shown in Figure 29, substantiating the presence of YCC on flame-annealed Au-on-mica surfaces and single-crystal Au(111)-electrode surfaces, respectively. Single-molecule AFM in aqueous buffer shows lateral tip convolution, but vertical dimensions that accord with the crystallographic dimensions. Voltammetric signals on this kind of surfaces have been observed. Figure 29, middle shows an *in situ* STM image of YCC on a Au(111)-surface under electrochemical potential control. The lateral dimensions accord with the crystallographic structure whereas the vertical height is now much smaller in spite of vertical in situ Au-step calibration. This observation is common for protein mapping but not for small rigid molecules and will be readdressed below. In some ways the "fragile" binding mode of YCC on single-crystal Au(111)-electrode surfaces can be turned to the better in the way of creating mesoscopic YCC surface organizations, Figure 29, right.

6.2.2.3. De Novo Designed Synthetic 4-Alpha Helix Bundle Heme Proteins. The use of mutant proteins has long been a powerful tool in bioelectrochemistry. Different strategies toward electrochemical interfacial "bioelectronics" have been based on de novo totally synthetic "metalloproteinoids" among which 4-α helix bundle structures outfitted with a suitable linker group, Figure 28 have come to stand forward.[48–50]

De novo totally synthetic 4-α helix bundle one- and two-heme proteins were introduced by Dutton and associates[388] and elaborated by Dutton,[48] Hahnel,[389] DeGrado,[371] Willner,[49] Jensen,[372] and their associates. Broad electrochemical characterization was also reported. De novo totally synthetic 4-α helix bundle proteins per se and with a heme group coordinated inside the protein structure have also been molecular targets in efforts toward single-molecule electrochemistry.[50,372]

The de novo totally synthetic 4-α helix bundle proteins can be immobilized on gold surfaces via suitable linker groups.[48–50] In situ STM of the de novo totally synthetic 4-α helix bundle proteins has also been introduced.[50,372] Two recent studies illustrate the potential and limitations of this approach. Synthetic alpha helices need a template where either a carbohydrate[372] or a cyclic peptide[50] has been offered. De novo carbohydrate-templated 4-α helix bundle proteins, so far without a redox active metal center can be immobilized on Au(111) surfaces and characterized by the voltammetry/XPS/in situ STM combination. Dense and structurally unresolved monolayers are identified. Electrochemical potential stepping toward the potential of reductive desorption of the thiol-based linker, however, discloses molecular-size strong in situ STM contrasts.[372] These testify to molecular resolution and expectable potential dependent

in situ STM contrast variation which is, however, fraught with the irreversible feature of the electrochemical desorption process.

Voltammetry at single-crystal Au(111) electrodes and in situ STM to single-molecule resolution of a de novo totally synthetic single-heme 4-α helix bundle protein was also reported[50] disclosing another element of in situ STM of redox (bio)molecules. Single-molecule imaging was clearly obtained but expected overpotential dependent redox-based in situ STM tunneling contrast variation could not be detected. This can probably be traced to the location of the heme group in the molecular structure of the protein. The heme group is coordinated between the four helices almost midway along the helices. This site is too remote from the electrode surface to be a dominating redox-based ET path. A multitude of other, essentially superexchange pathways compete and blur the redox pathway. This resembles the behavior of the Co complex discussed in section 5.5 Overall the de novo (metallo)proteins may have offered proof-of-principle single-molecule functionality but there is a way to go before they can compete with native and mutant protein function in pure and applied single-molecule "bioelectronics".

6.2.2.4. Other Cytochromes *c*: Two-Center Cytochrome c_4. A crucial notion in biological electron transport and enzyme catalysis is long-range ET between localized metal centers. A second feature is that ET function is frequently undertaken by proteins that contain several redox centers which "communicate" mutually by electrostatic forces or via the protein conformational system. The comprehensive mapping of cooperativity in the four-heme cytochromes c_3 has, for example led to microscopic understanding of this protein to an extent that resembles the cooperative oxygenation equilibria of the four heme groups in hemoglobin.[390] The large number of interheme contacts and microscopic redox potentials is, however, prohibitive for complete mapping. Redox metalloproteins with two centers offer special perspectives. Two-center proteins are prototypes for multicenter ET but structurally and functionally simple enough that complete thermodynamic, spectral and kinetic mapping is within reach.[391]

Two-center redox metalloproteins addressed along such lines include the modular redox metalloprotein *Desulfovibrio desulfuricans* desulfoferredoxin[392] and the diheme protein cytochrome c_4 from several bacterial species.[391] Cyt c_4 from *Pseudomonas stutzeri* has been a suitable target for electrochemical approaches to the electronic communication between the two centers.[385,391,393,394] The protein holds two almost equally sized domains each resembling cyt *c*, separated by a short peptide chain, Figure 28. The distance between the two Fe-atoms is 19 Å, with strong hydrogen bond contacts between a propionate from each heme group.

Rate constants for intermolecular electron exchange with organic and inorganic reaction partners of *P. stutzeri* cyt c_4 in solution have been mapped.[391,393,394] The dipolar nature of cyt c_4 offers the option that cyt c_4 can be immobilized on modified gold electrode surfaces in orientations with either the low- or the high-potential heme group adjacent to the surface.[385,393] Two-electron electrochemical processes then proceed only via intramolecular ET. This has provided values for the intramolecular ET rate constants and intriguing electrochemical "rectification" in the cyclic voltammograms, with perspectives for similar bioelectronics at the single-molecule level not available for single-center metalloproteins.

6.3. The Blue Copper Proteins

The blue copper-proteins and -enzymes as strategic targets in single-molecule in situ STM and bioelectrochemistry was introduced early.[116–118,395,396] The blue single-Cu ET protein azurin (*P. aeruginosa*) was in focus prompted by its intrinsic disulfide linker group,[116–118,395,396] now subjected to comprehensive studies,[116–122] further extended in.[47,123–126]

Azurin (*P. aeruginosa*) has inspired other studies toward the single-molecule level under nonelectrochemical, gas ambient conditions where the protein is exposed to very high voltages with expectations for electronic device function.[126,397] Focus in the present subsection is on azurin in electrochemically controlled environments. As a more challenging target molecule the blue copper enzyme, Cu-nitrite reductase is addressed in section 6.4.

6.3.1. The Blue Copper Protein Pseudomonas aeruginosa Azurin: A Nanoscale Bioelectrochemical Paradigm

In separate ways horse heart cyt *c* and *P. aeruginosa* azurin have emerged as electrochemical "paradigms" for protein interfacial electrochemical ET. Horse heart cyt *c* was the key target molecule in the pioneering studies by Kuwana, Niki, Hill, Bowden, and Hildebrandt,[345–347,376,378] and in later stages where for example spectroscopic techniques were introduced in metalloprotein electrochemistry. *P aeruginosa* azurin has been a central target protein also in recent efforts in protein electrochemistry, where physical electrochemical notions such as single-crystal electrode technology and in situ scanning probe microscopy have been in focus.[116,117,116–126]

6.3.1.1. *P. aeruginosa* Azurin on Bare Au(111)-Electrode Surfaces. *P. aeruginosa* azurin is robust to surface manipulation. The protein can be immobilized in dense, although not ordered monolayers directly on single-crystal Au(111) surfaces via disulfide adsorption structurally opposite to the Cu center, strongly evidenced by interfacial capacitance, XPS and other data.[118,120–126] The higher plant analogue, plastocyanin (*Populus nigra*) with an engineered disulfide group inserted has been shown to adsorb in a similar mode.[47,132] XPS of azurin displays, interestingly, signals from both Au−S binding and the S-ligands around the Cu-center. The surface organization is illuminated by in situ STM images, Figure 30 with voltammetric interfacial ET function in the adsorbed state retained.[121]

Attempts to record in situ STM spectroscopy of *P. aeruginosa* azurin adsorbed directly on Au(111)-electrode surfaces have been reported.[123,125,134] Indications of single-molecule redox features may have been discerned but the data were fraught with protein monolayer stability in the confined STM gap or elusive adsorption patterns.[123–125,134] Disulfide based azurin adsorption on gold tips and subsequent insertion in the in situ STM gap appears less compromising in these respects,[124,125] cf. discussion in section 3.

Insertion of the protein in gentler "biomimetic" electrochemical environments leads azurin to show a completely different behavior. *P. aeruginosa* azurin on Au(111)-electrode surfaces in the particular environment where the protein is adsorbed on highly ordered variable-length alkanethiol SAMs[122,384] appears to offer a unique option for fine-tuning and optimizing interfacial electrochemical redox metalloprotein performance.

6.3.1.2. *P. aeruginosa* Azurin on Alkanethiol Modified Au(111)-Electrode Surfaces. Robust and "well-behaved" voltammetry is the first sign that Au(111)-electrode surfaces

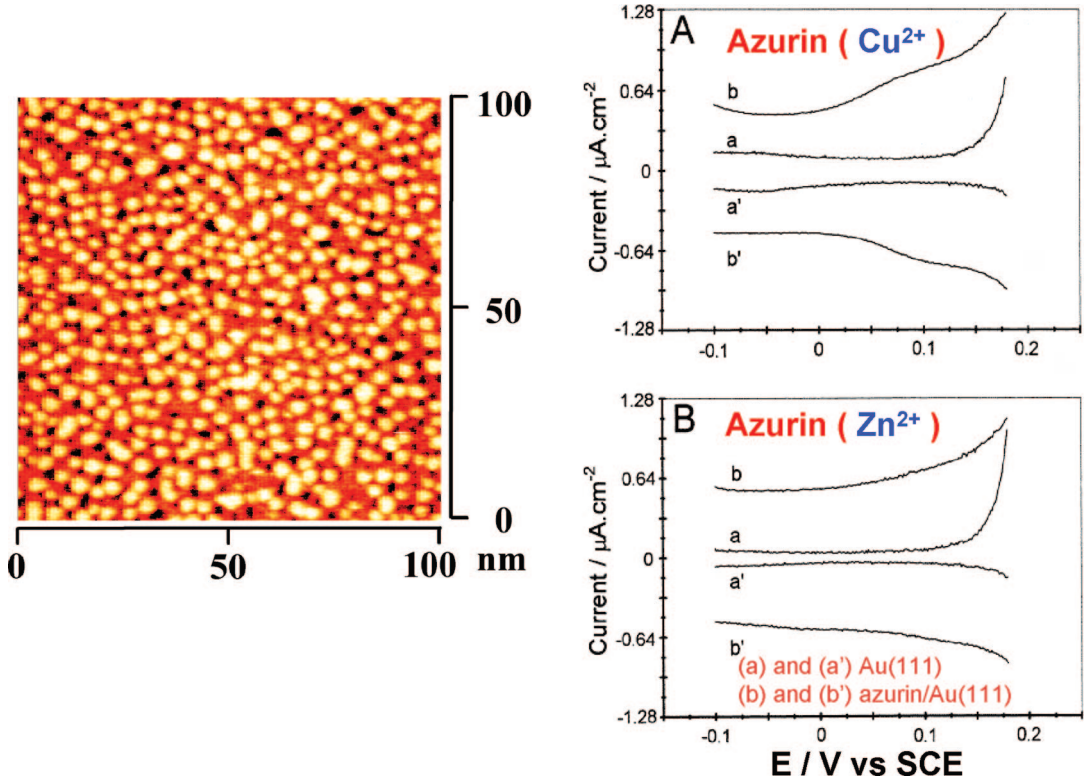

Figure 30. Left: In situ STM image of *P. aeruginosa* azurin on Au(111)-electrode surface. Five mM ammonium acetate. Right: Differential pulse voltammograms of native Cu-azurin and electrochemically inert Zn-substituted azurin. Reprinted with permission from ref 121. Copyright 2000 American Chemical Society.

modified by variable-length alkanethiols constitute close to optimal environment for *P. aeruginosa* azurin adlayer interfacial electrochemistry.[86,384] Figure 31 discloses what appears as almost "ideal" voltammetry. Chain lengths between six and ten carbon atoms give, notably, fast reversible monolayer voltammetry, while interfacial kinetic control, still with highly robust voltammetry takes over for longer chain lengths.

Such data warrant theoretical framing and consideration of *P. aeruginosa* azurin in molecular resolution by in situ STM of the protein in ET action on the modified electrode surfaces. Figure 31, top left, shows an in situ STM image of the protein adlayer. The bright spots are individual azurin molecules. Figure 31, bottom left shows quadratic free energy relations associated with meaningful reorganization free energies, 0.3−0.5 eV, section 3, indicative of strong electronic coupling to the protein and solvent environment. Figure 31, bottom right, shows a bimodal distance dependence of the interfacial electron exchange rate constant. No distance dependence is detectable below a chain length of about ten carbon atoms. Exponential distance decay is observed above this length. The decay factor is ≈1.0 per methylene group, strongly indicative that electron tunnelling across the alkanethiol layer is now a controlling factor. Adsorption isotherms, and kinetic deuterium isotope effects represent other information available by such high-resolution voltammetry.[86,384]

Comparison of the image in Figure 31, left with the voltammograms in Figure 31, middle adds to a standing issue in protein film voltammetry, i.e. the amount of adsorbed protein molecules that retains interfacial ET function, cf. section 6.2.1. Virtually all adsorbed *P. aeruginosa* azurin molecules retain full functionality in the case of undecanethiol-modified Au(111) electrodes. The variable-length, intermediate-size (eight-to-eleven carbon atoms) alkanethiols on the highly uniform Au(111)-electrode surfaces thus point to close to optimal function of immobilized *P. aeruginosa* azurin. Together with the uniform surface structure (compare with a recent quartz crystal microbalance study[398]) this is perhaps rooted in the "biomimetic" environment constituted by a delicate balance between the robust but structurally "soft", hydrophobic microenvironment of the intermediate-length Au(111)-alkanethiol layers and the hydrophobic functional protein. Similar "surface-padding" has been exploited in other recent studies of azurin mutants.[399]

P. aeruginosa azurin on alkanethiol-modified Au(111)-electrode surfaces is, finally, robust enough that single-molecule in situ scanning tunnelling *spectroscopy* can be recorded. Resonance features of the same electronic origin as discussed in section 3 and displayed by Fe-protoporphyrin IX and the Os-complexes, section 5 emerge at the single-molecule level. Figure 32shows a series of in situ STM images of single azurin molecules on a Au(111)-electrode surface modified by a highly ordered undecanethiol SAM, recorded at different overpotentials. The bias voltage is constant, i.e. substrate and tip potentials are varied in parallel as for Fe-protoporphyrin IX.[83] The structural resolution is demonstrated by the single-molecule features of both the azurin molecules and of the ordered alkanethiol monolayer underneath. The tunneling spectra are recorded as normalized "apparent heights" in the constant current mode rather than directly as current as for the Os complexes. A robust resonance feature appears close to the equilibrium redox potential, with a maximum about nine times higher than the background.[86]

The comprehensive data for electrochemical azurin surface dynamics have pointed toward meritorious properties of this metalloprotein as a target molecule for combining bioelec-

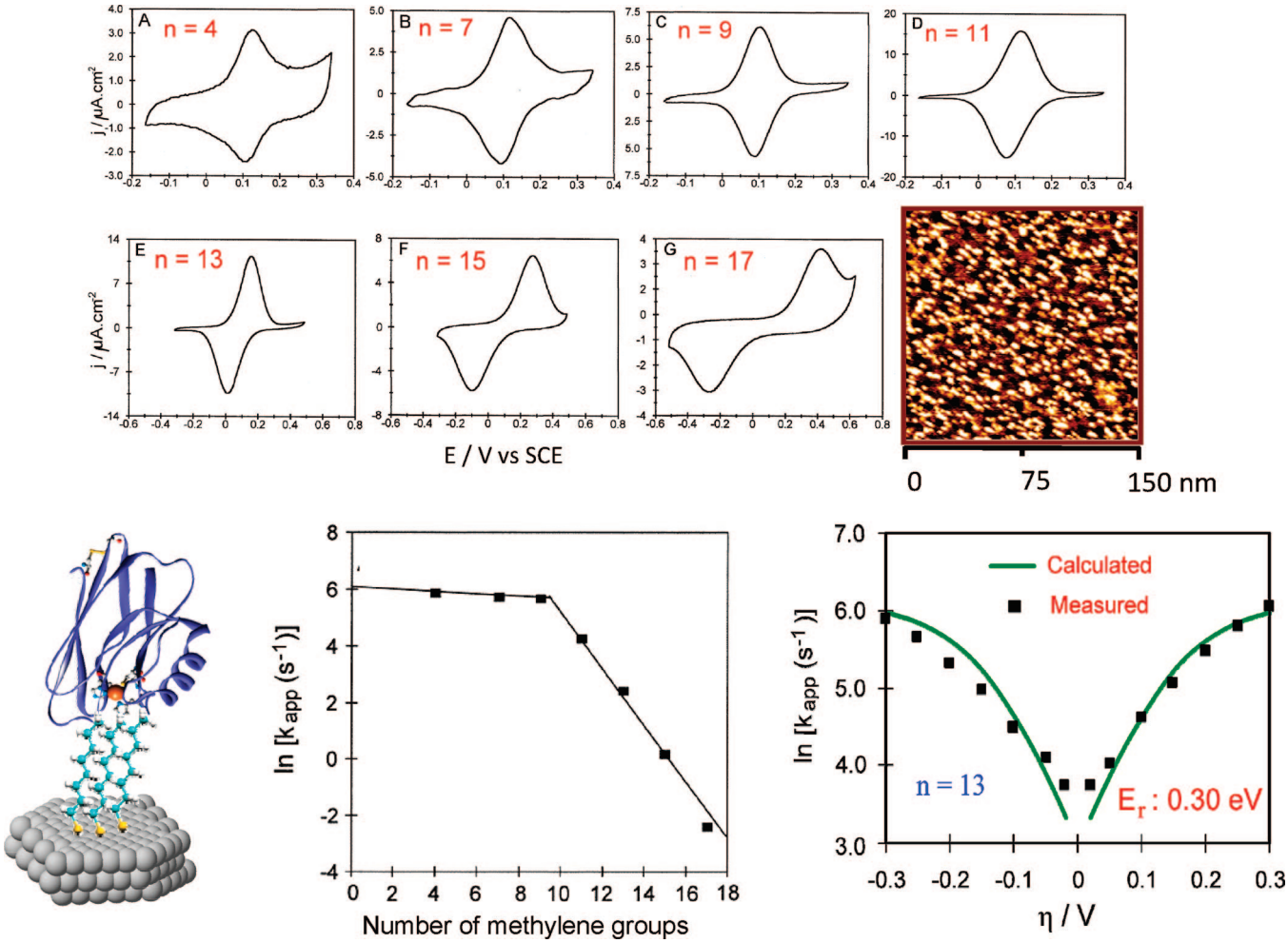

Figure 31. Top: Top row: Cyclic voltammograms of *P. aeruginosa* azurin on variable-length alkanethiol-modified Au(111)-electrode surfaces. The number of methylene groups indicated by the quantity *n*. The in situ STM image shows *P. aeruginosa* azurin on undecanethiol-modified Au(111)-electrode surface. Working electrode potential +0.20 V (SCE), $V_{bias} = -0.20$ V. Bottom, left: Schematic view of *P. aeruginosa* azurin on the alkanethiol-modified Au(111)-electrode surface. Bottom middle: Dependence of the electrochemical exchange rate constant k_{app} (s^{-1}) on the number of CH_2-units. Bottom right: Quadratic dependence of the electrochemical ET rate constant, on the overpotential on $CH_3(CH_2)_{13}S$-modified Au(111)-electrode surface. Data from refs 86 and 384.

trochemistry with single-crystal electrodes and in situ scanning probe microscopies. The robust and well-defined protein film voltammetry, high-resolution in situ STM and feasibility of in situ scanning tunneling spectroscopy have further warranted the use of theoretical notions to an extent comparable to that for transition metal complexes and other "small" molecules, cf. section 3.10.

6.4. Redox Metalloenzymes in Electrocatalytic Action at the Single-Molecule Level: The Multicopper and Multiheme Nitrite Reductases

The nitrite reductases are central in the bacterially controlled global biological nitrogen cycle where they catalyze the reduction of nitrite to lower oxidation states of nitrogen, in some cases right down to ammonia.[400–402] There are three major classes of nitrite reductases. The copper nitrite reductases, CuNiR are trimeric enzymes where each 36 kDa monomer contains a type I Cu center for electron acceptance from an external reducing reaction partner and a type II center for catalytic NO_2^- reduction to nitrogen monoxide, Figure 33.[400] The second, heme or cyt *c* based nitrite reductase class is a homodimeric enzyme holding altogether ten redox active heme groups.[352,401] Notably, the equilibrium redox potentials of the heme groups in this composite redox metalloenzyme have been resolved.[352,400] The third class is the two-heme cyt cd_1-type nitrite reductases.[383,402] All the three enzyme classes have been structurally resolved to high resolution. Rationales for CuNiR as novel single-molecule targets are:

The type I center resembles the type I center of the simpler ET protein azurin, which offers comprehensive reference frames. As also for azurin, the protein surface around the type I center is largely hydrophobic but as a difference from azurin, with discrete charges scattered over the surface, Figure 33 (pH 6−7). The two Cu-centers are connected via a direct covalent link for facile ET between the Cys130 ligand in the type I center and the His129 ligand in the type II center, Figure 34.

Intramolecular ET between the two centers coupled with electrons from an external donor into the protein at one center and out of the protein in NO_2^--reduction at the other center, is a crucial feature of the enzyme function. The electrons are supplied from the electrode to the type I center in the voltammetric processes, Figure 34.

A final aspect is that the substrate, i.e., nitrite is a small molecule structurally not detectable by in situ STM on the enzyme background. As frequently observed in the enzyme voltammetry including that of CuNiR, binding of substrate

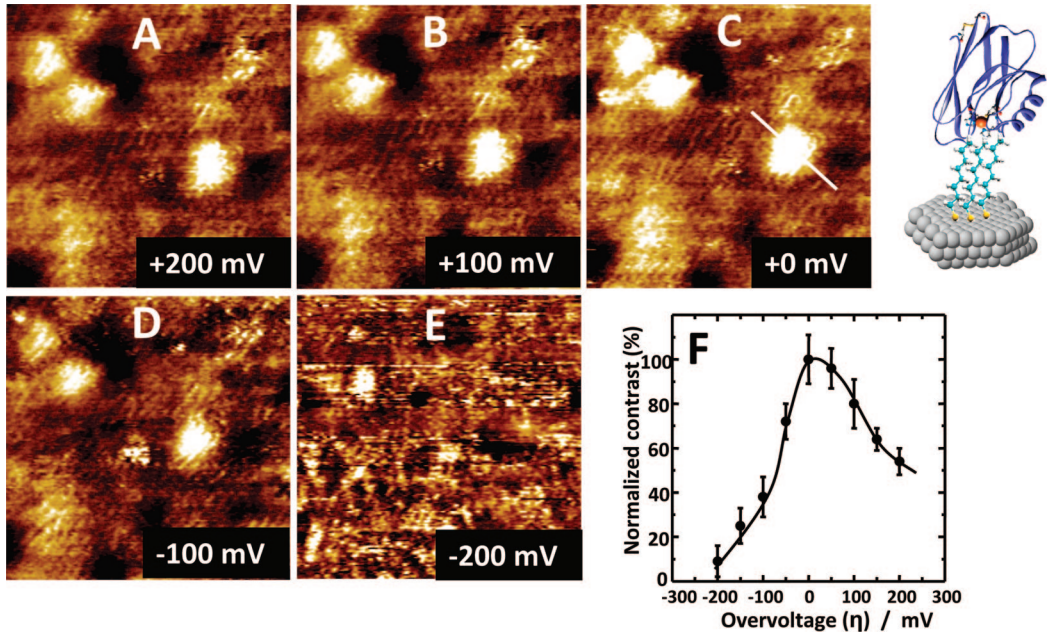

Figure 32. Sequence of in situ STM images of redox gated electron tunneling through a single *P. aeruginosa* azurin molecule on top of a highly ordered octanethiol monolayer (distinguished underneath the azurin molecules) covering the Au(111)-electrode surface. Five mM ammonium acetate, pH 4.6. $V_{bias} = -0.2$ V. Variable overpotential as shown. Figure at the bottom right shows the normalized tunneling contrast with a resonance feature close to the equilibrium potential. Data from ref 86.

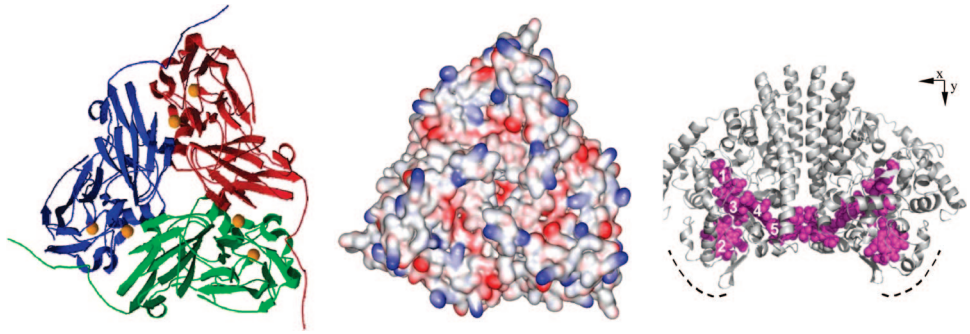

Figure 33. Left: Three-dimensional structure of *A. xylosoxidans* CuNiR (PDB 1HAU). The view is along the 3-fold axis and the three monomeric units are indicated by different colors. Middle: Same view of CuNiR showing the protein surface electrostatic charge distribution. Red represents negative and blue positive surface charges. Right: View of *E. coli* deca-heme nitrite reductase (PDB1GU6). Data from Protein Data bank.

induces, however, significant electronic changes in the enzyme, notably in the contact between the electron acceptance center and the electrode surface.[135,136] This holds other prospects for electronic mapping of the enzyme directly in action at the single-molecule level.

Achromobacter xylosoxidans CuNiR as a representative of the CuNiR class is electrocatalytically active on modified Au(111)-electrode surfaces.[135] The voltammetric patterns are controlled by subtle combinations of hydrophilic and hydrophobic surface properties of many noncovalent surface linker molecules tested.[136] Combined electrocatalytic voltammograms and in situ STM of the enzyme in catalytic action, Figure 35, are illustrative. "Good" electrocatalytic voltammetry with close to full catalytic activity compared with homogeneous solution is observed using several linker molecules. In some but far from all cases noncatalytic voltammetry as well as bidirectional catalysis are also found. Subtle structural changes on substrate binding transmitting to the (modified) electrode/metalloenzyme contact must here be involved. Wijma and associates[403] reported recently a voltammetric study of another CuNiR (*Alcaligenes faecalis* S-6) on edge-plane pyrolytic graphite electrode. In spite of structural inhomogeneity of the electrode surface ("distributions of the heterogeneous ET rates") the study could map

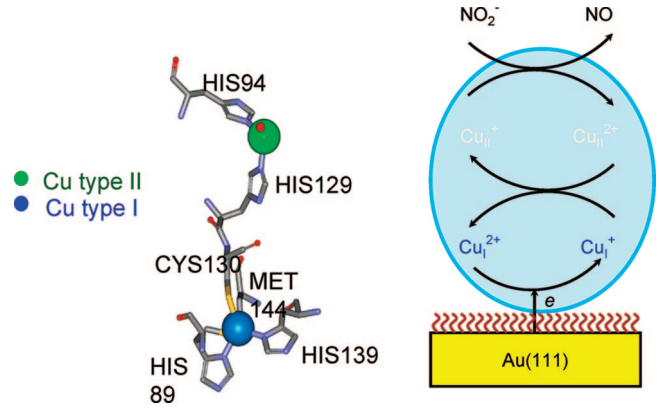

Figure 34. Left: covalent link between the Cys130 ligand of the type I Cu-center and the His129 ligand of the type II Cu-center in *A. xylosoxidans* CuNiR, offering a facile intramolecular ET route between the two centers. Right: Schematic view of CuNiR on a modified Au(111)-electrode surface. The electrode supplies the electrons which are transmitted from the type I center to catalytic action at the type II center by intramolecular ET.

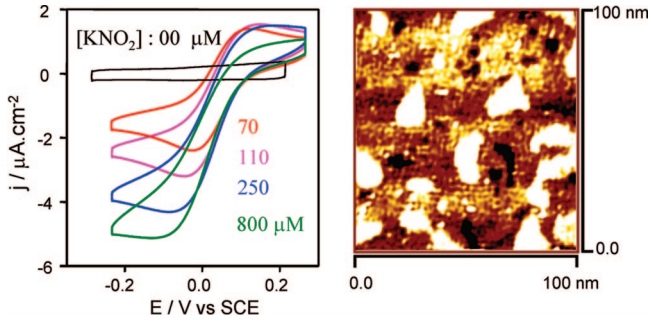

Figure 35. Left: Cyclic voltammograms for nitrite reduction catalyzed by a CuNiR submonolayer on cysteamine-modified single-crystal Au(111)-electrode. Five mM acetate buffer pH 6.0. Right: In situ STM image of CuNiR molecules in electrocatalytic action on the same surface. Reprinted with permission from ref 135. Copyright 2003 American Chemical Society.

the electrocatalytic NO_2^- reduction mechanism including the disclosure of a dual path mechanism and interconversion between active and inactive catalytic type II states.

A notable outcome of the studies in refs 135 and 136 is that the enzyme "in action" on cysteamine- and benzylthiol-modified Au(111)-electrode surfaces can be directly observed at the level of the single molecule, Figure 35. Enzyme molecules even with the triangular crystallographic CuNiR substructure visible are thus observed. These structures only appear when nitrite substrate is present. While presently not as advanced as single-molecule fluorescence-induced enzyme blinking, section 2, the electrochemical single-molecule CuNiR patterns thus still hold a perspective for following single-molecule electrochemical redox metalloenzyme activity. The choice of electrochemical redox enzymes and structurally small substrate molecules that only induce electronic but no molecular structural features are paramount in these observations.

Butt and associates have studied the voltammetry of the (*Escherichia coli*) deca-heme class of nitrite reductases.[352] Well-defined although unstable catalytic multielectron voltammetric reduction of nitrite by the enzyme immobilized by adsorption on bare Au(111)-electrode surfaces is notable. Electrode prefunctionalization is otherwise broadly needed in metalloenzyme monolayer voltammetry. The decaheme nitrite reductase constitutes a second case for in situ STM of a redox metalloenzyme to single-molecule resolution but precise image interpretation is presently not at the level for CuNiR.[137] Molecular-scale structures can be observed on the Au(111)-electrode surface under conditions where the enzyme is electrocatalytically active, with both the natural dimer and surface-dissociated monomer enzyme structures identified. In contrast to CuNiR, molecular conductivities (in situ STM contrasts) are little distinctive between enzyme and active enzyme/substrate states. Even though the enzyme is macroscopically active, direct immobilization on the pure Au(111)-electrode surface is probably still too strongly invasive on the enzyme structure and function.

The single-molecule electrochemical studies of the nitrite reductases suggest further strategies. Suitable electrode surface modification can stabilize the metalloenzyme monolayers. Together with the strategic choice of enzymes with structurally small substrate molecules, the electronic structural changes on enzyme/substrate complex formation can, further be isolated from molecular structural changes in the in situ STM mapping. A study by Heering and associates of *Paracoccus denitrificans* cyt cd_1 CuNiR on polycrystalline gold surfaces[383] suggests other strategies. The enzyme gives no electrochemical signals of its own but electron relay via coadsorbed YCC, Section 6.2.2.2 arouses cyt cd_1 CuNiR signals even at the zeptomole level. Combination with single-crystal electrode surfaces and scanning probe microscopies could take this sensitivity further toward the single-molecule level.

6.5. A Few Notes on Single-Molecule Bioelectrochemistry

Protein film voltammetry of both small ET metalloproteins and composite metalloenzymes have evolved over the past decade, and single-crystal electrodes have paved the way for the scanning probe microscopies, STM and AFM in new bioelectrochemistry. The discussion above has illuminated the combination of protein film voltammetry with these new technologies. High-resolution images have been achieved for the intermediate-size molecular promoters and "building blocks" of the biological macromolecules, i.e., amino acids and related types of molecules which form highly ordered monolayers on Au(111)-electrode surfaces. Dynamic surface phenomena such as phase transitions can also be followed. The degree of image detail in both individual adsorbate molecules and their lateral organization holds clearly perspectives for the understanding of the interaction of "biological liquids" with solid surfaces.

Improved voltammetric resolution of redox metalloproteins on modified Au(111)-electrodes and single-molecule structural resolution have been achieved for the three classes of ET metalloproteins and two composite multicenter redox metalloenzymes under conditions where the molecules are fully active in ET or enzyme function. This opens the perspective that not only structural mapping, but given adequate theoretical support, ET and redox enzyme function can also be addressed at the level of the single molecule.

The behavior of P. aeruginosa azurin supported by studies of smaller redox molecules has illuminated these perspectives. The comprehensive data for electrochemical P. aeruginosa azurin surface dynamics have disclosed meritorious properties of this metalloprotein as a target for combining bioelectrochemistry with single-crystal electrodes, surface spectroscopy, and in situ scanning probe microscopies. The robust and well-defined protein film voltammetry, high-resolution in situ STM imaging, and feasibility of in situ STS have, further warranted theoretical notions to an extent comparable to that for transition metal complexes and other "small" molecules.

7. Electrochemical Biomolecular Metalloprotein/Inorganic Hybrid Structures

Inorganic structures in the form of particles, tubes and other forms of controlled size and shape have reached the same size range as molecules and biomolecules such as proteins and DNA-fragments. This is also a core size range of physical and chemical nanotechnology where properties such as the electronic structure is gradually transformed from macroscopic solid state to single-molecule behavior. The combination of inorganic metallic and semiconductor structures with comparable-size (bio)molecules into biological/inorganic "hybrid" structures with highest possible controlled stoichiometries is therefore an important new notion.[54,55,104–110,168,186,368,404,405] Nanoparticle- and nano-

wire-based electroanalytical chemistry and biological diagnostics go far beyond the "proof-of-principle" level and have come to real applications of importance.[54,55] The molecular electronics aspect involving one-, two, and three-dimensional molecular-scale nanoparticle-based hybrid structures offer other technological perspectives but presently rather at the level where working principles have been identified and documented, section 2.

The scope of the final Section of the present review is first to address some issues of variable-size gold nanoparticles (Au-NP) at electrochemical surfaces and electrochemical in situ STM where the variable size is directly reflected in electrochemical and in situ STM charging behavior. This will be followed by discussion of some bulk and electrochemical properties of "hybrids" between Au-NPs and (a) redox metalloprotein(s)[114,405] as well as a few observations on biomolecular/nanotube hybrids.[104–110] We refer to recent reviews for the chemical synthesis, surface assembly and architectures, and hybrid-based nanocircuitry, as well as biological sensing and other technology perspectives.[54,55,243,406–409]

7.1. Variable-Size Gold Nanoparticles in Electrochemistry and In Situ STM

7.1.1. A Primer of Au-NP Physical Properties in Liquid-State Environment

Physical and chemical properties of solute pure and monolayer-coated ("capped") Au-NPs affect a range of pure and applied colloid and surface science even with a historical dimension of several thousands years.[407–409] Facile chemical synthesis introduced by Schmid[409] and by Brust and Schiffrin[410] have boosted Au-NP and other metal-NP science toward characterization of the physical properties of these core nanoscale metallic entities by multifarious techniques and in a variety of UHV and aqueous or other liquid-state environments. Physical properties in Au-NP focus have been the surface Plasmon optical extinction band (i.e., absorption and scattering),[411–413] scanning and transmission electron microscopy and electrochemical properties of surface-immobilized coated Au-NPs.[413–419] The latter include a range of studies that cover not only solid/electrolyte interfaces but also interfaces between two immiscible liquids.[420,421] To this adds an impressive variety of Au-NP cross-linked molecular and biomolecular structures with real and putative applications in (electro)analytical chemistry, biological diagnostics, and in other ways.[54,55,407,408] The 1−5 nm size range is critical for the electronic properties of the Au-NPs. The smallest, i.e., ≤1 nm, particles behave like a similar-sized molecule with a discrete electronic spectrum or a wide HOMO/LUMO gap.[242–244] Intermediate-sized Au-NPs, say 1.6 nm (Au_{145}) to 2.5 nm (already many hundred Au-atoms) display electrochemically detectable Coulomb charging effects at room temperature[242–244,417–419] while the Coulomb energy spacings in larger Au-NPs (≥3−5 nm) are too close for discreteness-of-charge effects at room temperature.

7.1.2. Single-Electron Charging of Coated Au-NPs in Voltammetry and In Situ STM

Metallic NPs, from now on Au-NPs in size ranges below 3−5 nm offer a case for observation of single-electron Coulomb charging (Coulomb blockade) at room temperature and for following the transition from almost bulk metal behavior (>5 nm) via the Coulomb blockade pattern, down to single-molecule behavior, < 1 nm radius.[242,416–418]

Successive Coulomb charging is associated with the electrostatic charging energy increments of the particle,[242] cf. eq 82

$$E_{\text{el.stat.}} = \left(z - \frac{1}{2}\right)\frac{e^2}{C_{\text{NP}}} C_{\text{NP}} = \varepsilon_s R_{\text{NP}} \tag{90}$$

where z is the number of electronic charges (e) already on the particle, and C_{NP} the capacitance of a spherical particle of radius R_{NP}. ε_s is the static dielectric constant of the surrounding medium. The energy separation between successive charge states exceeds the thermal energy, $k_B T$ if

$$\frac{e^2}{C_{\text{NP}}} > k_B T;\ R_{\text{NP}} < \frac{e^2}{\varepsilon_s k_B T} \tag{91}$$

At room temperature this condition accords formally with R_{NP} < 33 nm in vacuum ($\varepsilon_s = 1$) and with R_{NP} < 6−7 nm and R_{NP} < 0.5 nm if the short-range ($\varepsilon_s = 5$) and bulk static dielectric constant of water ($\varepsilon_s = 80$) applies, respectively. These radii should be corrected by the thickness of the protective coating monolayer. 1.6 nm Au-NPs, Au_{145}, are observed to give electrochemical energy spacings of about 0.17 eV,[416–418] corresponding to an "effective" dielectric constant of $\varepsilon_{\text{eff}} \approx 20$ if the radius of the naked particle is used and to $\varepsilon_{\text{eff}} \approx 13$ if the coated particle radius is used.

Quantized electrochemical capacitive charging of variable-size Au-NP monolayers with various protective monolayer coatings in aqueous and organic solvents have been reported.[242–244,406,414–416] Figure 36 shows two examples based on Au_{145} differential pulse voltammetry (DPV). The upper trace shown to the left shows a sequence of no less than 15 successive, almost evenly 170 mV spaced charge states distributed almost symmetrically on either side of the potential of zero charge (pzc). The lower trace shows a quite different pattern for a layer of smaller, Au_{38} (0.8 nm) particles. Successive charge states can still be distinguished but more widely spaced and with a large HOMO/LUMO gap around the pzc, much closer to single-molecule behavior.[417] Figure 36, right shows that successive Coulomb charging can be entangled with other specific effects. The charge steps in this system are only apparent on the anodic side of the pzc, ascribed to specific ion pairing and the degree of hydrophobicity of the electrolyte ions involved.[416]

The importance of metallic NPs intermediate between bulk and molecular scale states prompted early the use of STM for NP-characterization with observed Coulomb charging ("staircases") in tunneling current/bias voltage correlations (at cryogenic temperatures).[422,423] Murray and associates also observed a close correlation between electrochemical capacitive Coulomb charging of hexanethiol-protected Au_{145} in toluene/acetonitrile and a Coulomb staircase in the current/bias voltage relation of the particles at the single- (or few-) particle level in STM.[242,413] The latter was, however, under UHV conditions and at 83 K, i.e. rather different from the electrochemically mapped charging peaks.

A recent study reported Coulomb charging of water-soluble protected 1.6 nm Au-NPs by DPV and electrochemical in situ STM under the same aqueous electrolyte and room temperature conditions, Figure 37.[418] Multiple 0.15 V spaced peaks were observed on the anodic side of the pzc both in

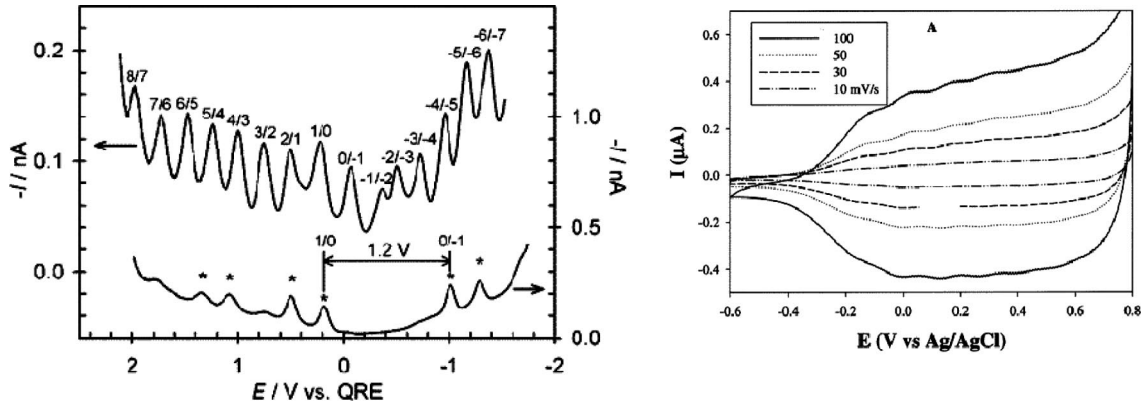

Figure 36. Left: Top: Differential pulse voltammogram (DPV) of hexanethiol-coated Au_{147}−NPs (1.6 nm) in 1,2-dichloroethane solution showing 15 successive redox charge states. Bottom: DPV of similarly coated Au_{38}NPs showing a wide HOMO/LUMO gap. Right: Cyclic voltammogram for butanethiol-coated 2 nm AuNPs in aqueous 0.1 M NH_4PF_6, showing a range of voltammetric capacitive peaks but only in the anodic scan. Reprinted with permission from refs 416 and 417. Copyright 2001 and 2003 American Chemical Society.

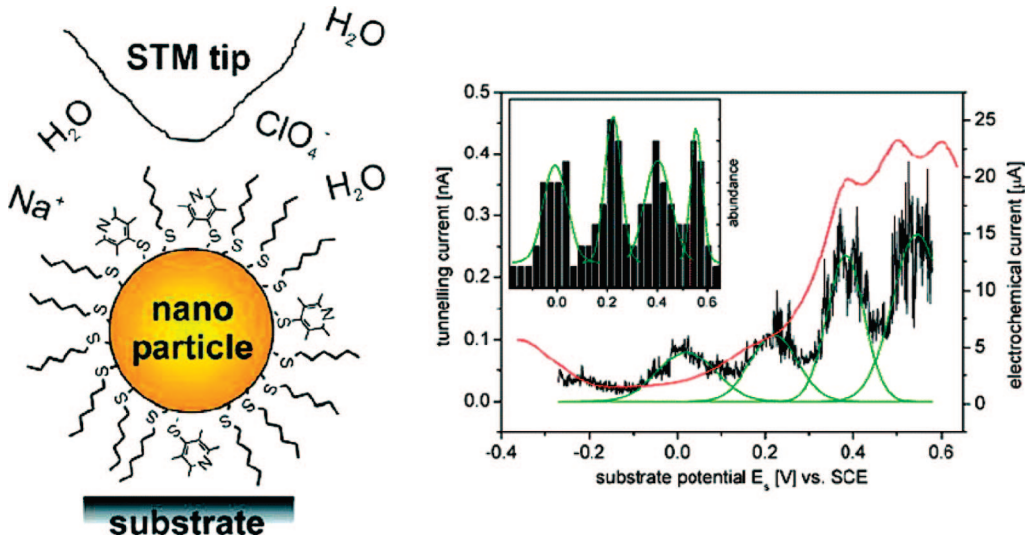

Figure 37. Left: Au_{145} AuNP (1.6 nm) coated with a mixed hexanethiol/mercaptopyridine monolayer in electrochemical in situ STM (schematic). Right: Sequential charging in DPV (red) and in situ STM tunneling current/overpotential correlation at constant bias voltage, 0.05 V (black). 0.1 M $KClO_4$ aqueous solution. Inset: Abundance distribution of the tunnelling current peak positions. Reprinted with permission from ref 418. Copyright 2007 American Chemical Society.

DPV and in situ STM current/overpotential correlation (fixed bias voltage), cf. sections 3, 5 and 6. The peak positions corresponded to 1.1 and 0.9 aF per particle from DPV and in situ STM, respectively. The observations raise the issue whether a molecular-sized AuNP, here 1.6 nm in these contexts is best regarded as a ("quasi-")molecule or as a small metallic entity. The environmental dynamics would strongly affect the ET processes in the former case whereas these effects are minor in the latter case. The former view was taken as the basis of the data treatment but this issue is presently under study.

7.2. Electrocatalysis and Bioelectrocatalysis by Gold Nanoparticles

Protected Au-NPs have been combined with redox metallo- and nonmetalloproteins[114,368,421,424] into covalently, chemisorptively or electrostatically linked "hybrids" of supramolecular biostructures. A seminal report by Xiao and associates,[368] cf. ref 55 illustrates such research. Glucose oxidase could be reconstituted in the chemisorbed state on a 1.4 nm AuNP integrated into a conducting film on an electrode surface. In this state the AuNP acts as a highly efficient electronic relay ("nanoplug") between the electrode and the enzyme with an order of magnitude higher ET rate than in the natural enzyme function.

Au-NP/protein hybrids have become broadly important in electrocatalysis, bioelectrochemistry extending to large protein complexes such as cyt c oxidase, biological recognition, and other areas[54,55] with links even toward notions such as protein-based "nanocircuitry".[368] We note here some issues relevant to the understanding of the protein/NP interactions as reflected in electronic NP/biomolecule interactions and in interfacial electrochemical ET of a protein/NP hybrid with well-defined composition.

Protected Au-NPs immobilized on Au-electrode surfaces are efficient electrocatalysts of both small molecules[424–426] and redox metalloproteins.[54,114,420] A recent study illustrates catalytic and electronic aspects.[114] Strongly positively charged HHC, section 6.2.2 could be linked electrostatically to strongly negatively charged water soluble thioctic acid-protected 3 nm Au-NPs, Figure 38. The stoichiometry appears, notably as 1:1 from the cyt *c* Soret band/NP plasmon

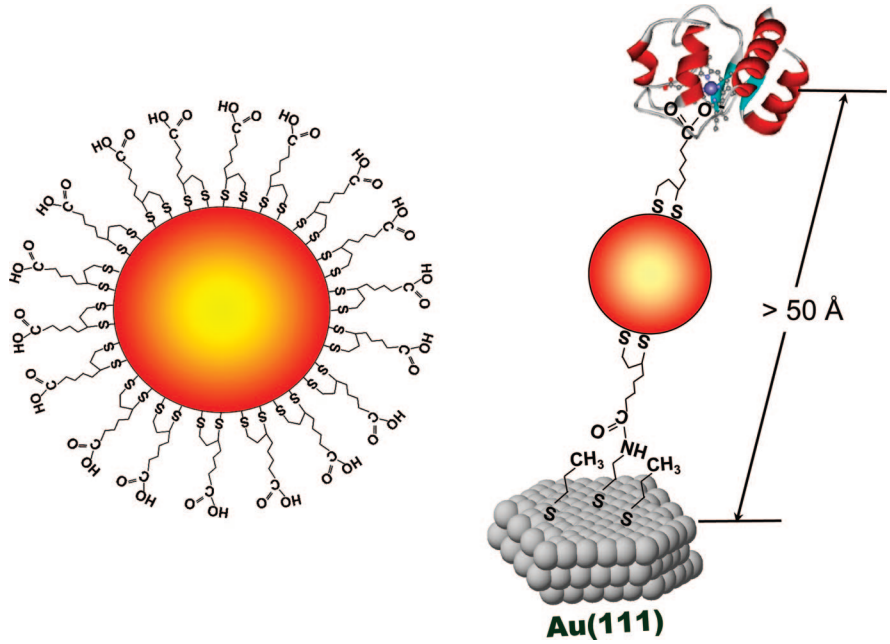

Figure 38. Left: Schematic view of AuNP coated by thioctic acid. Right: HHcyt *c* electrostatically linked to the coated AuNP which is in turn linked by amide bonding to a cysteamine-covered Au(111)-electrode. Reprinted with permission from ref 114. Copyright 2007 American Chemical Society.

absorbance ratio, Figure 39. The plasmon band of the 1:1 Au-NP/cyt *c* hybrid also shows a small but consistent band broadening compared with the pure protected Au-NP, ascribed to lifetime broadening by interfacial ET in the Au-NP/cyt *c* hybrid.[114] Well-defined protected Au-NPs in narrow size ranges can be deposited on Au(111)-electrode surfaces by covalent linking to a cysteamine adlayer. Au-NP electrostatic linking to HHC here evokes at least an order of magnitude interfacial electrochemical ET rate enhancement compared to HHC voltammetry on similar (undecanoic acid-modified) Au-NP-free surfaces. A second observation is that a two-step, HHC/Au-NP and Au-NP/electrode ET mechanism accords with the data with the former step as rate determining. Interfacial Au-NP/electrode ET thus appears as virtually activationless compared to the protein/Au-NP ET step. This pattern follows other observations by Murray, Haiss, Fermin, and associates.[424–426]

Au-NPs inserted between the electrode surface and redox molecules or proteins therefore both work as effective linkers and can be brought to exert efficient electrocatalysis. The electronic structures of the Au-NPs and the electronic interactions between the Au-NPs and both the electrode surface and the reacting molecules must be key factors in these scenarios. Other theoretical observations were noted in section 3.9

7.3. Nanotubes and Nanorods as Bioelectrochemical Nanoscale Wires and Sensors

Carbon nanotubes immobilized on solid electrochemical electrode surfaces have been introduced as efficient 1−2 nm diameter molecular-scale "wires" between the electrode surface and biological molecules with reconstituted redox enzymes such as glucose oxidase, GOx as a primary focus class.[55,403,404,427] Together with wider, >20 nm silicon "nanorods", a different electrochemical functional principle of carbon nanotubes is also being established.[104–110] This is of importance in interfacial electrochemical ET and electronic interactions between small assemblies of probe molecules, ultimately a single molecule, and the solid conducting wall surface of the carbon nanotubes or silicon nanorod, Figure 40.

Lieber and associates have developed the three-terminal Si-nanorod based concept toward multifarious bioelectrochemical-like sensoric principles. In basic terms, the conductivity of the nanorod at given bias voltage and gate potential in aqueous buffer is the core observable.[105] The conductivity is extremely sensitive to adsorption of biological molecules such as proteins and DNA fragments and also to different chemical states of the adsorbates. DNA duplication and telomerase activity, protein and enzyme processes, cancer diagnostic marking, and whole virus detection are processes recorded to a level of detection of a few hundred molecules or so.[104–106] The working principle of the solid state FET-based ultrasensitive detection device is shown schematically in Figure 40, left.

The three-terminal solid state FET source/drain/gate electrode system has been worked into a full (aqueous) liquid state electrochemical analogue where the solid state gate electrode is replaced by an electrochemical reference electrode, Figure 40, right.[108] This has enabled recording carbon nanotube conductivity signals on molecular and biomolecular adsorption with electrochemical potential control of the enclosing electrodes. Nanotube dimensions at the molecular scale, however, only apply to the nanotube cross section. As (bio)molecular adsorption can be expected all along the mesoscopically long nanotubes, conductivity recording therefore requires very small bias voltages in order to ascertain adequate electrochemical potential control at all the adsorption sites along the tube.

MacPherson, Heering, Dekker, and their associates have brought these notions into a "proof-of-principle" state using small redox molecules and redox proteins, respectively as probe molecules.[108–110] GOx, showed not only conductance signals on enzyme adsorption but also conductance changes on substrate glucose addition to the adsorbed enzyme.[108] [NiFe]-hydrogenase has also been addressed at these levels

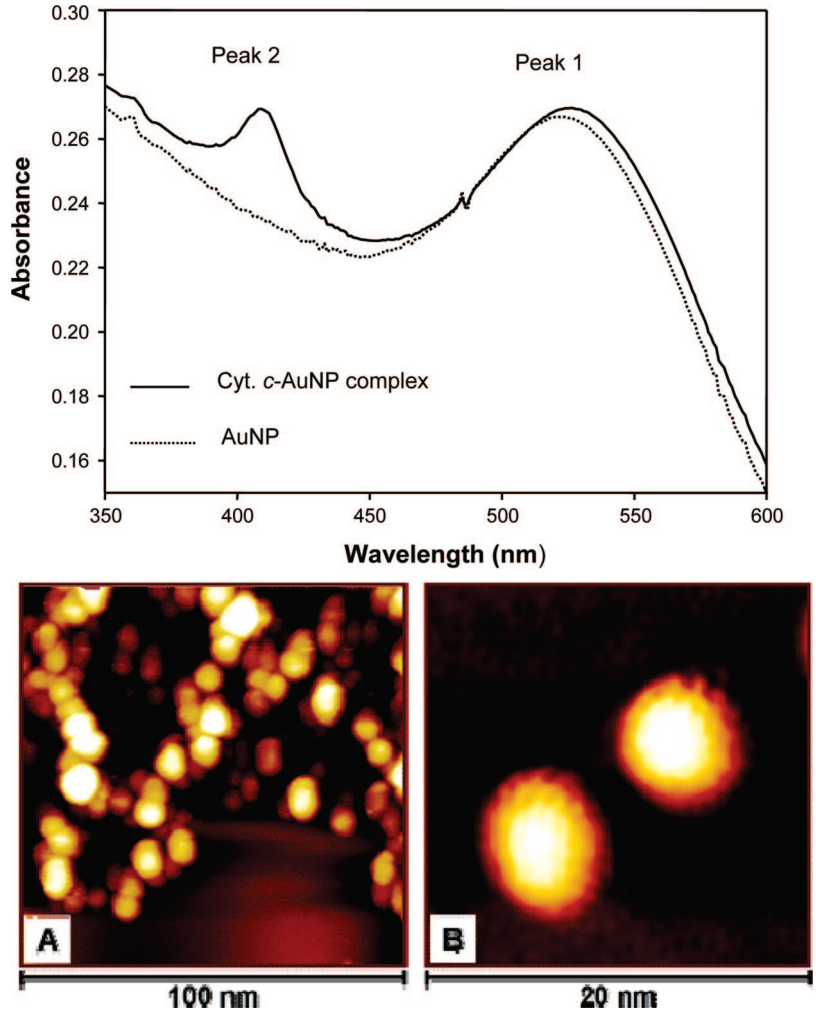

Figure 39. Top: Absorption spectrum of 1:1 hybrid between 3 nm thioctic acid-coated AuNP and HHcyt *c*. The two peaks show the AuNP plasmon band (peak 1) and the Soret band of HHcyt *c*. (peak 2). Bottom: STM image (in air) of two 3 nm thioctic-coated AuNPs. Reprinted with permission from ref 114. Copyright 2007 American Chemical Society.

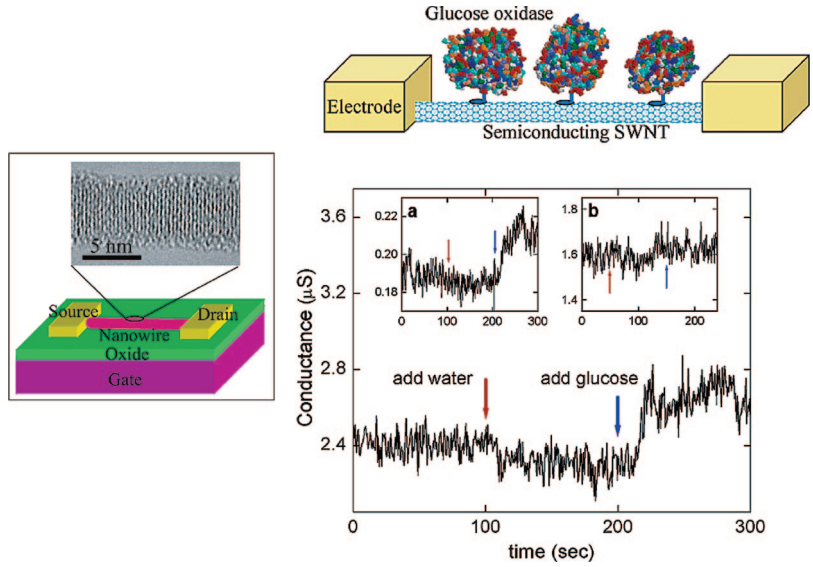

Figure 40. Left: Working principle in semiconductor-based solid state nanoscale biosensor. The Si-nanotube is mounted between a source and a drain electrode, the potentials of which are controlled relative to a gate electrode. The Si-tube conductance changes on adsorption of even a small number of biomolecules from aqueous buffer. Reprinted with permission from ref 105. Copyright 2006 American Chemical Society. Right, top: Schematic view of a related working principle where a single-wall carbon nanotube connects two electrodes and the solid state gate electrode is replaced by an electrochemical reference electrode.[108] The nanotube conductance of the glucose oxidase (GOx) covered C-nanotube changes on addition of the GOx substrate glucose. Right, bottom: Real-time conductance response on glucose addition. Insert a shows a similar measurent with a smaller conductance and inset b a blank experiment in the absence of GOx. Reprinted with permission from ref 108. Copyright 2003 American Chemical Society.

of resolution.[110] Theoretical notions are, however, different from those of in situ STM and in contrast to the latter, largely absent. Rather than on direct interfacial electrochemical ET, theoretical notions of (bio)molecular adsorption-induced nanotube conductance changes rest on subtle charge density changes in the nanotube caused by the (bio)molecular adsorption and reactivity in the adsorbed state. Understanding of these subtle effects will be a new challenge in theoretical electrochemistry.

8. Outlook and Some Perspectives

Molecular electronic properties (molecular "electronics") and interfacial molecular ET toward or at the single-molecule level have evolved over the past decade-and-a-half. We have aimed at overviewing particular facets of this exciting and broad interdisciplinary area, namely experimental and theoretical aspects associated with ultrasmall scale interfacial molecular and biomolecular electrochemistry. This notion distinguishes our approach from the broad areas of single-molecular conductivity under UHV and at cryogenic temperature conditions to which most reported theoretical approaches apply. At the same time, molecular-scale (bio)molecular interfacial electrochemical ET is kept distinct from the impressive variety of small-scale metallic and semiconductor structures which can now also be controlled electrochemically toward the mesoscopic and molecular-scale levels.

We have overviewed inorganic and metalloprotein-based system classes which accord to various extents with these notions. We have also addressed proof-of-principle electrochemical ET in well-defined (single-crystal surface) microenvironments and in nontraditional in situ STM and nanogap electrode confinements. These designs have been brought to materialize and to extensive characterization in both experimental studies and theoretical support. Notably, the latter has disclosed novel interfacial ET phenomena specific to the single-molecule and in situ STM or nanogap electrode configurations.

As in other areas of new ultrasmall and molecular-scale science, technology perspectives have been a conspicuous driving force in the development of interfacial electrochemical ET toward these levels of resolution. The new nanoscale and single-molecule electrochemistry has, however, also added new insight into the fundamental structure of the electrochemical interface and interfacial electrochemical ET processes including the disclosure of new ET.

9. Acknowledgments

Financial support from The Danish Council for Technology and Production Sciences, Grant Nos. 26-00-0034 and 274-07-0272 (J.Z., Q.C., T.A., and J.U.), Brødrene Hartmann's, the Carlsberg, and the Lundbeck Foundations (J.Z., Q.C., and J.U.), and Russian Foundation for Basic Research, Grant No. 06-03-32193 (A.M.K. and I.G.M.) is acknowledged.

10. References

(1) Furtak, T. E.; Kliewer, K. L.; Lynch, D. W., Eds.; *Non-traditional Approaches to the Study of the Solid-electrolyte Interface*; North-Holland: Amsterdam, 1980; p 101.
(2) Hansen, W. N.; Kolb, D. M.; Lynch, D. W., Eds.; *Electronic and Molecular Structure of Electrode-Electrolyte Interfaces*; Elsevier: Amsterdam, 1983; p 150.
(3) Wieckowski, A., Ed.; *Interfacial Electrochemistry. Theory, Experiment and Applications*; Dekker: New York, 1999.
(4) Kolb, D. M. *Angew. Chem., Int. Ed.* **2000**, *40*, 1162.
(5) Hubbard, A. T. *Acc. Chem. Res.* **1980**, *13*, 177.
(6) Clavilier, J.; Faure, R.; Guinet, G.; Durand, R. *J. Electroanal. Chem.* **1980**, *107*, 205.
(7) (a) Hamelin, A. *J. Electroanal. Chem.* **1996**, *407*, 1. (b) Hamelin, A.; Martins, A. M. *J. Electroanal. Chem.* **1996**, *407*, 13.
(8) Furtak, T. E.; Lynch, D. W. *J. Electroanal. Chem.* **1977**, *79*, 1.
(9) Kolb, D. M.; Kötz, R. *Surf. Sci.* **1977**, *64*, 96.
(10) Bewick, A. *J. Electroanal. Chem.* **1983**, *150*, 481.
(11) Hansen, W. N.; Osteryoung, R. A.; Kuwana, T. *J. Am. Chem. Soc.* **1966**, *88*, 1062.
(12) Furtak, T. E. *J. Electroanal. Chem.* **1983**, *150*, 375.
(13) Jeanmaire, D. L.; Van Duyne, R. P. *J. Electroanal. Chem.* **1977**, *84*, 1.
(14) Nuzzo, R. G.; Allara, D. L. *J. Am. Chem. Soc.* **1983**, *105*, 4481.
(15) Schumacher, R. *Angew. Chem., Int. Ed.* **1990**, *29*, 329.
(16) Carnie, S. L.; Torrie, G. M. *Adv. Chem. Phys.* **1984**, *56*, 141.
(17) Henderson, D.; Blum, L. *J. Electroanal. Chem.* **1982**, *132*, 1.
(18) Badiali, J. P.; Rosinberg, M. R.; Goodisman, *J. Electroanal. Chem.* **1981**, *130*, 31.
(19) Badiali, J. P. *Electrochim. Acta* **1986**, *31*, 149.
(20) Kornyshev, A. A., In: Dogonadze, R. R.; Kálmán, E.; KornyshevA. A.; Ulstrup, Eds.; *The Chemical Physics of Solvation. Part C. Solvation Phenomena in Specific Physical, Chemical and Biological Systems*; Elsevier: Amsterdam, 1988; p 355.
(21) Lustenberger, P.; Rohrer, H.; Christoph, R.; Siegenthaler, H. *J. Electroanal. Chem.* **1988**, *243*, 225.
(22) Wiechers, J.; Twomey, T.; Kolb, D. M.; Behm, R. J. *J. Electroanal. Chem.* **1988**, *248*, 451.
(23) Nichols, R. J.; Magnussen, O. M.; Hotlos, J.; Twomey, T.; Behm, R. J.; Kolb, D. M. *J. Electroanal. Chem.* **1990**, *290*, 21.
(24) Gewirth, A. A.; Niece, B. K. *Chem. Rev.* **1997**, *97*, 1129–1162.
(25) Lorenz, W. J.; Plieth, W., Eds.; *Electrochemical Nanotechnology*; Wiley-VCH: Weinheim, Germany, 1998.
(26) (a) Mujica, V.; Kemp, M.; Ratner, M. A. *J. Chem. Phys.* **1994**, *101*, 6849. (b) Mujica, V.; Kemp, M.; Ratner, M. A. *J. Chem. Phys.* **1994**, *101*, 6856. (c) Kemp, M.; Mujica, V.; Ratner, M.W. J. *Chem. Phys.* **1994**, *101*, 5172.
(27) (a) Mujica, V.; Roitberg, A. E.; Ratner, M. *J. Chem. Phys.* **1998**, *109*, 5036. (b) Mujica, V.; Roitberg, A. E.; Ratner, M. *J. Chem. Phys.* **2000**, *112*, 6834. (c) Mujica, V.; Ratner, M. A. *Chem. Phys.* **2006**, *326*, 197.
(28) Hall, L. E.; Reimers, J. R.; Nush, N. S.; Silverbrook, K. *J. Chem. Phys.* **2000**, *112*, 1510.
(29) Reimers, J. R.; Cai, Z.-L.; Bilič, A.; Hush, N. S.; Reimers, J. R.; Picconatto, C. A.; Ellenbogen, J. C.; Shashidhar, R. *Molecular Electronics III, N.Y. Acad. Sci.* **2003**, *1006*, 235.
(30) (a) Solomon, G. C.; Reimers, J. R.; Hush, N. S. *J. Chem. Phys.* **2005**, *122*, 224502. (b) Solomon, G. C.; Gagliardi, A.; Pecchia, A.; Frauenheim, T.; Di Carlo, A.; Reimers, J. R.; Nush, N. S. *J. Chem. Phys.* **2007**, *125*, 184702. (c) Reimers, J. R.; Solomon, G. C.; Gagliardi, A.; Bilič, A.; Hush, N. S.; Frauenheim, T.; Di Carlo, A.; Pecchia, A. *J. Phys. Chem. A* **2007**, *111*, 5592.
(31) Stadtler, R.; Jacobsen, K. W. *Phys. Rev. B* **2006**, *74*, 161405.
(32) Taylor, J.; Brandbyge, M.; Stokbro, K. *Phys. Rev. B* **2003**, *68*, 121101.
(33) Zhang, J.; Bilič, A.; Reimers, J. R.; Hush, N. S.; Ulstrup, J. *J. Phys. Chem. B.* **2005**, *109*, 15355.
(34) Kuznetsov, A. M.; Sommer-Larsen, U. *J. Surf. Sci.* **1992**, *275*, 52.
(35) (a) Kuznetsov, A. M.; Ulstrup, J. *J. Phys. Chem. A* **2000**, *104*, 11531. (b) Errata: J. Phys. Chem.A 2001, *105* 7494.
(36) Kuznetsov, A. M.; Ulstrup, J. *J. Electroanal. Chem.* **2004**, *564*, 209.
(37) Zhang, J.; Chi, Q.; Kuznetsov, A. M.; Hansen, A. G.; Wackerbarth, H.; Christensen, H. E. M.; Andersen, J. E. T.; Ulstrup, J. *J. Phys. Chem. B* **2001**, *105*, 1131.
(38) Kuznetsov, A. M.; Medvedev, I. G.; Ulstrup, J. *J. Chem. Phys.* **2007**, *127*, 104708.
(39) Hill, H. A. O. *Coord. Chem. Rev.* **1996**, *151*, 115.
(40) Armstrong, F. A. *J. Chem. Soc., Dalton Trans.* **2002**, 661.
(41) Armstrong, F. A. *Curr. Opin. Chem. Biol.* **2005**, *9*, 110.
(42) Hammerich, O.; Ulstrup, J., Eds. *Bioinorganic Electrochemistry*; Elsevier: Amsterdam, 2007.
(43) Landau, L. D.; Lifshitz, E. M. *Quantum Mechanics*, 2nd ed.; Pergamon Press: Oxford,1965.
(44) Bell, R. P. *Tunnelling in Chemistry*; Chapman and Hall: London, 1980.
(45) Duke, C. B. *Tunneling in Solids*; Academic Press: New York, 1969.
(46) Davis, J. J.; Hill, H. A. O. *Chem. Comm.* **2002**, 303.
(47) Bizzarri, A. R.; Bonnanni, B.; Costantini, G.; Cannistraro, S. *ChemPhysChem* **2003**, *4*, 1189.
(48) Chen, X. X.; Discher, B. M.; Pilloud, D. L.; Gibner, B. R.; Moser, C. C.; Dutton, P. L. *J. Phys. Chem. B* **2002**, *106*, 617.
(49) Willner, I.; Heleg-Shabtai, V.; Katz, E.; Rau, H. K.; Haehnel, W. *J. Am. Chem. Soc.* **1999**, *121*, 6455.

(50) Albrecht, T.; Li, W. W.; Ulstrup, J.; Haehnel, W.; Hildebrandt, P. *ChemPhysChem* **2005**, *6*, 961.
(51) Wagenknecht, H.-A., Ed. *Charge Transfer in DNA* 2005, Wiley-VCH, Weinheim.
(52) (a) O'Kelley, S.; Jackson, N. M.; Hill, M. G.; Barton, J. K. *Angew. Chem., Int. Ed.* **1999**, *38*, 941–945. (b) Jackson, N. M.; Hill, M. G. *Curr. Opin. Chem. Biol.* **2001**, *5*, 209.
(53) Mearns, F. J.; Wong, E. L. S.; Short, K.; Hibbert, D. B.; Gooding, J. J. *Electroanalysis* **2006**, *18*, 1971.
(54) Palaček, E.; Scheller, F.; Wang, J. *Electrochemistry of Nucleic Acids and Proteins: Towards Electrochemical Sensors for Genomics and Proteomics*; Elsevier: Amsterdam, 2005.
(55) Katz, E.; Willner, I. *Angew. Chem., Int. Ed.* **2004**, *43*, 6042.
(56) Kouwenhoven, L. P.; Austing, D. G.; Tarucha, S. *Rep. Prog. Phys.* **2001**, *64*, 701.
(57) Kubatkin, S.; Danilov, A.; Hjort, M.; Cornil, J.; Bredas, J.-L.; Stuhr-hansen, N.; Bjørnholm, T. *Nature* **2003**, *425*, 698.
(58) (a) Nakamura, H.; Karube, I. *Anal. Bianal. Chem.* **2003**, *377*, 446. (b) Murphy, L. *Current Opinion Chem. Biol.* **2006**, *10*, 177. (c) Oumera, M.; Sanchez, S.; Ichinose, I.; Tang, J. *Sensors Actuators B* **2007**, *123*, 1195.
(59) (a) Drummond, T. G.; Hill, M. G.; Barton, J. K. *Nat. Biotechnol.* **2003**, *21*, 1192. (b) Wanekaya, A. K.; Chen, W.; Myung, N. V.; Mulchandani, A. *Electroanalysis* **2006**, *18*, 533.
(60) Basché, T.; Moerner, W. E.; Orrit, M.; Wild, U. P., Eds.; *Single Molecule Optical Detection, Imaging and Spectroscopy*; Verlag Chemie: Munich, 1996.
(61) Moerner, W. E. *J. Phys. Chem. B* **2002**, *106*, 910.
(62) Orrit, M.; Bernard, J.; Personov, R. I. *J. Phys. Chem.* **1993**, *97*, 10290.
(63) Xie, X. S.; Dunn, R. C. *Science* **1994**, *265*, 361.
(64) Lu, H. P.; Xie, S. *Nature* **1997**, *385*, 143.
(65) Stip, P.; Rezaei, M. A.; Ho, W. *Phys. Rev. Lett.* **1999**, *82*, 1724.
(66) Min, W.; Gopich, I. V.; English, B. P.; Kou, S. C.; Xie, X. S.; Szabo, A. J. *Phys. Chem. B* **2006**, *110*, 20093.
(67) Min, W.; English, B. P.; Luo, G.; Cherayil, B. J.; Kou, S. C.; Xie, X. S. *Acc. Chem. Res.* **2005**, *38*, 923.
(68) Kienberger, F.; Ebner, A.; Gruber, H. J.; Hinterdorfer, P. *Acc. Chem. Res.* **2006**, *39*, 29.
(69) Thormann, E.; Hansen, P. L.; Simonsen, A. C.; Mouritsen, O. G. *Colloid. Surf. B-Biointerfaces* **2006**, *53*, 149.
(70) Valkunas, L.; Janusonis, J.; Rutkauskas, J.; Van Grondelle, R. *J. Lumin.* **2007**, *127*, 269.
(71) Rogers, C. T.; Buhrman, R. A. *Phys. Rev.* **1985**, *55*, 859.
(72) Farmer, K. R.; Rogers, C. T.; Buhrman, R. A. *Phys. Rev. Lett.* **1987**, *58*, 2255.
(73) He, H. X.; Zhu, J. S.; Tao, N.; Nagahara, L.; Amlani, T.; Tsui, R. *J. Am. Chem. Soc.* **2001**, *123*, 7730.
(74) Blanter, Y. A.; Buttiker, M. *Phys. Rept.* **2000**, *336*, 1.
(75) Galperin, M.; Nitzan, A.; Ratner, M. A. *Phys. Rev. B* **2006**, *74*, 075326, and references therein.
(76) Velonia, K.; Flomenbom, O.; Loos, D.; Masuo, S.; Cotlet, M.; Engelborghs, Y.; Hofkens, J.; Rowan, A. E.; Klafter, J.; Nolte, R. J. M.; De Schryver, F. C. *Angew. Chem., Int. Ed.* **2005**, *44*, 560.
(77) Engelkamp, H.; Hatzakis, N. S.; Hofkens, J.; De Schryver, F. C.; Rowan, A. E. *Chem. Comm.* **2006**, 935.
(78) Stéfanini, M. O.; McKane, A. J.; Newman, T. J. *Nonlinearity* **2005**, *18*, 1575.
(79) (a) Bar-Haim, A.; Klafter, J.; Kopelman, R. *J. Am. Chem. Soc.* **1997**, *119*, 6197. (b) Bar-Haim, A.; Klafter, J. *J. Lumin.* **1998**, *76 & 77*, 197. (c) Bar-Haim, A.; Klafter, J. *J. Phys. Chem. B* **1998**, *102*, 1662.
(80) Austin, R. H.; Beeson, K. W.; Eisenstein, L.; Frauenfelder, H.; Gunsalus, I. C. *Biochemistry* **1975**, *14*, 5355.
(81) Frauenfelder, H.; Wolynes, P. G.; Austin, R. H. *Rev. Mod. Phys.* **1999**, *71*, S419.
(82) Frauenfelder, H.; McMahon, B. H.; Austin, R. H.; Chu, K.; Groves, J. T. *Proc. Nat. Acad. Sci. U.S.A.* **2001**, *98*, 2370.
(83) Tao, N. *Phys. Rev. Lett.* **1996**, *76*, 4066.
(84) Albrecht, T.; Guckian, A.; Ulstrup, J.; Vos, J. G. *IEEE Trans. Nanotechnology* **2005**, *4*, 430.
(85) Albrecht, T.; Guckian, A.; Ulstrup, J.; Vos, J. G. *Nano Lett.* **2005**, *5*, 1451.
(86) Chi, Q.; Farver, O.; Ulstrup, J. *Proc. Nat. Acad. Sci. U.S.A.* **2005**, *102*, 16203.
(87) Li, Z.; Han, G.; Meszaros, G.; Pobelov, I.; Wandlowski, T. H. *Faraday Discuss.* **2006**, *131*, 121.
(88) Haiss, W.; van Zalinge, H.; Bethell, D.; Ulstrup, J.; Schiffrin, D. J.; Nichols, R. J. *Faraday Discuss.* **2006**, *131*, 253.
(89) Xiao, X.; Nagahara, L. A.; Rawlett, A. M.; Tao, N. *J. Am. Chem. Soc.* **2005**, *127*, 9235.
(90) Li, X.; Xu, B.; Xiao, X.; Yang, X.; Zang, L.; Tao, N. *Faraday Discuss.* **2006**, *131*, 111.
(91) Chen, F; He, J.; Nuckolls, C.; Roberts, T.; Klare, J. E.; Lindsay, S. *Nano Lett.* **2005**, *5*, 503.
(92) He, J.; Lindsay, S.; Ciszek, J. W.; Tour, J. M. *J. Am. Chem. Soc.* **2006**, *128*, 14828.
(93) Papers in: Z. Phys. Chem. 2007 221, Issue 9−10.
(94) (a) Leatherman, G.; Durantini, E. N.; Gust, D.; Moore, T. A.; Moore, A. L.; Stone, S.; Zhou, Z.; Rez, P.; Liu, Y. Z.; Lindsay, S. M. *J. Phys. Chem. B* **1999**, *103*, 4006. (b) Rawlett, A. M.; Hopson, T. J.; Nagahara, L. A.; Tsui, R. K.; Ramachandran, G. K.; Lindsay, S. M. *Appl. Phys. Lett.* **2002**, *81*, 3043. (c) Ramachandran, G. K.; Tomfohr, J. K.; Li, J.; Sankey, O. F.; Zarate, X.; Primak, A.; Terazono, Y.; Moore, T. A.; Moore, A. L.; Gust, D.; Nagahara, L. A.; Lindsay, S. M. *J. Phys. Chem.* **2003**, *107*, 6162.
(95) (a) Macpherson, J. V.; de Mussy, J. P. G.; Delplancke, J. L. *Electrochem. Sol. State Lett.* **2001**, *4*, E33. (b) Gardner, C. E.; Macpherson, J. V. *Anal. Chem.* **2002**, *74*, 576A
(96) Chen, C. J. *Introduction to Scanning Tunneling Microscopy*; Oxford University Press: New York, 1993.
(97) Gewirth, A. A., Siegenthaler, H., Eds.; *Nanoscale Probes of the Solid/Liquid Interface*; Kluwer: Dordrecht, 1995.
(98) Danilov, A. I. *Usp.Khim.* **1995**, *64*, 818.
(99) Whangbo, M. H. *Surface Analysis with STM and AFM*; Verlag Chemie: Weinheim, 1996.
(100) Wolf, E. L. *Physics and Nanotechnology*; Wiley-VCH: Weinheim, 2004.
(101) (a) Boussaad, S.; Tao, N. J. *Appl. Phys. Lett.* **2002**, *80*, 2398. (b) He, H. X.; Boussaad, S.; Xu, B. Q.; Li, C. Z.; Tao, N. J. *J. Electroanal. Chem.* **2002**, *522*, 167. (c) Xu, B.; Tao, N. J. *Science* **2003**, 301–1221.
(102) (a) Xiang, J.; Liu, S.-T.; Wu, B.; Ren, F.-Z.; Yang, B.-W.; Mao, Y. L.; Chow, Z.-Q.; Tian, Z.-Q. *Angew. Chem., Int. Ed.* **2005**, *44*, 1265. (b) Xang, J.; Liu, B.; Liu, B.; Ren, Z.-Q.; Tian, Z.-Q. *Electrochem. Commun.* **2006**, *8*, 577–580.
(103) Tian, J. H.; Liu, B.; Li, X. L.; Yang, Z. L.; Ren, B.; Wu, S. T.; Tao, N. J.; Tian, Z.-Q. *J. Am. Chem. Soc.* **2006**, *128*, 14748.
(104) (a) Cui, Y.; Zhong, Z.; Wang, D.; Wang, W. U.; Lieber, C. M. *Nano Lett.* **2003**, *3*, 149. (b) Zheng, G.; Lu, W.; Jin, S.; Lieber, C. M. *Adv. Mater.* **2004**, *16*, 1890–1893.
(105) Patolsky, F.; Zheng, G.; Lieber, C. M. *Anal. Chem.* **2006**, *78*, 4261.
(106) Chen, D.; Wang, G.; Li, J. *J. Phys. Chem. C* **2007**, *111*, 2351.
(107) Rosenblatt, S.; Yaish, Y.; Park, J.; Gore, J.; Sazonova, V.; McEuen, P. L. *Nano Lett.* **2002**, *2*, 869.
(108) Besteman, K.; Lee, J.-O.; Wiertz, F. G. M.; Heering, H. A.; Dekker, C. *Nano Lett.* **2003**, *3*, 727.
(109) Day, T. M.; Wilson, N. R.; Macpherson, J. V. *J. Am. Chem. Soc.* **2004**, *126*, 16724.
(110) Heller, I.; Kong, J.; Williams, K. A.; Dekker, C.; Lemay, S. G. *J. Am. Chem. Soc.* **2006**, *128*, 7353.
(111) Liang, W.; Shores, M. P.; Bockrath, M.; Long, J. R.; Park, H. *Nature* **2002**, *417*, 725.
(112) Park, J.; Pasupathy, A. N.; Goldsmith, J. I.; Chang, C.; Yaish, Y.; Petta, J. R.; Rinkoski, M.; Sethna, J. P.; Abruna, H. D.; McEuen, P. L.; Ralph, D. C. *Nature* **2002**, *417*, 722.
(113) Albrecht, T.; Moth-Poulsen, K.; Christensen, J. B.; Bjørnholm, T.; Ulstrup, J. *J. Am. Chem. Soc.* **2006**, *128*, 6574.
(114) Jensen, P. S.; Chi, Q.; Grumsen, F. B.; Abad, J. M.; Horsewell, A.; Schiffrin, D. J.; Ulstrup, J. *J. Phys. Chem. C* **2007**, *111*, 6124.
(115) (a) Galperin, M.; Nitzan, A.; Ratner, M. A. *Phys. Rev. B* **2006**, *73*, 045314. (b) Galperin, M.; Ratner, M. A.; Nitzan, A. *J. Phys.-Condensed Matter* **2007**, *19*, 103201.
(116) Friis, E. P.; Andersen, J. E. T.; Madsen, L. L.; Møller, P.; Ulstrup, J. *J. Electroanal. Chem.* **1997**, *431*, 35.
(117) Iversen, G.; Friis, E. P.; Kharkats, Y. U. I.; Kuznetsov, A. M.; Ulstrup, J. *J. Biol. Inorg. Chem.* **1998**, *3*, 229.
(118) Chi, Q.; Zhang, J.; Friis, E. P.; Andersen, J. E. T.; Ulstrup, J. *Electrochem. Commun.* **1999**, *1*, 91.
(119) Friis, E. P.; Andersen, J. E. T.; Kharkats; Yu., I; Nichols, R. J.; Zhang, J.; Ulstrup, J. *Proc. Nat. Acad. Sci. U.S.A.* **1999**, *96*, 1379.
(120) Zhang, J.; Chi, Q.; Kuznetsov, A. M.; Hansen, A. G.; Wackerbarth, H.; Christensen, H. E. M.; Andersen, J. E. T.; Ulstrup, J. *J. Phys. Chem. B* **2001**, *105*, 1131.
(121) Chi, Q.; Zhang, J.; Nielsen, J. U.; Friis, E. P.; Chorkendorff, I.; Canters, G. W.; Andersen, J. E. T.; Ulstrup, J. *J. Am. Chem. Soc.* **2000**, *122*, 4047.
(122) Chi, Q.; Zhang, J.; Jensen, P. S.; Christensen, H. E. M.; Ulstrup, J. *Faraday Discuss.* **2006**, *131*, 181.
(123) (a) Facci, P.; Alliata, S.; Cannistraro, S. *Ultramicsoscopy* **2001**, *89*, 291–298. (b) Alessandrini, A.; Salerno, M.; Frabboni, S.; Facci, P. *Appl. Phys. Lett.* **2005**, *86*, 133902.
(124) (a) Andolfi, L.; Bruce, D.; Cannistraro, S.; Canters, G. W.; Davis, J. J.; Hill, H. A. O.; Crozier, J.; Verbeet, M. P.H.; Wrathmell, C. L.; Astier, Y. *J. Electroanal. Chem.* **2004**, *565*, 21. (b) Alessandrini, A.; Facci, P. *Meas. Sci. Technol.* **2005**, *16*, R65.
(125) Alessandrini, A.; Corni, S.; Facci, P. *Phys. Chem. Chem. Phys.* **2006**, *38*, 4383.

(126) Bonnanni, B.; Andolfi, L.; Bizzarri, A. R.; Cannistraro, S. *J. Phys. Chem.* **2007**, *111*, 5062.
(127) (a) Davis, J. J.; Morgan, D. A.; Wrathmell, C. L.; Axford, D. N.; Zhao, J.; Wang, N. *J. Mater. Chem.* **2005**, *15*, 2160. (b) Axford, D.; Davis, J. J.; Wang, N.; Wang, D. X.; Zhang, T. T.; Zhao, J. W.; Peters, B. *J. Phys. Chem. B* **2007**, *111*, 9062.
(128) Davis, J. J.; Wang, N.; Morgan, A.; Zhang, T.; Zhao, J. *Faraday Discussions* **2006**, *131*, 167, and references therein.
(129) Andersen, J. E. T.; Møller, P.; Pedersen, M. V.; Ulstrup, J. *Surf. Sci.* **1995**, *325*, 193.
(130) Zhang, J.; Chi, Q.; Dong, S.; Wang, E. *Bioelectrochem. Bioenerg.* **1996**, *39*, 267.
(131) Hansen, A. G.; Boisen, A.; Nielsen, J. U.; Chorkendorff, I.; Andersen, J. E. T.; Zhang, J.; Ulstrup, J. *Langmuir* **2003**, *19*, 3419.
(132) (a) Bonanni, B.; Alliata, D.; Bizzari, A. R.; Cannistraro, S. *ChemPhysChem.* **2003**, *4*, 1183. (b) Delfino, I.; Bonanni, B.; Andolfi, L.; Baldacchini, C.; Bizzarri, A. R.; Cannistraro, S. *J. Phys.-Condensed Matter* **2007**, *19*, 225009.
(133) Zhang, J.; Christensen, H. E. M.; Ooi, B. L.; Ulstrup, J. *Langmuir* **2004**, *20*, 10200.
(134) Zhang, J.; Kuznetsov, A. M.; Ulstrup, J. *J. Electroanal. Chem.* **2003**, *541*, 133.
(135) Zhang, J; Welinder, A. C.; Christensen, H. E. M.; Ulstrup, J. *J. Phys. Chem. B* **2003**, *107*, 12480.
(136) Welinder, A. C.; Zhang, J.; Hansen, A. G.; Moth-Poulsen, K.; Christensen, H. E. M.; Kuznetsov, A. M.; Bjørnholm, T.; Ulstrup, J. *Z. Phys. Chem.* **2007**, *221*, 1343.
(137) Gwyer, J. D.; Zhang, J.; Butt, J. N.; Ulstrup, J. *Biophys. J.* **2006**, *91*, 3897.
(138) (a) Nitzan; Ratner, M. A. *Science* **2003**, *300*, 1384. (b) Kushmerick, J. G.; Pollack, S. K.; Yang, J. C.; Naciri, J.; Holt, D. B.; Ratner, M. A.; Shashidhar, R.; Reimers, J. R.; Picconatto, C. A.; Ellenbogen, J. C.; Shashidhar, R. *Ann. N.Y. Acad. Sci.* **2003**, *1006*, 277. (c) Weiss, E. A.; Wasielewski, M. R.; Ratner, M. A. *Top. Curr. Chem.* **2005**, *257*, 103.
(139) Nitzan, A. *Annu. Rev. Phys. Chem.* **2001**, *52*, 681.
(140) (a) Troisi, A.; Ratner, M. A. *Small* **2006**, *2*, 172. (b) Jones, D. R.; Troisi, A. *J. Phys. Chem. C* **2007**, *111*, 14567.
(141) Chen, F.; Hihath, J.; Huang, Z.; Li, X.; Tao, N. J. *Annu. Rev. Phys. Chem.* **2007**, *58*, 535.
(142) See ref 42, Chapters 6 and 8.
(143) Bonnell, D., Ed.; *Scanning Probe Microscopy and Spectroscopy: Theory, Techniques, and Applications*, 2nd ed.; Wiley-VCH: New York, 2000.
(144) Meyer, E.; Hug, H. J.; Bennewitz, R. *Scanning Probe Microscopy: The Lab on a Tip* Springer: Berlin, 2004.
(145) Radmacher, M.; Fritz, M.; Hansma, H. G.; Hansma, P. K. *Science* **1994**, *265*, 1577.
(146) Rief, M.; Gautel, M.; Osterhelt, F.; Fernandez, J. M.; Gaub, H. E. *Science* **1997**, *276*, 1109.
(147) Rounsewell, R.; Forman, J. R.; Clarke, J. *Methods* **2004**, *34*, 100.
(148) Forman, J. R.; Clarke, J. *Curr. Opion. Struct. Biol.* **2007**, *17*, 58.
(149) (a) Hugel, T.; Grosholz, M.; Clausen-Schaumann, H.; Pfau, A.; Gaub, H. E.; Seitz, S. S. *Macromolecules* **2001**, *34*, 1039.
(150) Mitsui, K.; Nakajima, K.; Arakawa, H.; Hara, A. M.; Ikai, M. *Biochem. Biophys. Res. Commun.* **2000**, *272*, 55.
(151) Strunz, T.; Oroszlan, K.; Schäfer, R.; Güntherodt, H.-J. *Proc. Nat. Acad. Sci. U.S.A.* **1999**, *96*, 11277.
(152) (a) Bustamente, C.; Smith, S. B.; Liphardt, J.; Smith, D. *Curr. Opin. Struct. Biol.* **2000**, *10*, 279. (b) Williams, M. C.; Rouzina, I. *Curr. Opion. Struct. Biol.* **2002**, *12*, 330.
(153) Zhang, X.; Moy, V. T. *Biophys. Chem.* **2003**, *104*, 271.
(154) Kienberger, F.; Ebner, A.; Gruber, H. J.; Hinterdorfer, P. *Acc. Chem. Res.* **2006**, *29*, 29.
(155) (a) Neuert, G.; Hugel, T.; Netz, R. R.; Gaub, H. E. *Macromolecules* **2006**, *39*, 789. (b) Butt, H. J. *Macromol. Chem. Phys.* **2006**, *207*, 573.
(156) Kornyshev, A. A.; Kuimova, M.; Kuznetsov, A. M.; Ulstrup, J.; Urbach, M. *J. Phys.: Condens. Matter* **2007**, *19*, 375111.
(157) Balzani, V.; Venturi, M.; Credi, A. *Molecular Devices and Machines: A Journey into the Nanoworld* Wiley-VCH: Weinheim, Germany, 2003.
(158) Mahler, G.; May, V.; Schreiber, M. *Molecular electronics: Properties, Dynamics, and Applications*; M. Dekker: New York, 1996.
(159) Jortner, J.; Ratner, M., Eds.; *Molecular electronics*; Blackwell: Oxford, 1997.
(160) (a) Aviram A.; Ratner, M., Eds.; *Molecular Electronics*; NY Acad. Sci.: New York, 1998. (b) Aviram, A.; Ratner, M.; Mujica, V., Eds. *Molecular Electronics II*; NY Acad. Sci.: New York, 2002. (c) Reimers, J. R.; Picconatto, C. A.; Ellenbogen, J. C.; Shashidhar, R., Eds.; *Molecular Electronics III*; N.Y. Acad. Sci.: New York, 2003.
(161) (a) Haiss, W.; Nichols, R. J.; Van Zalinge, H.; Higgins, S.; Bethell, D.; Schiffrin, D. J. *J. Am. Chem. Soc.* **2003**, *125*, 15294. (b) Haiss, W.; Nichols, R. J.; Van Zalinge, H.; Higgins, S.; Bethell, D.; Schiffrin, D. J. *Phys. Chem. Chem. Phys.* **2004**, *6*, 4330.
(162) Haiss, W.; Nichols, R. J.; van Zalinge, H.; Higgins, S.; Bethell, D.; Schiffrin, D. J. *Langmuir* **2004**, *20*, 7694.
(163) Haiss, W.; Albrecht, T.; Van Zalinge, H.; Higgins, S. J.; Bethell, D.; Höbenreich, H.; Schiffrin, D. J.; Nichols, R. J.; Kuznetsov, A. M.; Zhang, J.; Chi, Q.; Ulstrup, J. *J. Phys. Chem. B* **2007**, *111*, 6703.
(164) Lindsay, S. M.; Ratner, M. A. *Adv. Mater.* **2007**, *19*, 23.
(165) Nazmudtinov, R. R.; Zhang, J.; Zinkicheva, T. T.; Manyurov, I. R.; Ulstrup, J. *Langmuir* **2006**, *22*, 7556.
(166) See for example: Bilič, A.; Reimers, J. R.; Hush, N. S. *J. Chem. Phys.* **2005**, *122*, 094708, and references therein.
(167) Vericat, C.; Vela, M. E.; Benitez, G. A.; Gago, J. A. M.; Torelles, X.; Salvarezza, R. C. *J. Phys.: Condens. Matter* **2006**, *18*, R867.
(168) Love, J. C.; Estroff, L. A.; Kriebel, J. K.; Nuzzo, R. G.; Whitesides, G. M. *Chem. Rev.* **2005**, *105*, 1103.
(169) Kuznetsov, A. M.; Ulstrup, J. *Chem. Phys.* **1991**, *157*, 25.
(170) Widrig, C.; Schmickler, W. *J. Electroanal. Chem.* **1992**, *336*, 213.
(171) (a) Jaklevic, R. C.; Lambe, J. *Phys. Rev. Lett.* **1966**, *17*, 1139. (b) Lambe, J.; Jaklevic, R. C. *Phys. Rev.* **1968**, *165*, 821.
(172) Wolfram, T., Ed.; *Inelastic Electron Tunneling Spectroscopy*; Springer: New York, 1978.
(173) Hla, S.-W.; Rieder, K.-H. *Annu. Rev. Phys. Chem.* **2003**, *54*, 307.
(174) Kuznetsov, A. M. *Faraday Discuss.* **2006**, *131*, 79.
(175) Yu., L. H.; Heane, Z. K.; Ciszek, J. W.; Cheng, L.; Stewart, M. P.; Tour, J. M.; Natelson, D. *Phys. Rev. Lett.* **2004**, *93*, 266802.
(176) (a) Qiu, X. H.; Nazin, G. V.; Ho, W. *Phys. Rev. Lett.* **2004**, *20*, 206102. (b) Lee, H. J.; Lee, J. H.; Ho, W. *ChemPhysChem* **2005**, *6*, 971.
(177) (a) Pradhan, N. A.; Liu, N.; Ho, W. *J. Chem. Phys.* **2004**, *120*, 11371. (b) *J. Phys. Chem. B* **2005**, *109*, 8513.
(178) Osorio, E. A.; O'Neill, K.; Stuhr-Hansen, N.; Nielsen, O. F.; Bjørnholm, T.; van der Zant, H. S. J. *Adv. Mater.* **2007**, *19*, 281.
(179) Park, H.; Park, J.; Lim, A. K. L.; Anderson, E. H.; Alivisatos, P.; McEuen, P. L. *Nature* **2000**, *407*, 57.
(180) Scudiero, L.; Barlow, D. F.; Hipps, K. W. *J. Phys. Chem. B* **2000**, *104*, 11899.
(181) Deng, W.; Hipps, K. W. *J. Phys. Chem. B* **2003**, *107*, 10736. (b) Natelson, D.; Yu, L. H.; Ciszek, J. W.; Keane, Z. K.; Tour, J. M. *Chem. Phys.* **2006**, *324*, 267.
(182) Metzger, R. M. *Chem. Rev.* **2003**, *103*, 3803.
(183) Xiao, X.; Brune, D.; He, J.; Lindsay, S.; Gorman, C. B.; Tao, N. *Chem. Phys.* **2006**, *326*, 138.
(184) Han, W.; Durantini, E. N.; Moore, T. A.; Moore, A. L.; Gust, D.; Leatherman, G.; Deely, G. R.; Tao, N.; Lindsay, S. M. *J. Phys. Chem.* **1997**, *101*, 10719.
(185) (a) Kaba, M. S.; Song, J. K.; Barteau, M. A. *J. Phys. Chem.* **1996**, *100*, 19577. (b) *J. Vac. Sci. Technol.* **1997**, *15*, 1299.
(186) Gittins, G. I.; Bethell, D.; Schiffrin, D. J.; Nichols, R. J. *Nature* **2000**, *40*, 67.
(187) Khomutov, G. B.; Belovolova, L. V.; Gubin, S. P.; Khanin, V. V.; Obydenov, A. Y. U.; Sergeev-Cherenkov, A. N.; Soldatov, E. S.; Trifonov, A. S. *Bioelectrochem. Bioeng.* **2001**, *55*, 177.
(188) Itaya, K. *Prog. Surf. Sci.* **1998**, *58*, 121.
(189) (a) Medvedev, I. G. *Russian J. Electrochem.* **2005**, *41*, 259. (b) J. Electroanal. Chem. 2007, *600*, 151, and references therein.
(190) Beckman, R.; Beverly, K.; Boukai, A.; Bunimovich, Y. U.; Choi, J. W.; Delonno, E.; Green, J.; Johnston-Helperin, E.; Luo, Y.; Sheriff, B.; Stoddart, J. F.; Heath, J. R. *Faraday Discuss.* **2006**, *131*, 9.
(191) Flood, A. H.; Peters, A. J.; Vignon, S. A.; Steuerman, D. W.; Tseng, H.-R.; Kang, S.; Heath, J. R.; Soddart, J. F. *Chem. Eur. J.* **2004**, *10*, 6558.
(192) Liu, Y.; Flood, A. H.; Stoddart, J. F. *J. Am. Chem. Soc.* **2004**, *126*, 9150.
(193) Luo, Y.; Collier, P.; Jeppesen, J. O.; Nielsen, K. A.; DeIonno, E.; Ho, G.; Perkins, J.; Tseng, H.-R.; Yamamoto, T.; Stoddart, J. F.; Heath, J. R. *ChemPhysChem* **2002**, *3*, 519.
(194) (a) Van der Molen, S. J.; van der Vegte, H.; Kudernac, T.; Amin, I.; Feringa, B. L.; van Wees, B. J. *Nanotechnology* **2006**, *17*, 310. (b) De Feyter, S.; Uji-I, H.; Mamdouh, V.; Miura, A.; Zhang, J.; Jonkheijm, P.; Schenning, A.P.H.J.; Meijer, E. W.; Chen, Z.; Wurthner, F.; Schuurmans, N.; van Esch, J.; Feringa, B.; Dulcey, A. E.; Persec, V.; de Schruyver, F. C. *Int. J. Nanotechnol.* **2006**, *17*, 462.
(195) (a) Hush, N. S. *Z. Elektrochem.* **1957**, *61*, 738. (b) *J. Chem. Phys.* **1958** *28*, 962. (c) *Trans. Faraday Soc.* **1961** *57*, 557. (d) *J. Electroanal. Chem.* **1999**, *460*, 170. (e) *J. Electroanal. Chem.* **1999**, *470*, 5.
(196) Marcus, R. A. *Can. J. Chem.* **1959**, *37*, 155.
(197) Gerischer, H. *Z. Phys. Chem NF.* **1960**, *26*, 223–325.
(198) (a) Dogonadze, R. R.; Chizmadzhev, Y. U. A. *Dokl.Akad.Nauk SSSR* **1962**, *144*, 1077. (b) Dogonadze, R. R.; Chizmadzhev Yu., A. *Dokl.Akad.Nauk SSSR* **1962**, *145*, 848.

(199) (a) Dogonadze, R. R.; Kuznetsov, A. M.; Vorotyntsev, M. A. *J. Electroanal. Chem.* **1970**, *215*, 17. (b) *Croatica Chem.Acta.* **1972**, *44*, 257.
(200) (a) Marcus, R. A. *Annu. Rev. Phys. Chem.* **1964**, *15*, 155. (b) Levich, V. G. *Adv. Electrochemistry Electroeng.* **1966**, *4*, 249. (c) Reynolds, W. L.; Lumry, R. W. *Mechanisms of Electron Transfer*; The Ronald Press Company: New York, 1966.
(201) Marcus, R. A.; Sutin, N. *Biochim. Biophys. Acta* **1987**, *811*, 265.
(202) (a) Kuznetsov, A. M. *Charge Transfer in Physics, Chemistry and Biology*; Gordon & Breach: Reading, 1995. (b) Kuznetsov, A. M. *Charge Transfer in Chemical Reaction Kinetics*; Press polytechniques et universitaires romandes: Lausanne, 1997.
(203) (b) Kuznetsov, A. M.; Ulstrup, J. *Electron Transfer in Chemistry and Biology: An Introduction to the Theory*; Wiley: Chichester, U.K., 1999.
(204) Jortner, J.; Bixon, M. *Adv. Chem. Phys.* **1999**, *106*, 107 Electron Transfer - from Isolated Molecules to Biomolecules, Parts 1 and 2.
(205) (a) Meyer, T. J.; Newton, M. D. *Chem. Phys.* **1993**, *176*, 289649. Special issue on electron transfer. (b) Arnaut, L. *J. Photochem. Photobiol. A* **1994**, *82*, 1232. Special issue on electron transfer.
(206) (a) Kornyshev, A. A.; Newton, M. D.; Ulstrup, J.; Sanderson, B. *Chem. Phys.* **2005**, *319*, 1428. Special issue in honour of Alexander M. Kuznetsov. (b) Reimers, J. R.; Ulstrup, J.; Meyer, T. J.; Solomon, G. C. *Chem. Phys.* **2006**, *324*, 1–292. (c) Reimers, J. R.; Ulstrup, J.; Meyer, T. J.; Solomon, G. C. *Chem. Phys.* **2006**, *326*, 1272. Special issues in honour of Noel Sydney Hush.
(207) Kuznetsov, A. M. Ulstrup, J.;ref 42, Chapter 6.
(208) Schmickler, W *J. Electroanal. Chem.* **1986**, *204*, 31.
(209) Feldberg, S. W.; Sutin, N. *Chem. Phys.* **2006**, *324*, 216.
(210) Gosavi, S.; Marcus, R. A. *J. Phys. Chem. B* **2000**, *104*, 2067.
(211) Kuznetsov, A. M.; Medvedev, I. G.; Sokolov, V. V. *J. Chem. Phys.* **2004**, *120*, 7616.
(212) Finklea, H. O. *Electroanal. Chem.* **1996**, *19*, 109.
(213) Sikes, H. D.; Smalley, J. F.; Dudek, S. P.; Cook, A. R.; Newton, M. D.; Chidsey, C. E. D.; Feldberg, S. W. *Science* **2001**, *291*, 1519.
(214) Kuznetsov, A. M.; Ulstrup, J. *Surf. Coat. Technol.* **1994**, *67*, 193.
(215) Kuznetsov, A. M.; Schmickler, W. *Chem. Phys.* **2002**, *282*, 371.
(216) (a) Kuznetsov, A. M.; Ulstrup, J. *Elektrokhimiya* **1995**, *31*, 221. (b) Kuznetsov, A. M.; Ulstrup, J. *Probe Microscopy* **2001**, *2*, 187.
(217) Schmickler, W. *Surf. Sci.* **1993**, *295*, 43. (b) Schmickler, W.; Tao, N. *Electrochim. Acta* **1997**, *42*, 2809. (c) Schmickler, W. *Surf. Sci.* **1993**, *295*, 43.
(218) (a) Sumi, H. *Chem. Phys.* **1997**, *222*, 269. (b) Sumi, H.; Hori, Y.; Mukai, K. *J. Electroanal. Chem.* **2006**, *592*, 46.
(219) Albrecht, T; Moth-Poulsen, K.; Christensen, J. B.; Guckian, A.; Bjørnholm, T.; Vos, J. G.; Ulstrup, J. *Faraday Discuss.* **2006**, *131*, 265.
(220) Medvedev, I.G. J. *Electroanal. Chem.* **2006**, *598*, 1.
(221) Kuznetsov, A. M.; Medvedev, I. G. *J. Electroanal. Chem.* **2001**, *502*, 15.
(222) Kuznetsov, A. M.; Medvedev, I. G.; Sokolov, V. V. *J. Electroanal. Chem.* **2003**, *552*, 231.
(223) Kuznetsov, A. M.; Medvedev, I. G. *Electrochem. Commun.* **2007**, *9*, 1343.
(224) Andersen, J. E. T.; Kornyshev, A. A.; Kuznetsov, A. M.; Madsen, L. L.; Møller, P.; Ulstrup, J. *Electrochim. Acta* **1997**, *42*, 819.
(225) Kokkanen, A. A.; Kuznetsov, A. M.; Medvedev, I. G. *Russ. J. Electrochem.* **2007**, *43*, 1033.
(226) Medvedev, I. G. *Russ. J. Electrochem.* **2003**, *39*, 44.
(227) Kuznetsov, A. M.; Schmickler, W. *Chem. Phys. Lett.* **2000**, *327*, 314.
(228) Schlottmann, P. *Z. Phys. B* **1982**, *49*, 109.
(229) Kast, S. M.; Nicklas, K.; Bar, H. J.; Brickmann, J. *J. Chem. Phys.* **1994**, *100*, 566.
(230) Kast, S. M.; Brickmann, J. *J. Chem. Phys.* **1996**, *104*, 3732.
(231) Glazman, L. I.; Shehkter, R. I. *Zhur. Eksp. Theor. Fiz.* **1988**, *94*, 292–306; Sov. Phys. JETP 1988, 67, 163.
(232) Wingreen, N. S.; Jacobsen, K. W.; Wilkins, J. W. *Phys. Rev. B* **1989**, *40*, 11834.
(233) Santos, E.; Koper, M. T. M.; Schmickler, W. *Chem. Phys. Lett.* **2006**, *419*, 421.
(234) (a) Mohr, J.-H.; Schmickler, W. *Phys. Rev. Lett.* **2000**, *84*, 1051. (b) Mohr, J.-H.; Schmickler, W.; Badiali, J. P. *Chem. Phys.* **2006**, *324*, 140.
(235) Jauho, A. P.; Wingreen, N. S.; Meir, Y. *Phys. Rev. B* **1994**, *50*, 5528.
(236) Kuznetsov, A. M.; Nazmutdinov, R. R.; Schmickler, W. *J. Electroanal. Chem.* **2002**, *532*, 171.
(237) Likharev, K. K. *IBM J. Res. Devel.* **1988**, *32*, 144.
(238) Devoret, M. H.; Esteve, D.; Urbina, C. *Nature* **1992**, *360*, 547.
(239) Likharev, K. K.; Claeson, T. *Sci. Am.* **1992**, *266*, 80.
(240) Grabert, H.; Devoret, M. H., Eds., *Single Charge Tunneling*; Plenum: New York, 1992.
(241) Kuznetsov, A. M.; Ulstrup, J. *J. Electroanal. Chem.* **1993**, *362*, 147.
(242) Chen, S.; Murray, R. W.; Feldberg, S. W. *J. Phys.Chem. B* **1998**, *102*, 9898.
(243) Chen, S.; Ingram, R. S.; Hostetler, M. J.; Pierton, J. J.; Murray, R. W.; Schaaff, T. G.; Khoury, J. T.; Alvarez, M. M.; Whetten, R. L. *Science* **1998**, *280*, 2098.
(244) Ingram, R. S.; Hostetler, M. J.; Murray, R. W.; Schaaff, T. G.; Khoury, J. T.; Bigioni, T. P.; Guthrie, D. K.; First, P. N. *J. Am. Chem. Soc.* **1997**, *119*, 9279.
(245) Fan, F. R. F.; Bard, A. J. *Science* **1997**, *277*, 1791.
(246) Albrecht, T.; Mertens, S. F. L.; Ulstrup, J. *J. Am. Chem. Soc.* **2007**, 129–9162.
(247) Kornyshev, A. A.; Kuznetsov, A. M. *ChemPhysChem* **2006**, *7*, 1036.
(248) Haiss, W.; van Zalinge, H.; Bethell, D.; Ulstrup, J.; Schiffrin, D. J.; Nichols, R. J. *Faraday Discuss.* **2006**, *131*, 253.
(249) Kornyshev, A. A.; Kuznetsov, A. M.; Ulstrup, J. *Proc. Natl. Acad. Sci. U.S.A.* **2006**, *103*, 6799.
(250) Jortner, J.; Bixon, M.; Langenbacher, T.; Michel-Beyerle, M. E. *Proc. Natl. Acad. Sci. U.S.A.* **1998**, *95*, 12559.
(251) Bixon, M.; Jortner, J. *Chem. Phys.* **2005**, *319*, 273.
(252) Bixon, M.; Jortner, J. *Chem. Phys.* **2006**, *326*, 252.
(253) Berlin, Y. A.; Burin, A. L.; Ratner, M. A. *J. Phys. Chem. A* **2000**, *104*, 443.
(254) Berlin; Yu., A.; Kurnikov, I. V.; Beratan, D.; Ratner, M. A.; Burin, A. I.; Schuster, G. B. *Top. Curr. Chem.* **2004**, *237*, 1.
(255) Li, X.-Q.; Zhang, H.; Yan, Y.-J. *J. Phys. Chem. A* **2001**, *105*, 9563.
(256) Giese, B.; Amaudrut, J.; Köhler, A.-K.; Spormann, M.; Wessely, S. *Nature* **2001**, *412*, 318.
(257) McConnell, H. M. *J. Chem. Phys.* **1961**, *35*, 508.
(258) (a) Dogonadze, R. R.; Ulstrup, J.; Kharkats, Y. I. *Dokl.Akad.Nauk SSSR* **1972**, *207*, 640. (b) *J. Electroanal. Chem.* **1972**, *39*, 47. (c) *J. Theor. Biol.* **1973**, *259*, 279.
(259) Kharkats, Y. I. *Elektrokhimiya* **1972**, *8*, 1300.
(260) Kharkats, Y. I.; Madumarov, A. K.; Vorotyntsev, M. A. *J. Chem. Soc. Faraday Trans. II* **1974**, *70*, 1578.
(261) Dogonadze, R. R.; Kuznetsov, A. M. *Prog. Surf. Sci.* **1975**, *6*, 1.
(262) (a) Kuznetsov, A. M.; Kharkats, Y. I. *Soviet Electrochemistry* **1976**, *12*, 1170. (b) *Soviet Electrochemistry* **1977**, *13*, 1283.
(263) Kuznetsov, A. M.; Ulstrup, J. *J. Chem. Phys.* **1981**, *75*, 2047.
(264) *Coord. Chem. Rev.*, **2005**, 249; Issues 3−3, 273−516. Special issues in honour of Henry Taube.
(265) Friis, E. P.; Kharkats, Y. I.; Kuznetsov, A. M.; Ulstrup, J. *J.Phys.Chem.A* **1998**, *102*, 7851.
(266) (a) Koch, J.; von Oppen, F. *Phys. Rev. Lett.* **2005**, *94*, 206804. (b) Koch, J.; von Oppen, F.; Andreev, A. V. *Phys. Rev. B* **2006**, *74*, 205438.
(267) Sumi, H. *J. Phys. Chem. B* **1998**, *102*, 1833.
(268) Andersen, J. E. T.; Kornyshev, A. A.; Kuznetsov, A. M.; Møller, P.; Ulstrup, J. *Russ. J. Electrochem.* **1995**, *31*, 907.
(269) Albrecht, T.; Guckian, A.; Kuznetsov, A. M.; Vos, J. G.; Ulstrup, J. *J. Am. Chem. Soc.* **2006**, *128*, 17132.
(270) Visoly-Fisher, I; Daie, K.; Terazono, Y.; Herrero, C.; Fungo, F.; Otero, L.; E.; Durantini, J. J.; Silber, Sereno, L.; Gust, D.; Moore, T. A.; Moore, A. L.; Lindsay, S. M. *Proc. Natl. Acad. Sci. U.S.A.* **2006**, *103*, 8686.
(271) Medvedev, I. G. *J. Electroanal. Chem.* **2007**, *600*, 151.
(272) Kornyshev, A. A.; Kuznetsov, A. M. *Chem. Phys.* **2006**, *324*, 276.
(273) Boese, D.; Schoeller, H. *Europhys. Lett.* **2001**, *54*, 668.
(274) McCarthy, K. D.; Prokof'ev, N.; Tuominen, M. T. *Phys. Rev. B* **2003**, *67*, 245415.
(275) Mitra, A.; Aleiner, I.; Millis, A. J. *Phys. Rev. B* **2004**, *69*, 245302.
(276) Braig, S.; Flensberg, K. *Phys. Rev. B* **2003**, *68*, 205324.
(277) Kornyshev, A. A.; Kuznetsov, A. M. *Electrochem. Commun.* **2006**, *8*, 679.
(278) Medvedev, I. G. *Russ. J. Electrochem.* **2005**, *41*, 368–380.
(279) Aviram, A.; Ratner, M. A. *Chem. Phys. Lett.* **1974**, *29*, 277.
(280) Zhang, J.; Chi, Q.; Albrecht, T.; Kuznetsov, A. M.; Grubb, M.; Hansen, A. G.; Wackerbarth, H.; Welinder, A. C.; Ulstrup, J. *Electrochim. Acta* **2005**, *50*, 3143.
(281) Schmickler, W.; Rampi, M. A.; Tranc, E.; Whitesides, G. M. *Faraday Dscuss.* **2004**, *125*, 171.
(282) Tranc, E.; Duati, M.; Whitesides, G. M.; Rampi, M. A. *Faraday Discuss.* **2006**, *131*, 197.
(283) Kuznetsov, A. M. *Elektrokhimiya* **2007**, *43*, 1335.
(284) Kuznetsov, A. M.; Ulstrup, J. *J. Chem. Phys.* **2002**, *116*, 2149.
(285) Kuznetsov, A. M. *J. Chem. Phys.* **2007**, *127*, 084710.
(286) Kuznetsov, A. M. *Electrochim. Acta* **2000**, *46*, 247.
(287) Korotkov, A. N. *Phys. Rev. B* **1994**, *49*, 10381.
(288) Feldheim, D. L.; Keating, C. D. *Chem. Soc. Rev.* **1998**, *27*, 1.
(289) Kornyshev, A. A.; Kuznetsov, A. M.; Ulstrup, J. *ChemPhysChem* **2005**, *6*, 583.
(290) (a) Zhang, J.; Grubb, M.; Hansen, A. G.; Kuznetsov, A. M.; Boisen, A.; Wackerbarth, H.; Ulstrup, J. *J. Phys.: Condensed Matter* **2003**,

15, S1873. (b) Hansen, A. G.; Wackerbart, H.; Nielsen, J. U.; Zhang, J.; Kuznetsdov, A. M.; Ulstrup, J. *Russ. J. Electrochem.* **2003**, *39*, 108.
(291) Cunha, F.; Tao, N. J.; Wang, X. W.; Jin, Q.; Duong, B.; D-Agnese, J. *Langmuir* **1996**, *12*, 6410.
(292) Wandlowski, T. *J. Electroanal. Chem.* **1995**, *395*, 83.
(293) Zhang, J.; Chi, Q.; Ulstrup, J. *Langmuir* **2006**, *22*, 6203.
(294) Zhang, J.; Demetriou, A.; Welinder, A. C.; Albrecht, T.; Nichols, R. J.; Ulstrup, J. *Chem. Phys.* **2005**, *319*, 210.
(295) Zhang, J.; Chi, Q.; Nielsen, J. U.; Friis, E. P.; Andersen, J. E. T.; Ulstrup, J. *Langmuir* **2000**, *16*, 7229.
(296) Kühnle, A.; Linderoth, T. R.; Hammer, B.; Besenbacher, F. *Nature* **2002**, *415*, 891.
(297) Dakkouri, A. S.; Kolb, D. M.; Edelstein-Shima, R.; Mandler, D. *Langmuir* **1996**, *12*, 2849.
(298) Xu, Q.; Wan, L.; Wang, C.; Bai, C.; Wang, Z.; Nozawa, T. *Langmuir* **2001**, *17*, 6203.
(299) Bunge, E.; Port, S. N.; Roelfs, B.; Meyer, H.; Baumgärtl, H.; Schiffrin, D. J.; Nichols, R. J. *Langmuir* **1997**, *13*, 85.
(300) (a) Bunge, E.; Nichols, R. J.; Roelfs, B.; Meyer, H.; Baumgärtl, H. *Langmuir* **1996**, *12*, 3060. (b) Roelfs, B.; Bunger, E.; Schroter, C.; Solomun, T.; Meyer, H.; Nichols, R. J.; Baumgärtl, H. *J. Phys. Chem. B* **1997**, *101*, 754. (c) Talonen, P.; Sundholm, G.; Floate, S.; Nichols, R. J. *Phys. Chem. Chem. Phys.* **1999**, *1*, 3661.
(301) (a) Su, G. J.; Zhang, H. M.; Wan, L. J.; Bai, C. L.; Wandlowski, T. J. *Phys. Chem. B* **2004**, *108*, 1931. (b) Li, Z.; Han, B.; Wan, L. J.; Wandlowski, T. *Langmuir* **2005**, *21*, 6915.
(302) Cunha, F.; Jin, Q.; Tao, N. J.; Li, C. Z. *Surf. Sci.* **1997**, *389*, 19.
(303) Kunitake, M.; Batina, N.; Itaya, K. *Langmuir* **1995**, *11*, 2337.
(304) Yoshimoto, S.; Tada, A.; Suto, K.; Narita, R.; Itaya, K. *Langmuir* **2003**, *19*, 672. (b) Yoshimoto, S.; Tada, A.; Suto, K.; Itaya, K. J. *Phys. Chem. B* **2003**, *107*, 5836.
(305) (a) Yoshimoto, S.; Tsutsumi, E.; Suto, K.; Honda, Y.; Itaya, K. *Chem. Phys.* **2005**, *319*, 147, and references therein. (b) Yoshimoto, S.; Itaya, K. J. *Porphyrins Phthalocyanins* **2007**, *11*, 313.
(306) Ulman, A. *Chem. Rev.* **1996**, *96*, 1533.
(307) Poirier, G. E. *Chem. Rev.* **1997**, *97*, 1117.
(308) Café, P.; Larsen, A. G.; Yang, W.; Bilič, A.; Blake, I. M.; Crossley, M. J.; Zhang, J.; Wackerbarth, H.; Ulstrup, J.; Reimers, J.R. J. *Phys. Chem. C* **2007**, *111*, 17285.
(309) Dameron, A. A.; Charles, L. F.; Weiss, P. S. *J. Am. Chem. Soc.* **2005**, *127*, 8697.
(310) Zhang, J.; Chi, Q.; Ulstrup, J. *J. Phys. Chem. B* **2006**, *110*, 1102.
(311) Wang, Y.; Hush, N. S.; Reimers, J. R. *J. Phys. Chem. C* **2007**, *111*, 10787.
(312) Widrig, C. A.; Chung, C.; Porter, M. D. *J. Electroanal. Chem.* **1991**, *310*, 335.
(313) Heyrovsky, M.; Mader, P.; Vesela, V.; Fedurco, M. *J. Electroanal. Chem.* **1994**, *369*, 53.
(314) (a) Ralph, T. R.; Hitchman, M. L.; Millington, J. P.; Walsh, F. C. *J. Electroanal. Chem.* **1994**, *375*, 1. (b) *J. Electroanal. Chem.* **1994**, *375*, 17.
(315) (a) Fawcett, W. R.; Fedurco, M.; Kovazova, Z.; Borkowska, Z. *J. Electroanal. Chem.* **1994**, *368*, 275. (b) *Langmuir* **1994**, *10*, 912.
(316) References in refs164−166 and 296−298.
(317) Molina, L. M.; Hammer, B. *Chem. Phys. Lett.* **2002**, *360*, 264. (b) Di-Felice, R.; Selloni, A. *J. Phys. Chem. B* **2003**, *197*, 1151. (c) Di Felice, R.; Selloni, A. *J. Chem. Phys.* **2004**, *120*, 4906.
(318) (a) Katz, E.; Filanovsky, B.; Willner, I. *New J. Chem.* **1999**, *23*, 481. (b) Willner, I.; Katz, E.; Patolsky, F.; Buckmann, A. F. *J. Chem. Soc., Perkin Trans.* **1998**, *2*, 1817. (c) Kharitonov, A. B.; Zayats, M.; Alfonta, L.; Katz, E.; Willner, I. *Sensors Actuators B* **2001**, *B76*, 203.
(319) Wirde, M.; Gelius, U.; Nyholm, L. *Langmuir* **1999**, *15*, 6370.
(320) (a) Michota, A.; Kudelski, A.; Bukowska, J. *Langmuir* **2000**, *16*, 10236. (b) *J. Raman Spectrosc.* **2001**, *32*, 345. (c) *Surf. Sci.* **2002**, *502*−*503*, 214.
(321) Haiss, W.; Wang, C. S.; Grace, I.; Batsanov, A. S.; Schiffrin, D. J.; Higgins, S.; Bryce, M. R.; Lambert, C. J.; Nichols, R. J. *Nat. Mat.* **2006**, *5*, 995.
(322) Li, X. L.; Hihath, J.; Chen, F.; Masuda, T.; Zang, L.; Tao, N. J. *J. Am. Chem. Soc.* **2007**, *129*, 11535.
(323) Chen, F.; Nuckolls, C.; Lindsay, S. *Chem. Phys.* **2006**, *324*, 236.
(324) Cui, X. D.; Primak, A.; Zarate, X.; Tomfohr, J.; Sankey, O. F.; Moore, A. L.; Moore, T. A.; Gust, D.; Nagahara, L. A.; Lindsay, S. M. *J. Phys. Chem. B* **2002**, *106*, 8609.
(325) O'Boyle, N. M.; Albrecht, T.; Murgida, D. H.; Cassidy, L.; Ulstrup, J.; Vos, J. G. *Inorg. Chem.* **2007**, *46*, 117.
(326) Tran, E.; Duati, M.; Whitesides, G. M.; Rampi, M. A. *Faraday Discuss.* **2006**, *131*, 197.
(327) (a) Bard, A. J.; Fan, F. R. F. *Acc. Chem. Res.* **1996**, *29*, 572. (b) Fan, F. R. F.; Kwak, J.; Bard, A. J. *J. Am. Chem. Soc.* **1996**, *118*, 9669.
(328) Zevenbergen, M. A. G.; Krapf, D.; Zuiddam, M. R.; Lemay, S. G. *Nano Letters* **2007**, *7*, 384.
(329) White, R. J.; White, H. S. *Langmuir* **2008**, *24*, 2850.
(330) Lee, G.; Evans, D. F.; Elings, V.; Edstrom, R. D. *J. Vac. Sci. Technol. B* **1991**, *9*, 1236.
(331) Feng, L.; Hu, C. Z.; Andrade, J. D. *J. Colloid Interface Sci.* **1988**, *126*, 650.
(332) Leatherbarrow, R. J.; Stedman, M.; Wells, T. N. C. *J. Mol. Biol.* **1991**, *221*, 361.
(333) Welland, M. E.; Miles, M. J.; Lambert, N.; Morris, V. J.; Coombs, J. H.; Pethica, J. B. *Int. J. Biol. Macromol.* **1989**, *11*, 29.
(334) Nawaz, Z.; Cataldi, T. R.; Knall, J.; Somekh, R.; Pethica, J. B. *Surf. Sci.* **1992**, *265*, 139.
(335) Zhang, J.-D.; Chi, Q.; Dong, S.-J.; Wang, E. *J. Electroanal. Chem.* **1994**, *379*, 535.
(336) (a) Leggett, G. J.; Davies, M. C.; Jackson, D. E.; Roberts, C. J.; Tendler, S. J. B.; Williams, P. M. *J. Phys. Chem.* **1993**, *97*, 8852. (b) Zhang, J.-D.; Chi, Q.-J.; Dong, S.-J.; Wang, E.-K. *Electroanalysis* **1998**, *10*, 738.
(337) Chi, Q.; Zhang, J.; Dong, S.; Wang, E. *J. Chem. Soc. Faraday Trans.* **1994**, *90*, 2057.
(338) Haggerty, L.; Lenhoff, A. M. *Biophys. J.* **1993**, *64*, 886.
(339) Diemann, E.; Branding, A.; Müller, A. *Naturwiss.* **1992**, *79*, 267.
(340) Lee, I.; Lee, R. J.; Warmack, R. J.; Allison, D. P.; Greenbaum, E. *Proc. Nat. Acad. Sci. U.S.A.* **1995**, *92*, 1965.
(341) Andersen, J. E. T.; Olesen, K. G.; Danilov, A. I.; Foverskov, C. E.; Møller, P.; Ulstrup, J. *Bioelectrochem. Bioeng.* **1997**, *44*, 57.
(342) Davis, J. J.; Hill, H. A. O.; Kurz, A.; Jacob, C.; Maret, W.; Vallee, B. L. *Phys. Chem. Comm.* **1998**, Art. No. 2.
(343) Mukhopadhyay, R.; Davis, J. J.; Kyritsis, P.; Hill, H. A. O.; Meyer, J. *J. Inorg. Biochem.* **2000**, *78*, 251.
(344) Davis, J. J.; Djuricic, D.; Lo, K. K. W.; Wallace, F. N. K.; Wong, L. L.; Hill, H. A. O. *Faraday Discuss.* **2000**, *116*, 15.
(345) Yeh, P.; Kuwana, T. *Chem. Lett.* **1977**, *10*, 1145.
(346) Niki, K.; Yagi, T.; Inokuchi, H.; Kimura, K. *J. Am. Chem. Soc.* **1979**, *101*, 3335.
(347) (a) Eddowes, M. J.; Hill, H. A. O. *J. Chem. Soc. Chem. Comm.* **1977**, 771. (b) Eddowes, M. J.; Hill, H. A. O. *J. Am. Chem. Soc.* **1979**, *101*, 4461.
(348) Angrove, H. C.; Cole, J. A.; Richardson, D. J.; Butt, J. *J. Biol. Chem.* **2003**, *277*, 23374.
(349) Reference 42, Chapter 4.
(350) Reda, T.; Hirst, J. *J. Phys. Chem. B* **2006**, *110*, 1394.
(351) (a) Armstrong, F. A.; Heering, H. A.; Hirst, J. *Chem. Soc. Rev.* **1997**, *26*, 169. (b) Armstrong, F. A. *J. Chem. Soc., Dalton Trans.* **2002**, 661. (c) Ferantipova, E. E.; Gorton, L. *Electroanal.* **2003**, *15*, 484. (d) Vincent, K. A.; Parkin, A.; Armstrong, F. A. *Chem. Rev.* **2007**, *107*, 4366.
(352) Gwyer, J. D.; Richardson, D. J.; Butt, J. N. *Biochem. Soc. Trans.* **2006**, *34*, 133.
(353) (a) Heering, H. A.; Weiner, J. H.; Armstrong, F. A. *J. Am. Chem. Soc.* **1997**, *119*, 11628. (b) Leger, C.; Elliott, S. J.; Hoke, H. R.; Jeucken, L. J. C.; Jones, A. K.; Armstrong, F. A. *Biochemistry* **2003**, *42*, 8353. (c) Hudson, J. M.; Heffron, K.; Kotlyar, V.; Sher, Y.; Maklashina, E.; Cecchini, G.; Armstrong, F. A. *J. Am. Chem. Soc.* **2005**, *127*, 6977, and references therein.
(354) (a) Pershad, H. R.; Hirst, J.; Cochran, B.; Ackrell, B. A. C.; Armstrong, F. A. *Biochim. Biophys. Acta - Bioenergetics* **1999**, *1412*, 262. (b) Leger, C.; Heffron, K.; Pershad, H. R.; Maklashina, E.; Luna-Chavez, C.; Cecchini, G.; Ackrell, B. A. C.; Armstrong, F. A. *Biochemistry* **2001**, *40*, 11234.
(355) Anderson, L. J.; Richardson, D. J.; Butt, J. *Biochemistry* **2001**, *40*, 11294.
(356) Elliott, S. J.; McElhaney, A. E.; Feng, C.; Enemark, J. H.; Armstrong, F. A. *J. Am. Chem. Soc.* **2002**, *124*, 11612.
(357) Zu, Y.; Shannon, R. J.; Hirst, J. *J. Am. Chem. Soc.* **2003**, *125*, 6020.
(358) Johnson, D. L.; Thompson, J. L.; Brinkmann, S. M.; Schuller, K. A.; Martin, L. L. *Biochemistry* **2003**, *42*, 10229.
(359) Tarasevich, M. R.; Chirkov, Y. G.; Bogdanovskaya, V. A.; Kapustin, A. V. *Electrochim. Acta* **2005**, *51*, 418.
(360) Bernhardt, P. V.; Honeychurch, M. J.; McEwan, A. G. *Electrochem. Commun.* **2006**, *8*, 257.
(361) Ferapontova, E. E.; Ruzgas, T.; Gorton, L. *Anal. Chem.* **2003**, *75*, 4841–4850.
(362) Shleev, S.; Tkac, J.; Christenson, A.; Ruzgas, T.; Yaropolov, A. I.; Whittaker, J. W.; Gorton, L. *Biosens. Bioelectron.* **2005**, *20*, 2517.
(363) (a) Scheller, F. W.; Wollenberger, U.; Warsinke, A.; Lisdat, F. *Curr. Opin. Biotechnol.* **2001**, *12*, 35. (b) Lisdat, F.; Ge, B.; Meyerhoff, M. E.; Scheller, F. W. *Probe Micros.* **2001**, *2*, 113.
(364) Ge, B.; Scheller, F. W.; Fisdat, F. *Biosens. Bioelectron.* **2003**, *18*, 295.
(365) Gilardi, G.; Fantuzzi, A.; Sadeghi, S. J. *Curr. Opin. Struct. Biol.* **2001**, *11*, 491.

(366) Gilardi, G.; Fantuzzi, A. *Trends Biotechnol.* **2001**, *19*, 468.
(367) (a) Shipway, A. N.; Willner, I. *Acc. Chem. Res.* **2001**, *34*, 421. (b) Willner, B.; Katz, E.; Willner, I. *Curr. Opin. Biotech.* **2006**, *17*, 589.
(368) Xiao, Y.; Patolsky, F.; Katz, E.; Hainfeld, J. F.; Willner, I. *Science* **2003**, *299*, 1877.
(369) Baron, R.; Lioubashevski, O.; Katz, E.; Niazov, T.; Willner, I. *J. Phys. Chem. A* **2006**, *110*, 8548.
(370) (a) Wong, E. L. S.; Gooding, J. J. *Aust. J. Chem.* **2005**, *58*, 280. (b) Wong, E. L. S.; Chow, E.; Gooding, J. J. *Langmuir* **2005**, *21*, 6957. (c) Mearns, F. J.; Wong, E. L. S.; Short, K.; Hibbert, D. B.; Gooding, J. J. *Electroanalysis* **2006**, *18*, 1971.
(371) (a) DeGrado, W. F.; Summa, C. M.; Pavone, V.; Nastri, F.; Lombardo, A. *Annu. Rev. Biochem.* **1999**, *68*, 779. (b) Brask, J.; Jensen, K. J. *Bioorg. Med. Chem. Lett.* **2001**, *11*, 697.
(372) Brask, J.; Wackerbarth, H.; Jensen, K. J.; Zhang, J.; Chorkendorff, I.; Ulstrup, J. *J. Am. Chem. Soc.* **2003**, *125*, 94.
(373) Zhang, J.; Ulstrup, J. *J. Electroanal. Chem.* **2007**, *599*, 213.
(374) Nielsen, M. S.; Harris, P.; Ooi, B. L.; Christensen, H. E. M. *Biochemistry* **2004**, *43*, 5188.
(375) Hasan, M. N.; Kwakernaak, C.; Sloof, W. G.; Hagen, W. R.; Heering, H. A. *J. Biol. Inorg. Chem.* **2006**, *11*, 651.
(376) (a) Tarlov, M. J.; Bowden, E. F. *J. Am. Chem. Soc.* **1991**, *113*, 1847. (b) Song, S.; Clark, R. A.; Bowden, E. F.; Tarlov, M. J. *J. Phys. Chem.* **1993**, *97*, 6564. (c) Xu, J. S.; Bowden, E. F. *J. Am. Chem. Soc.* **2006**, *128*, 6813. (d) Nakano, K.; Yoshitake, T.; Yamashita, Y.; Bowden, E. F. *Langmuir* **2007**, *23*, 6270.
(377) (a) Wei, J.; Liu, H.; Khoshtariya, D. E.; Yamamoto, H.; Dick, A.; Waldeck, D. H. *Angew. Chem., Int. Ed.* **2002**, *41*, 4700. (b) Wei, J.; Liu, H.; Dick, A. R.; Yamamoto, H.; He, Y.; Waldeck, D. H. *J. Am. Chem. Soc.* **2002**, *124*, 9501. (c) Khoshtariaya, D. E.; Wei, J.; Liu, H.; Yue, H.; Waldeck, D. H. *J. Am. Chem. Soc.* **2003**, *125*, 7704.
(378) (a) Murgida, D. H.; Hildebrandt, P. *J. Phys. Chem. B* **2001**, *105*, 1578. (b) J. Phys. Chem. B 2002, *106*, 12814. (c) Acc. Chem. Res. 2004, *37*, 854.
(379) Yue, H.; Khoshtariya, D.; Waldeck, D. H.; Grochol, J.; Hildebrandt, P.; Murgida, D. H. *J. Phys. Chem. B* **2006**, *110*, 19906.
(380) (a) Avila, A.; Gregory, B. W.; Niki, K.; Cotton, T. W. *J. Phys. Chem. B* **2000**, *104*, 2759. (b) Wei, J. J.; Liu, H.; Niki, K.; Waldeck, D. H. *J. Phys. Chem. B* **2004**, *108*, 16912.
(381) Scott, R. A.; Mauk, A. G. *Cytochrome c A Multidisplinary Approach*; University Science Books: Sausalito, CA, 1995.
(382) Telford, J. R.; Wittung-Stafshede, P.; Gray, H. B.; Winkler, J. R. *Acc. Chem. Res.* **1998**, *31*, 755, and references therein.
(383) Heering, H. A.; Wiertz, F. G. M.; Dekker, C.; de Vries, S. *J. Am. Chem. Soc.* **2004**, *126*, 11103.
(384) Chi, Q.; Zhang, J.; Andersen, J. E. T.; Ulstrup, J. *J. Phys. Chem. B* **2001**, *105*, 4669.
(385) Chi, Q.; Zhang, J.; Jensen, P. S.; Nazmudtinov, R. R.; Ulstrup, J. J. *Phys. C: Cond. Matter Phys.* **2008**, in press.
(386) Zhang, B. L.; Zhu, Y. M.; Dong, S. J.; Wang, E. *Int. J. Biol. Macromol.* **2001**, *21*, 251–261.
(387) (a) Hansen, A. G.; Mortensen, M. W.; Andersen, J. E. T.; Ulstrup, J.; Kühle, A.; Garnæs, J.; Boisen, A. *Probe Micros.* **2001**, *2*, 139. (b) Zhang, J.; Ulstrup, J. Unpublished. (c) Kang, J.;; Rowntree, P. A. *Langmuir* **2007**, *23*, 509.
(388) Robertson, D. E.; Farid, R. S.; Moser, C. C.; Urbauer, J. L.; Mulholland, S. E.; Pidikiti, R.; Lear, J. D.; Wand, A. J.; Degrado, W. F.; Dutton, P. L. *Nature* **1994**, *368*, 425.
(389) Rau, H. K.; deJonge, N.; Haehnel, W. *Angew. Chem., Int. Ed.* **2000**, *39*, 250.
(390) (a) Louro, R. O.; Catarino, T.; Paquete, C. M.; Turner, D. L. *FEBS Lett.* **2004**, *576*, 77. (b) Paquete, C. M.; Turner, D. L.; Louro, R. L.; Xavier, A. V.; Catarino, T. *Biochim. Biophys. Acta - Bioenergetics* **2007**, *1767*, 1169, and references therein.
(391) Andersen, N. H.; Christensen, H. E. M.; Iversen, G.; Nørgaard, A.; Scharnagle, C.; Thuesen, M. H.; Ulstrup, J. Cytochrome *c*4. Messerschmidt, A.; Huber, R.; Poulos, T. L.; Wieghardt, K., Eds.; In *Handbook of Metalloproteins*; Wiley:Chichester, U.K., 2001; p100.
(392) Andersen, N. H.; Harnung, S. E.; Trabjerg, I.; Moura, I.; Moura, J. J. G.; Ulstrup, J. *Dalton Trans.* **2003**, 3328.
(393) Karlsson, J. J.; Nielsen, M. F.; Thuesen, M. H.; Ulstrup, J. *J. Phys. Chem. B* **1997**, *101*, 2430.
(394) Conrad, L. S.; Karlsson, J. J.; Ulstrup, J. *Eur. J. Biochem.* **1995**, *231*, 133.
(395) (a) Andersen, J. E. T.; Jensen, M. H.; Madsen, L. L.; Møller, P.; Ulstrup, J Proc. Snowdonia Conf. on Electrified Interfaces 1995,Harlech, Poster and Abstr. No. 26. (b) Andersen, J. E. T.; Friis, E. P.; Madsen, L. L.; Møller, P.; Ulstrup, J. Proc. Eurobic3, Noordwijkerhout, The Netherlands 1996,Poster and Abstr. No. A27. (c) Andersen, J. E. T.; Kornyshev, A. A.; Kuznetsov, A. M.; Madsen, L. L.; Møller, P.; Ulstrup, J. *Electrochim. Acta* **1997**, *42*, 819. (d) Friis, E. P.; Andersen, J. E. T.; Madsen, L. L.; Bonander, N.; Møller, P.; Ulstrup, J. *Electrochim. Acta* **1997**, *42*, 2889.
(396) (a) Friis, E. P.; Iversen, G.; Kharkats, Y. U. I.; Kuznetsov, A. M.; Ulstrup, J. *J. Biol. Inorg. Chem.* **1998**, *3*, 229. (b) Friis, E. P.; Andersen, J. E. T.; Madsen, L. L.; Møller, P.; Nichols, R. J.; Ulstrup, J. *Electrochim. Acta* **1998**, *43*, 2889.
(397) Rinaldi, R.; Cingolani, R. *Physica E* **2004**, *21*, 45, and references there.
(398) Fleming, B. D.; Praporski, S.; Bond, A. M.; Martin, L. L. *Langmuir* **2007**, *24*, 323.
(399) Fujita, K.; Nakamura, N.; Ohno, H.; Niki, K.; Gray, H. B.; Richards, J. H. *J. Am. Chem. Soc.* **2004**, *126*, 13954.
(400) (a) Richardson, D. J.; Watmough, N. J. *Curr. Opin. Chem. Biol.* **1999**, *3*, 207. (b) Adman, E. T.; Murphy, M. E. P. in: Messerschidt, A. ; Huber, R.; Poulos, T.; Wieghardt, K., Eds.; *Handbook of Metalloproteins*; Wiley: Chichester, 2001; Vol. 2, p 1381.
(401) (a) Simon, J. *FEMS Microbiol. Rev.* **2002**, *26*, 285. (b) Bamford, V. A.; Angove, H. C.; Seward, H. E.; Thomson, A. J.; Cole, J. A.; Butt, J. N.; Hemmings, A. M.; Richardson, D. J. *Biochemistry* **2002**, *41*, 2921.
(402) (a) Williams, P. A.; Fulop, V.; Garman, E. F.; Saunders, N. F. W.; Ferguson, S. J.; Hajdu, J. *Nature* **1997**, *389*, 406. (b) Gordon, E. H. J.; Sjögren, T.; Löfqvist, M.; Richter, C. D.; Allen, J. W. A.; Higham, C. W.; Hajdu, J.; Fulop, V.; Ferguson, S. J. *J. Biol. Chem.* **2003**, *278*, 11773.
(403) Wijma, H. J.; Jeuken, L. J. C.; Verbeet, M. P. H.; Armstrong, F. A.; Canters, G. W. *J. Am. Chem. Soc.* **2007**, *128*, 8557.
(404) (a) Gooding, J. J.; Wibowo, R.; Liu, J. Q.; Yang, W. R.; Losic, D.; Orbons, S.; Mearns, F. J.; Shapter, J. G.; Hibbert, D. B. *J. Am. Chem. Soc.* **2003**, *125*, 9006. (b) Gooding, J. J. *Electrochim. Acta* **2005**, *50*, 3049.
(405) (a) Gooding, J. J.; Chou, A.; Liu, J. Q.; Losic, D.; Shapter, J. G.; Hibbert, D. B. *Electrochem. Commun.* **2007**, *9*, 1677. (b) Yang, W. R.; Thordarson, P.; Gooding, J. J.; Ringer, S. P.; Braet, F. *Nanotechnology* **2007**, *18*, 412001.
(406) (a) Matoussi, H.; Mauro, J. M.; Goldman, E. R.; Andersen, G. P.; Sundar, V. C.; Mikulec, F. V.; Bawendi, M. G. *J. Am. Chem. Soc.* **2000**, *122*, 12142. (b) Ackerson, G. J.; Jadzinsky, P. D.; Kornberg, R. D. *J. Am. Chem. Soc.* **2005**, *127*, 6550. (c) Abad, J. M.; Mertens, S. F. L.; Pita, M.; Fernández, V. M.; Schiffrin, D. J. *J. Am. Chem.* **2005**, *127*, 5689.
(407) Daniel, M.-C.; Astruc, D. *Chem. Rev.* **2004**, *104*, 293.
(408) Templeton, A. C.; Wuelfing, W. P.; Murray, R. W. *Acc. Chem. Res.* **2000**, *33*, 27.
(409) (a) Schmid, G., Ed.; *Nanoparticles: From Theory to Applications* Wiley-VCH: Weinheim, Germany, 2004. (b) Rotello, V., Ed. *Nanoparticles. Building Blocks for Nanotechnology*; Springer: New York, 2004. (c) Schmid, G.; Pfeil, R.; Boese, R.; Bandermann, F.; Meyer, S.; Calis, G. H. M.; Vandervelden, W. A. *Chem. Ber. Rec.* **1981**, *114*, 3634. (d) Schmid, G. *Chem. Rev.* **1992**, *92*, 1709.
(410) Brust, M.; Walker, M.; Bethell, D.; Schiffrin, D. J.; Whyman, R. *J. Chem. Soc. Chem. Comm.* **1994**, *7*, 801.
(411) (a) Mulvaney, P. *Langmuir* **1996**, *12*, 788. (b) Ygerabide, J.; Ygerabide, E. E. *Anal. Biochem.* **1998**, *262*, 137, and references therein. (c) Bohren, C. F.; Huffman, D. R. *Absorption and Scattering of Light by Small Particles*; Wiley: Chichester, U.K., 1998.
(412) Alvarez, M. M.; Khoury, J. T.; Schaaf, T. G.; Shafigullin, M. N.; Vezmar, I.; Whetten, R. L. *J. Phys. Chem. B* **1997**, *101*, 3706.
(413) (a) Hicks, J. F.; Zamborini, F. P.; Murray, R. W. *J. Phys. Chem. B* **2002**, *106*, 7751. (b) Hoswell, S. L.; O'Neill, I. A.; Schiffrin, D. J. *J. Phys. Chem. B* **2003**, *107*, 4844.
(414) Su, B.; Girault, H. H. *J. Phys. Chem. B* **2005**, *109*, 23925.
(415) Ranganathan, S.; Guo, R.; Murray, R. W. *Langmuir* **2007**, *23*, 7372, and references there.
(416) (a) Chen, S.; Murray, R. W. *J. Phys. Chem. B* **1999**, *103*, 9996. (b) Chen, S. *J. Phys. Chem. B* **2000**, *104*, 663–667. (c) Chen, S.; Pei, R. *J. Am. Chem. Soc.* **2001**, *123*, 10607.
(417) Quinn, B. M.; Liljeroth, P.; Ruiz, V.; Laaksonen, T.; Kontturi, K. *J. Am. Chem. Soc.* **2003**, *125*, 6644.
(418) Albrecht, T.; Mertens, S. F. L.; Ulstrup, J. *J. Am. Chem. Soc.* **2007**, *129*, 9162.
(419) (a) Su, B.; Eugster, N.; Girault, H. H. *J. Am. Chem. Soc.* **2006**, *127*, 10760. (b) Galletto, P.; Girault, H. H.; Gomis-Bas, C.; Schiffrin, D. J.; Antoine, R.; Broyer, M.; Brevet, P. F. *J. Phys.: Condens. Matter* **2007**, *19*, 375108.
(420) (a) Cheng, Y. F.; Schiffrin, D. J. *J. Chem. Soc. Faraday Trans.* **1996**, *92*, 3865. (b) Knake, R.; Fahmi, A. W.; Tofail, S. A. M.; Clohessy, J.; Mihov, M.; Cunnane, V. J. *Langmuir* **2005**, *21*, 1001.
(421) (a) Ralph, D. C.; Black, C. T.; Tinkham, M. *Phys. Rev. Lett.* **1995**, *74*, 3241. (b) Andres, R. P.; Bein, T.; Dorogi, M.; Feng, S.; Henderson, J. I.; Kubiak, C. P.; Mahoney, W.; Osifchin, R. G.; Reifenberger, R. *Science* **1996**, *272*, 1323.

(422) (a) Dubois, J. G. A.; Gerritsen, J. W.; Shafranjuk, S. E.; Boon, E. J. G.; Schmid, G.; van Kempen, H. *Europhys. Lett.* **1996**, *33*, 279. (b) Graf, H.; Vancea, J.; Hoffmann, H. *Appl. Phys. Lett.* **2002**, *80*, 1264.

(423) (a) Liu, T.; Zhong, J.; Gan, X.; Fan, C.; Li, G.; Matsuda, N. *ChemPhysChem* **2003**, *4*, 1364. (b) Aubin-Tam, M.-E.; Hamad-Schifferli, K. *Langmuir* **2005**, *21*, 12080. (c) Jiang, X.; Jiang, J.; Jin, Y.; Wang, E.; Dong, S. *Biomacromolecules* **2005**, *6*, 46. (d) Jiang, X.; Shang, L.; Wang, Y.; Dong, S. *Biomacromolecules* **2005**, *6*, 3030. (e) Pradeep, T.; Tom, R. T. *Langmuir* **2005**, *21*, 11896.

(424) (a) Xu, C. A.; van Zalinge, H.; Pearson, J. L.; Glidle, A.; Cooper, J. M.; Cumming, D. R.; Haiss, W.; Yao, J. L.; Schiffrin, D. J.; Prouin-Perez, M.; Cosstick, R.; Nichols, R. J. *Nanotechnology* **2006**, *17*, 3333. (b) Stolarczyk, K.; Bilewicz, R. *Electrochim. Acta* **2006**, *51*, 2358.

(425) Zhao, J.; Bradbury, C. R.; Huclova, S.; Potapova, I.; Carara, M.; Fermin, D. J. *J. Phys. Chem. B* **2005**, *109*, 22985.

(426) (a) Chen, S. *J. Mat. Chem.* **2007**, *17*, 4115. (b) Guo, S.; Wang, E. *Anal. Chim. Acta* **2007**, *598*, 181.

(427) Reference 42, Chapter 3.

CR068073+